THE UNIVERSITY OF MICHIGAN

INDUSTRY PROGRAM OF THE COLLEGE OF ENGINNERING

THE EFFECT OF FREE STREAM TURBULENCE ON THE LAMINAR BOUNDARY LAYER HEAT TRANSFER OF FLAT PLATES AND CIRCULAR CYLINDERS

Mahlon C. Smith

A dissertation submitted in partial fulfillment
of the requirements for the degree of
Doctor of Philosophy in the
University of Michigan
Department of Aeronautical and Astronautical Engineering
1964

May, 1964

IP-672

Doctoral Committee:

Professor Arnold M. Kuethe, Chairman
Professor Robert C. F. Bartels
Associate Professor Walter R. Debler
Associate Professor Arthur F. Messiter
Associate Professor Rudi S. B. Ong

ACKNOWLEDGEMENTS

The author expresses his appreciation for the constant stimulation of Professor A. M. Kuethe during the course of this research work. His thanks are given to the Aeronautical and Astronautical Engineering Department for their financial support. In addition, he is grateful to other members of the Department for their kind assistance with some of the apparatus, and in particular to Stanley A. Wallis for his friendly cooperation and advice regarding the conduct of the experiments.

The Bendix Corporation graciously provided one hour of computer time for the data correlation theory calculations.

TABLE OF CONTENTS

TABLE OF CONTENTS (CONT'D)

LIST OF TABLES

LIST OF FIGURES

LIST OF FIGURES (CONT'D)

LIST OF FIGURES (CONT'D)

LIST OF APPENDICES

1.0 INTRODUCTION

It has been known for a long time that the ideal condition of an undistrubed fluid being penetrated by a solid body is approached only approximately by placing a body in a wind tunnel and forcing the fluid past it. In particular, the effect of circulating the fluid through the tunnel is to generate velocity fluctuations in the flow. These fluctuations have been found to have a large effect on the aerodynamic characteristics of bodies, particularly on the drag of spheres, cylinders and smooth flat plates. It was found that increases of a few percent in the free stream turbulent fluctuations caused large decreases in the Reynolds number of transition of the boundary layer of a flat plate. With the spheres and cylinders it was found that boundary layer transition occurred at a smaller angle from the stagnation point when high levels of free stream turbulence existed. These boundary layer effects caused the changes observed in the drag.

Recent studies have been concerned with the effect free stream turbulence may have on heat transfer from bodies placed in the flow. These studies have included the total effect, the effect in the turbulent flow region and the effect in the laminar flow region. With a flat plate, the location of the transition region is moved forward with increasing free stream turbulence. This causes an increase in the total heat transfer since the heat transfer in the laminar and the turbulent regions is unchanged. With a circular cylinder, it has been found that the total heat transfer is increased because of increases all around the surface of the cylinder, including the front and the rear stagnation points.

In previous experimental tests, the clear tunnel free stream turbulence level was at least 0.5% and sometimes was as large as 1.6%. In addition, only a comparatively small amount of information was obtained concerning the mean velocity and the velocity fluctuations associated with the heat transfer. Finally, the data obtained by several investigators showed considerable scatter under approximately the same test conditions. Thus, it appeared desirable to repeat many of the experiments in the low turbulence wind tunnel available at the University of Michigan. In these experiments, both local heat transfer and local velocity measurements were made to determine the effect of the free stream turbulence in the laminar flow regions of flat plates and circular cylinders. The experimental data were obtained in wind tunnels with low free stream turbulence levels of less than 0.1%. These data are compared with data obtained with free stream turbulence levels of up to 6%, generated by placing grids in the tunnels.

An account of previous work related to this study is given in the following chapter.

2.0 HISTORICAL ACCOUNT OF RELATED WORK

This section contains a discussion of previous work related to the subject of the present study. The discussion is divided into three parts, 2.1 Flat Plate, 2.2 Circular Cylinder and 2.3 General. Both experimental and theoretical studies are reviewed. The review is not exhaustive, but rather the selection is intended to review the previous work most relevant to the problem.

2.1 Flat Plate

Sugawara and Sato (Reference 1) in 1952, performed experiments on the heat transfer from a flat plate aligned parallel to the free stream. They were not specifically interested in the effect of free stream turbulence on the laminar boundary layer heat transfer, but rather in the effect of the free stream turbulence on the turbulent boundary layer heat transfer. In addition, the clear tunnel had a rather high free stream turbulence level of 1% to 1.5% and the leading edge of the plate was blunted for the tests with the turbulence producing grid. Thus, they obtained no data revealing the effect of the free stream turbulence on the laminar boundary layer heat transfer. Some of their results are reproduced in Figures 2-1 and 2-2 showing the heat transfer with the clear tunnel with a smooth and blunt leading edge and with the grid with the blunt leading edge. With this grid, the free stream turbulence at the leading edge of the plate was about 4%. It is evident that, with the grid and the blunt leading edge, the extent of the laminar boundary layer was negligible, even at a Reynolds number as low as 10,000.

Edwards and Furber (Reference 2) in 1956, investigated the effect of free stream turbulence on the heat transfer from a flat plate. Their

data showed that a free stream turbulence level of 5% produced a large increase in the heat transfer, but did not produce a fully developed turbulent velocity profile. This is evident from Figure 2-3 reproduced from Reference 2. It can be concluded that transition was taking place in the Reynolds number region from about 100,000 to 200,000 when the large free stream turbulence was present. They did not find an effect on the heat transfer in the laminar flow region at the low Reynolds numbers. No velocity profile was obtained in this region when large free stream turbulence was present.

Wang (Reference 3) performed both a theoretical and an experimental study for the specific purpose of determining the effect of free stream turbulence on the laminar boundary layer heat transfer. Some of his experimental results, reproduced in Figures 2-4 and 2-5 show the effect of the free stream turbulence on the velocity profile and the heat transfer coefficient. He concludes from these results that the free stream turbulence has a negligible effect on the mean velocity profile and on the heat transfer in the laminar region. In this case, the large free stream turbulence level present with the grid amounted to about 3%. His data show a large effect of the free stream turbulence on both the mean velocity profile and the heat transfer at a location almost at the end of the transition region. These results are also shown in Figures 2-4 and 2-5. The clear tunnel turbulence level for these tests was about 0.7% to 1.6%. This rather high clear tunnel turbulence level causes transition of the boundary layer at a low Reynolds number. This is shown by Figure 2-6, reproduced from Wang's study, and is evident also from Figure 2-5.

Wang's theoretical results were similar to those previously obtained by several other authors, i.e., sinusoidal free stream oscilations in the stream direction have only a small second order effect on the laminar boundary layer heat transfer. Interestingly enough, the effect is to reduce heat transfer from the plate due to increasing the dissipation in the boundary layer.

One of the earliest theoretical studies of the effect of free stream oscillations on laminar boundary layer heat transfer was made by Lighthill, (Reference 4) in 1954. He linearized the equations, assumed sinusoidal stream oscillations, and calculated the effect of the oscillations on the phase and amplitude of the heat transfer and skin friction. Thus, no average effect on the heat transfer was determined.

Lin performed a similar, although non-linear, study in 1956 (Reference 5) and Moore and Ostrach published a relatively complete non-linear study in 1956 (Reference 6), based upon Moore's previous work (Reference 7) published in 1951. These two studies were based upon free stream flow disturbances consisting of streamwise variations in the velocity. Their results were all similar, i.e., the effect is very small and the heat transfer from the plate is reduced.

2.2 Circular Cylinder

One of the earliest experiments performed to determine the local heat transfer from a cylinder in crossflow was reported by Schmidt and Wenner in 1941 (Reference 8). Their results showed only nominal agreement with theory, and a recent attempt was made by Kestin, et al., (Reference 9)

to show that the discrepancies were due to free stream turbulence present in their tunnel and to its effect on the heat transfer.

Giedt (Reference 10) reported in 1951 the results of experiments designed to determine the effect of free stream turbulence on the local heat transfer and skin friction of circular cylinders. His results, reproduced in part in Figure 2-7, showed that with a free stream turbulence level of about 4%, the heat transfer at the stagnation point was increased about 30% over the clear tunnel value when the Reynolds number was 170,000. No effect on the skin friction near the stagnation point was detected. No measurements were made of the level of turbulence in the clear tunnel or with the rope grid in place.

Seban, et al., reported the results of a series of tests made with circular and elliptic cylinders. Their results, References 11 and 12 (1957 and 1960) showed an effect of the free stream turbulence on the stagnation point heat transfer similar to the effect measured by Giedt. No measurements were made by either Giedt or Seban to determine the characteristics of the flow field in the vicinity of the stagnation point.

Zapp (Reference 13) and Schnautz (Reference 14) reported in 1950 and 1958 the results of experiments in which they measured the heat transfer and mass transfer from cylinders exposed to crossflow with various turbulence levels. Their results, taken together, were rather complete in that local heat and mass transfer coefficients were measured from 0° to 180° around the cylinder. Data were taken from Reynolds numbers of 1000 to 210,000. The clear tunnel turbulence level

was 0.5% and grids were used to generate up to 11% turbulence. These turbulence levels were measured by the heated wake method. Since the mass transfer can be related to the heat transfer by analogy, these results can be used to obtain heat transfer estimates. Schnautz's results showed considerable scatter in the data, which was sometimes so large that the effect of increasing the turbulence was to decrease the mass transfer. Nevertheless, in general, the effect of the free stream turbulence on the heat and mass transfer was found to be significant, with increases of over 50% near the stagnation point.

Kestin, Maeder and Sogin published in 1961 a report (Reference 9) giving the results of a relatively extensive review and experimental investigation of the influence of free stream turbulence on the heat transfer of circular cylinders near the stagnation point. Their results were obtained in a tunnel with a free stream turbulence level of 0.5% to 1.0% without a grid. They obtained measurements of free stream turbulence intensity of 2.7% at a distance of 16 mesh lengths from a grid. This is only about half the value obtained in Reference 19 and the discrepancy is unexplained. Large increases in heat transfer near the stagnation point of up to 75% were obtained at Reynolds numbers of 220,000. Data were taken at Reynolds numbers of 140,000 to 220,000 and turbulence intensities of up to 2.7%. The interesting coalescing of the data at the higher turbulence levels, as noted in Figure 2-8, reproduced from Reference 9, the unexplained discrepancy in the free stream turbulence measurements behind the grid and the high level of free stream turbulence with the clear tunnel made it desirable to repeat some of their experiments as part of the present study.

Theoretical studies related to the phenomenon have been made by Glauert, Watson and others (References 15 and 16 respectively). These studies treated the problem of the skin friction and the heat transfer at a stagnation point when either streamwise or transverse disturbances are present in the free stream, or conversely, when the body is oscillating relative to the free stream, either in the streamwise direction or transversely. In general, the results show a vanishingly small effect on the average skin friction, and zero effect on the average heat transfer for this type of free stream oscillation. Thus, these studies show that a more complex representation of the problem is necessary. Such a representation was studied by Sutera, Maeder and Kestin and reported in Reference 17 in 1963. The study consisted of formulating a mathematical model in which vortices were carried up to a stagnation point by a free stream flow. These vortices had their axes aligned with the mean flow so that they would be stretched by the flow acceleration away from the stagnation point. The analysis consisted of an analog computer simulation. The results, using only one frequency for the vorticity, showed a 25% increase in the heat transfer with an increase in the skin friction of only 5%. The formulation of the problem did not provide for specification of the free stream "turbulence". Thus, no correlation with data was possible.

2.3 General

Some early studies reported by Dryden (Reference 18) in 1936 were concerned with the effect of free stream turbulence on the boundary layer of a flat plate. These were extensive studies involving measurement

of both the stream-wise velocity fluctuations and the mean velocity profiles in the boundary layer in both the laminar and the turbulent regions. The turbulence level of the clear tunnel was about 0.5% and the maximum grid generated turbulence level was about 3%. These results showed primarily the effect of the free stream turbulence on the transition Reynolds number. In these tests, the Reynolds number per foot was so large that the region of influence of the free stream turbulence on the mean velocity profile in the boundary layer occupied only a very short distance on the plate. As a result, no mean velocity profile measurements were obtained that showed this influence. Data obtained in the laminar region and in the turbulent region showed that the 3% free stream turbulence level did not measurably affect the mean velocity profiles in these regions.

Further studies by Dryden, et al., (Reference 19) made in 1937, established the nature of the turbulence generated by round rod, square mesh grids placed in a wind tunnel. In particular, the intensity as a function of distance from the grid was determined. The results are shown in Figure 7-13.

Finally, it is noted that Schnautz (Reference 14), Seban (Reference 12), and Short, Brown and Sage (Reference 22), obtained experimental data on elliptic cylinders and spheres which showed that the free stream turbulence causes increases in the stagnation point heat transfer that are comparable to the increase experienced on circular cylinders. Thus, the effect can be considered to exist, in general, whenever free stream turbulence exists in a flow around a blunt body.

3.0 EXPERIMENTAL APPARATUS

This chapter contains a description of the experimental apparatus used to obtain the data discussed herein. The chapter is divided into three parts containing descriptions of the flat plate, the circular cylinders and the auxiliary equipment including the wind tunnels and the electrical equipment used in the heat transfer measurements.

3.1 Flat Plate

This section contains the results of an error analysis, applicable to the design and construction of the flat plate, a description of the heat transfer apparatus, of the boundary layer probes, and of the flat plate used in the experiments. The details of the error analysis are given in Appendices 7.2, 7.3, and 7.4.

3.1.1 Error Analysis

Error analyses were made to determine the errors to be expected in the heat transfer measurements due to alternating current heating, thermocouple conduction and plate conduction. These analyses are described in Appendices 7.2, 7.3, and 7.4. The results indicate less than 1% loss in heat from the center portion of the plate, less than 1/2% difference in the maximum and average temperature of the ribbon due to AC heating, less than 0.01% error due to locating the thermocouples beneath the heating ribbon and less than 0.01% error due to heat conduction along the thermocouple wires. These results indicate that a negligible error exists in taking the thermocouple data as determining ΔT , the difference between the temperature of the plate and the temperature of the free stream.

3.1.2 Design and Construction

The important design features of the plate are shown in Figure 3-1. Basically, it consisted of an open grid, pine wood framework with 1/8" thick sheet balsa forming the surface of the plate. Model airplace cement was used on the joints. Fiberglass wool insulation filled the grid spaces and two thicknesses of heavy drawing paper separated the top and the bottom halves. These two halves were fabricated separately and were screwed together with countersunk machine screws. The sharp leading edge was built up of ribs and 1/16" thick sheet balsa. The openings were filled with fiberglass wool insulation. The leading edge with the semicylindrical cross-section was made of solid hardwood. A short, wooden, wedge shaped trailing edge was screwed to the rear of the plate. Both of the leading edges were screwed and glued to the plate proper and the juncture filled with spackling compound. After the compound hardened, the surface was sanded flush to make a smooth joint. The plate was hung from the removable ceiling of the tunnel for easy installation and removal.

3.1.3 Heating Ribbon

The heating ribbon, indicated in Figure 3-1, was stock ribbon manufactured by the Hoskins Company, Detroit, Michigan and given the name Chromel A . The ribbon had dimensions of 0.002" x 1.000" and had a resistance of 0.246 Ω/ft at room temperature. Resistance variation with temperature was negligible for the temperatures used, i.e., less than 50°F above room temperature. Measurements showed that the resistance variation along the ribbon was negligible. Seven strips of ribbon were placed on the top and bottom of the plate running streamwise. These strips

began at the juncture of the leading edge with the plate proper. The gap between the strips was about 0.01". The strips were attached to the plate by Permatex, a gasket material that remains pliable on exposure to heat and the atmosphere. The thickness of the Permatex was less than 0.01". These strips were connected in series at the leading and trailing edges of the plate. Approximately 1/8" overlap existed at the front of the plate. This was bent over so as not to interfere with the attachment of the leading edge.

3.1.4 Thermocouples

The thermocouple wires used were stock iron-constantan, enameled thermocouple wires manufactured by the Sigmund Cohn Company. The wire diameters were .003" and the lengths were selected as 10 feet, terminating at the manual switch at the top of the tunnel. These wires were cemented into groves cut in the balsa planking and running crosswise to the flow. The junctions were centered on the plate. Thus, the temperature of each wire was approximately constant over a length of approximately 2.5 inches (see Figure 7-16). The junctions were formed by sanding off the enamel, twisting tightly and dipping in melted solder. These wires were run to opposite sides of the plate from the identical top and bottom halves and then carried up the supports and out of the tunnel ceiling. The air stream thermocouple junction was mounted inside the tunnel above the plate, exposed to the free stream but shielded from radiation from the plate.

3.1.5 Pressure Taps

The pressure taps were 3/32" outside diameter, 1/16" inside diameter aluminum tubes flush mounted to the surface of the plate at the locations shown in Figure 3-1. Plastic tubing was attached to the

ends of the aluminum tubes, projecting down from the sheet balsa surface run out to the sides of the plate, up the supports and out the tunnel ceiling.

3.1.6 Boundary Layer Probes

A small "bridge" was constructed over the heating ribbons as shown in Figure 3-2. This bridge was screwed to the plate with machine screws and the micrometer probe mounted to it. The probes had extension arms about 2" long to bring the sensing element out of the influence of the bridge and the micrometer. An extension rod 1/8" in diameter extended through a hole in the tunnel ceiling for operating the screw. A telescope and a small inclined mirror permitted reading of the micrometer from outside the tunnel. Zeroing was done by reflection in the heating ribbon before each test.

3.1.7 Boundary Layer Bug

In addition to the boundary layer probe described in the preceding section, a boundary layer bug was made and taped to the surface of the plate for certain of the boundary layer measurements. This is shown in Figure 3-2. Measurement of the distance of the wire from the plate was done by use of a scale and a magnifying glass.

3.2 Circular Cylinders

This description of the circular cylinders follows that of the flat plate in all respects. Since some of the techniques were the same, reference will be made to the discussion in 3.1 Flat Plate where appropriate.

3.2.1 Error Analysis

The alternating current heating error and the thermocouple conduction error are as described in Section 3.1.1 Error Analysis.

The cylinder conduction error is comparable with that of the flat plate. The results of the analysis indicate that the errors are negligible in comparison with the temperature difference between the heating ribbon and the air stream.

3.2.2 Design and Construction

The cylinders were made of cast acrylic plastic of 3" and 8" diameter. These were stock cylinders from Cadillac Plastics Company, Detroit, Michigan and had wall thicknesses of 1/8" and 1/4" respectively. Both cylinders were mounted so that they, with their supports, extended from the floor to the ceiling of the wind tunnel. Thus end effects were negligible. One of the 3" cylinders and the 8" cylinder had heating ribbons and the thermocouples installed on them. These were filled with cotton to reduce internal convective heat transfer. The other 3" cylinder had the probe micrometer mechanism mounted within it. The cylinders and the micrometer probe are shown in Figures 3-3 and 3-4. The 3" cylinders were mounted so that they could be rotated from outside the tunnel. A protractor and indicator were used to determine the angle. The 8" cylinder could be rotated only from inside the wind tunnel. Angles were determined from marks on the cylinder and the support.

3.2.3 Heating Ribbon

The heating ribbon used on both cylinders was from the same roll of material as that used on the plate. On the 3" cylinder, the ribbon was wrapped around 7 times, and on the 8" cylinder 11 times, providing heated lengths of cylinder of 7" and 11", respectively.

Permatex was used for the attachment and thermal bond to the 3" cylinder and a thin stopcock grease was used on the 8" cylinder. The thickness of the bond was about 0.01" in each case. Wrapping the cylinders in the manner described resulted in a 0.002" x 0.01" gap between the ribbons running around the cylinder at angles of 6° and 2° on the 3" and the 8" cylinder respectively. These gaps were partially filled with the bonding material to minimize the effect of flow disturbance at the heating ribbon on the heat transfer measurements over the forward portion of the cylinder.

3.2.4 Thermocouples

The thermocouples were of 0.003" diameter iron-constantan as noted in Section 3.1.4 Thermocouples. The junctions were formed as previously described, and the wires were cemented in grooves scratched lengthwise in the surface of the cylinders. The junctions were placed under the center of the center ribbon and thus the thermocouple wires experienced lengths of 3.5" and 5.5" of approximately constant temperature on the 3" and the 8" cylinders respectively.

3.2.5 Pressure Taps

The pressure taps were located as shown in Figure 3-3. They were made by drilling holes in the cylinders and fixing 3/32" O.D. by 1/16" I.D. brass tubing in the holes, flush with the surface. The holes were located to an accuracy of about 0.1° by indexing on a machine. Plastic tubing was attached to the brass tubing projecting into the inside of the cylinder and was run out one end of the cylinder to the manometers.

3.2.6 Micrometer Probe

The micrometer probe was designed with a rack and screw so that the micrometer could be turned by an extension rod extending out of the end of the cylinder at the tunnel ceiling. A telescope was used to read the micrometer. The traverse prongs projecting out of the cylinder were steel needles about 0.02" in diameter. These fit snugly in holes drilled in the cylinder. As shown in Figure 3-4, projections were soldered to the needles to support the hot wire about 1/2" upstream of the needles. The hot wire was soldered to the probe and then etched in place by handling the whole cylinder. The distance from the wall was measured with a machine scale and a magnifying glass, and the angle $\theta = 0^\circ$ was taken as the angle for minimum current in the wire. It is noted that this angle was within a few tenths of a degree of the value obtained from the static pressure tap measurements.

3.2.7 Hot Wire Bugs

Several hot wire bugs were used in obtaining data on the flow near the surface of the culinder. The three basic types of bugs used are shown in Figure 3-5. These were used to measure the streamwise fluctuations at $\theta = \pm 10^\circ$, the u, v fluctuations at $\theta = 10^\circ$ and $\theta = 20^\circ$ and the mean speed at $y = 0.001"$. These bugs were cemented to the surface of the cylinder by Pliobond. This cement dries quite rapidly but is also quite soluble in acetone even when dry, thus permitting rapid attachment and detachment of the bugs.

3.3 General

This section contains descriptions of the wind tunnels, the hot wire equipment, the manometer equipment and the current and voltage measuring equipment used in the experiments.

3.3.1 Wind Tunnels

Two wind tunnels were used in the experiments. One tunnel, with a 2' x 2' test section is an open circuit tunnel with an 8' x 8' settling chamber mounting a honeycomb and four screens for reducing the turbulence level in the test section. The maximum speed with this tunnel is about 90 ft/sec without a grid, but only about 50 ft/sec with a 1" x 1/4" grid. The highest speed used in these tests was 40 ft/sec. The cylinder used in this tunnel had a diameter of 3", so a Reynolds number, based on the diameter, of 60,000 was attained. The free stream turbulence level with the grid was a function of the distance from the grid as shown in Figure 4-1. With no grid the free stream turbulence level is about 0.1% at all speeds used.

The larger tunnel, with a 5' x 7' test section, is a closed circuit tunnel with 4 screens in a 20' x 20' settling chamber. The free stream turbulence level is also 0.1%, but the turbulence level with the 1" x 1/4" grid was dependent upon the tunnel speed as shown in Figure 7-13. Undesirable tunnel vibration and noise, initiated by flow through the grid, limited the test speed to about 60 ft/sec, which, with a cylinder diameter of 8" yielded a Reynolds number of 240,000.

3.3.2 Hot Wire Equipment

The hot wire equipment used with the 2' x 2' wind tunnel was fabricated in the University of Michigan Aeronautical Engineering laboratories for use in turbulence investigations. This equipment was designed to utilize the constant current hot wire technique. Current for the wire was supplied by batteries. The amplifier had a constant

amplification over the frequency range of interest and the input-output relation was linear as shown in Figure 3-6.

The hot wire equipment used with the 5' x 7' tunnel was manufactured by the Shapiro-Edwards Company. The principle of operation and the performance was similar to that of the equipment described above.

3.3.3 Manometer Equipment

The tunnel manometer for the 2' x 2' tunnel was an inclined tube type with a 10 to 1 slope. The reservoir was adjustable. This manometer was checked with a Chattock Fry absolute manometer and found to be accurate to 1/2% in tunnel speed. A pitot tube was used for the sensing element. No correction was made for the size of the pitot tube. The effect of turbulence on the tunnel speed readings was found to be less than 1% and no correction was made.

The tunnel manometer for the 5' x 7' manometer was compared with a Meriam Company 34FB2 micromanometer. The comparison in tunnel speed was within 1%. The micromanometer was subsequently used with a pitot-static tube for the speed measurements.

3.3.4 Current and Voltage Equipment

The current into the heating ribbon was measured with a Weston AC ammeter, Model 433. The least scale dimension was 0.05 amperes and estimates were made to 0.01 amperes. Thus, approximately 1% error in the heating power resulted in the worst case due to reading error. Fluctuations, probably due to contact resistance, added perhaps another 1% to this error. The meter was calibrated to absolute current by the University of Michigan, Electrical Standards Laboratory,

(Figure 3-4), but meter error can be expected to add another 1% to the heating power yielding about 3% expected average error in the heating power. The thermocouple output voltage was read by use of a Kintel Model 204 AR electronic galvonometer. This is a chopper stabilized, transistorized, DC amplifier. It was calibrated periodically by the University of Michigan Electrical Standards Laboratory (Figure 3-8).

4.0 BASIC EXPERIMENTAL DATA

This chapter contains descriptions of the experimental procedures and the data obtained with the flat plate with a sharp leading edge and with the circular cylinders with no tail fairings or splitter plates, and using only the "standard" 1" x 1/4" grid. These data were obtained in both the 2' x 2' and the 5' x 7' tunnels. The readings taken, the data reduction and the data in the form of tables and figures are presented. The discussion is given in two sections referring to the flat plate and the circular cylinder, respectively.

The description of the experimental data taken with the plate with the hemicylindrical leading edge attached, with the vortex generators on the sharp leading edge and the data taken with splitters and tail fairings on the cylinder are given in Appendix 7.1 Supplementary Experimental Data and Observations.

4.1 Flat Plate

This section contains the results of the experiments made with the flat plate with the sharp leading edge. The discussion is divided into four parts. In summary, the data show that the free stream turbulence causes increases in the Nusselt number in the laminar boundary layer region, but not in the turbulent region. The transition region occurs at a much lower Reynolds number when high level grid generated free stream turbulence exists than when it does not. Most of the increase in the Nusselt number occurs after the beginning of transition. This corresponds with the relatively large change in the mean velocity profile that occurs in the transition region. A region of laminar flow exists,

even with 6% free stream turbulence, in which the heat transfer is unaffected by the turbulence, within the experimental error.

4.1.1 Heat Transfer Data

The procedure in obtaining the flat plate heat transfer data consisted of setting the tunnel speed and the plate heating current and reading the ammeter and the electronic galvanometer connected across the thermocouples. The data were taken with a clear tunnel and with a turbulence grid installed. The thermocouples were connected to a manual switch for switching the input to the galvanometer. Considerable care was taken to repeat the same tunnel speeds for the various runs. The distance from the plate to the grid was varied in order to vary the level of the free stream turbulence at the leading edge of the plate. The free stream turbulence level versus distance from the grid in the 2' x 2' tunnel is shown in Figure 4-1.

All of the heat transfer data for the flat plate were taken for the condition of approximately constant heat transfer along a length of the plate. The variation from constancy is about 1/2% per inch along the plate. This estimate is obtained by assuming that the constant current and the constant resistance of the heating ribbon result in constant generation of heat per unit area of the ribbon. Some of this heat is radiated by the ribbon and the remainder is carried away by the convective air flow. The temperature variation along the plate results in a variation in the radiated energy. Thus, the variation from a constant convective heat transfer amounts to about 10% distributed over about 20 inches of plate length. Considering the accuracy of the data and

approximations in the correction theory, calculation of the effect of the non-uniformities in heat transfer on the Nusselt number did not appear to be warranted.

It is noted that the maximum temperature difference between the plate and the free stream was less than 20°F. Thus, the assumption of constant air density was used in the data reduction.

The assumption of constant convective heat transfer permits the theory of Eckert for arbitrary heat flux along the plate (Appendix 7.6) and the results of his numerical calculations to be used for comparison with the experimental data. For this comparison the data are reduced to the form:

$$N_{u_x} = \frac{h_d x}{k} = \text{Nusselt number} \tag{4-1}$$

for

h_d = heat transfer coefficient from the data

x = distance from leading edge of plate

k = fluid thermal conductivity

The heat transfer coefficient is:

$$h_d = \frac{q_N}{\Delta T} \tag{4-2}$$

for

$$q_N = q - q_R = \text{convective heat transfer per second per unit area} \tag{4-3}$$

$$q = i^2 R = \text{electrical power dissipated in the ribbon per unit area} \tag{4-4}$$

i = heating current

R = resistance of ribbon per unit area

$$q_R = \sigma \epsilon T_o^4 \left[\frac{T}{T_o}^4 - 1 \right] = \text{radiant heat transfer rate from the heating ribbon per unit area} \quad (4\text{-}5)$$

$$\Delta T = T - T_o = \frac{\text{thermocouple output}}{30} \text{ (for iron-constantan)} \quad (4\text{-}6)$$

T = surface temperature

T_o = free stream temperature

σ = Stefan-Boltzman constant

ϵ = heating ribbon emissivity

The corresponding Reynolds number for each data point is calculated as:

$$R_{e_x} = \frac{U_o x}{\nu} \quad (4\text{-}7)$$

U_o = free stream velocity

ν = free stream kinematic viscosity

An example of flat plate heat transfer data reduction is given in Appendix 7.6.

Pressure tap data, to be discussed later, and the heat transfer data from the top and the bottom of the plate show flow symmetry in all cases. Flow symmetry was assumed to exist to an adequate extent when the data from the top and the bottom of the plate agreed to within about 2%. The data given here are averages over the top and bottom surfaces.

The boundary layer thickness δ at the trailing edge of the plate is approximately 3% of the distance between the plate and the tunnel wall. Thus, the displacement thickness, and the increase in

flow velocity due to the boundary layer growth, will be about 1%, over the length of the plate. No correction to the data was made for this slightly increased flow volecity.

All of the fluid properties for the calculation of the Nusselt and Reynolds numbers were taken at the free stream conditions.

The flat plate heat transfer data are plotted in Figures 4-2 through 4-5.

4.1.2 Static Pressure Data

These data were taken in the clear tunnel by use of a Hook gage. The longitudinal location of the pressure taps is as shown in Figure 3-1. The lateral location of the taps was 1" outside of the heating ribbons. The pressure data showed a maximum stream-wise velocity gradient of less than 0.8 ft/sec/ft. This gradient is considered negligible and no correction was made for it in the data reduction.

4.1.3 Hot Wire Mean Velocity Data

These data were taken by use of a hot wire sensitive to the average U component of velocity. The wire was mounted on a boundary layer micrometer probe. These data were reduced by conventional methods.

The results are given in Table 4-1 and Figure 4-6.

4.1.4 Velocity Fluctuation Data

The stream-wise component of the velocity fluctuations in the boundary layer was measured by means of a hot wire mounted on a "bug." The rms value of the fluctuation was obtained from the rms thermocouple output voltage and the calibration of the wire. The wire was calibrated by placing it in the free stream of the tunnel. The

experimental value of the mean velocity was used for the turbulence data reduction when available. In other cases mean velocity estimates were made either from theory or from data taken at another point in the flow. The results of these measurements are given in Table 4-1.

The spectral density of the stream-wise fluctuations at several locations in the flat plate boundary layer were also obtained as follows.

The one dimensional spectral density of the streamwise velocity fluctuations is defined such that:

$$\overline{u^2} = \int_0^n E \, dn \qquad (4\text{-}8)$$

The value of $\overline{u^2}$ was measured at the point at which the spectra was desired. The bandwidth used was 5 cps up to a frequency of about 100 cps and 25 cps at the higher frequencies. The fraction of $\overline{u^2}$ contained within the bandwidth Δn was obtained at various values of n, using the spectrum analyzer. An ordinate proportional to this fraction divided by Δn was plotted versus n. The area under this curve is proportional to $\overline{u^2}$. Thus, each ordinate is multiplied by the proportionality factor to obtain the value of E at each n.

It is assumed that the value of E at the last data point is maintained as n decreases. Also it is assumed that the total of $\overline{u^2}$ is contained within the frequency band available from the analyzer, i.e., $0 > n \leq 200$ cps, except when the data indicate that a significant portion of $\overline{u^2}$ lies at higher frequencies. In this case, an estimate of this portion is made based upon the slope and the magnitude of the measured data at $n = 200$ cps. The results of the spectra measurements are given in Figure 4-7.

The free stream grid generated turbulence spectra at three distances from the grid are also shown in this figure.

Oscillograms of the stream-wise fluctuations were also obtained with a Polaroid Land camera at two locations along the plate. These locations were at 8 inches and 12 inches from the leading edge, and at distances from the plate of $y/\delta = 0.1$ and $y/\delta = 3$. The value of δ was taken from the Blasius profile at $U/U_o = .997$. These data were taken at a free stream speed of 20 ft/sec. Both clear tunnel data and data with 6% free stream turbulence at the leading edge of the plate were obtained. The results are given in Figure 4-8.

4.2 Circular Cylinder

This section contains the results of the experiments made with the circular cylinders in the clear tunnel and with the 1" x 1/4" mesh grid installed. The data show that the effect of the free stream turbulence is to increase the heat transfer and the skin friction by approximately equal amounts relative to the laminar values on the forward portion of the circular cylinder. The effect increases linearly with the magnitude of the free stream turbulence in the range from 0 to 6 percent. The effect is larger at the larger Reynolds numbers, the increase amounting to about 70% at the largest test Reynolds number of 240,000. The boundary layer of the cylinder shows random velocity fluctuations caused by the free stream turbulence. These occur even at the stagnation point.

4.2.1 Heat Transfer Data

Heat transfer data were taken in both the 2' x 2' tunnel and the 5' x 7' tunnel. The procedure using the 2' x 2' tunnel was

identical to that used to obtain the flat plate data, Section 4.1.1. For tests in the 5' x 7' tunnel the time required to install the 1" grid was so great that all of the clear tunnel data were taken first, following which the grid was installed and the tests repeated. Check runs with the clear tunnel and with the grid installed, made over intervals of about one week, showed good agreement.

The constant heat transfer data in the case of the circular cylinder can be transformed to constant temperature data by using the results of Eckert as shown in Appendix 7.7. The data reduction then is based upon generating the two non-dimensional quantities:

$$N_{u_D} = \frac{hD}{k} \tag{4-9}$$

$$R_{e_D} = \frac{U_o D}{\nu} \quad . \tag{4-10}$$

The Reynolds number, R_{e_D}, is obtained using the free stream speed and fluid conditions. The Nusselt number is generated by using k for free stream conditions and finding the heat transfer coefficient h as follows:

$$T = \frac{\mu v}{30} \tag{4-11}$$

$$\mu v = C_1 \left(\mu v_{read} + \mu v_{calibration\ correction}\right) \tag{4-12}$$

where C_1 = correction for the potential drop due to the resistance of the thermocouple wires. (See Appendix 7.5.)

$$h = \frac{q_N}{\Delta T} \; ; \; q_N = q - q_R = \text{convective heat transferred.} \tag{4-13}$$

$$q = 0.280 \times 10^{-2}\ i^2\ \frac{BTU}{ft^2\ sec}\ \text{generated heat} \qquad (4\text{-}14)$$

i = current flow in heating ribbon in amperes

$$q_R = \sigma\ \epsilon\ T_o^4 \left[\frac{T^4}{T_o} - 1 \right] \frac{BTU}{ft^2\ sec}\ \text{radiant heat transfer} \qquad (4\text{-}15)$$

$\Delta T = T - T_o$ for T = cylinder temperature
T_o = air temperature (4-16)

It is noted that the maximum radiant heat transfer is about 4% of the convective heat transfer. An example calculation for reducing the data is given in Appendix 7.7. The reduced data are given in Table 4-2 and Figures 4-9 through 4-14. Figure 4-9 shows the stagnation point Nusselt number and Figures 4-10 through 4-14 show the Nusselt number as a function of θ, the angle around the cylinder.

4.2.2 Static Pressure Data

The static pressure data were obtained by using an inclined manometer with the 5' x 7' tunnel and a Hook gage with the 2' x 2' tunnel. All the data were taken either with a clear tunnel or with the 1" grid 15-1/2" upstream of the leading edge of the cylinder. At this distance the turbulence from the grid was about 6% at the cylinder leading edge. The pressure differential between the stagnation point tap on the cylinder and the static taps was used to determine the C_p as:

$$C_p = 1 - \frac{H}{H_o} = 1 - \frac{q}{q_o} \qquad (4\text{-}17)$$

where $q_o = H_o =$ tunnel dynamic head

$q = H =$ dynamic head at edge of boundary layer on cylinder. (4-18)

The results of the static pressure measurements are given in Figure 4-15.

The accuracy of the measurements was low, particularly at the lower tunnel speeds. Thus, only the data taken at the highest test speeds of 40 ft/sec in the 2' x 2' tunnel and at 60 ft/sec in the 5' x 7' tunnel were retained. Mean velocity data were derived from the static pressure data using Equation (4-17). The distribution of the ratio of the velocity averaged over $\pm \theta$ with the grid installed to that with the clear tunnel is shown in Figure 4-16.

4.2.3 Hot Wire Mean Velocity Data

The micrometer probe was used to measure the mean speed at several points external to the boundary layer. The data were obtained using the constant current method. The wire was calibrated in the clear tunnel using the potential theory mean speed at the stagnation point at a distance from the cylinder of 0.13", and the static pressure data at $\theta = \pm 10°$ and 20°. The results were averaged over $\pm \theta$ and are given in Figure 4-16 as the ratio of the mean speed with the grid installed to that with the clear tunnel.

In addition, the speed very close to the cylinder wall (y = .001") was obtained by cementing a Wollaston wire to the wall and then etching it in place. This technique was suggested by Professor W. W. Willmarth who, with Mr. Bo Jang Tu, devised the method. The results of these measurements, corrected for proximity to the wall according to the results of Reference 37, are given in Figure 4-17. The correction amounts to a factor of about 2.0 at the stagnation point, due to the low "mean speed," but becomes negligible between $\theta = 10°$ and $\theta = 20°$.

The approximate mean speed at the wire, necessary for calculating the correction, was obtained from the theory for the circular cylinder given in Reference 23.

4.2.4 Velocity Fluctuation Data

Velocity fluctuation measurements were made using the constant current hot wire method. These measurements were made with the micrometer probe; with an x wire bug for obtaining uv correlations and u' and v' magnitudes; and with the two single wire bugs placed at $\theta = \pm 10°$ to obtain correlation of the stream-wise velocity fluctuations and the u' magnitudes on opposite sides of the stagnation point.

The details of the configurations for the x wire measurements are given in Figure 4-18. It is noted that each wire was aligned to "about" 45° with the mean flow at each location. The geometric angle was measured by means of a telescope and protractor. By use of potential theory for the mean flow angle, the actual angle to the flow was determined. This flow angle was used in reducing the data according to the expression:

$$\overline{uv} = \frac{\overline{U^2}\,(\overline{de_4^2} - \overline{de_3^2}) - \alpha_1\,\overline{u^2} + \alpha_2\,\overline{v^2}}{\alpha_3} \tag{4-19}$$

for

$$\begin{aligned} \alpha_1 &= K_4^2 - K_3^2 \\ \alpha_2 &= K_4^2 \cot^2 \theta_4 - K_3^2 \cot^2 \theta_3 \\ \alpha_3 &= -2\,(K_4^2 \cot \theta_4 + K_3^2 \cot \theta_3)\,. \end{aligned} \tag{4-20}$$

It was found necessary to use this general relation as the angles θ_3 and θ_4 and the hot wire sensitivities, proportional to K_3 and K_4, could not be obtained with sufficient accuracy to make $\alpha_1 = \alpha_2 = 0$ and $\alpha_3 = -4K_4^2 = -4K_3^2$. Thus, the simplified expression for $\overline{uv}$ could not be used. The u', v' and $\overline{uv}$ results are given in Table 4-3.

The correlation measurements of the stream-wise velocity fluctuations at the wires placed at $\theta = \pm 10°$ were obtained for the conditions given in Figure 4-18. The correlations were calculated as:

$$\text{Correlation} = \frac{\overline{e_+^2} - \overline{e_-^2}}{4\sqrt{\overline{e_3^2}}\sqrt{\overline{e_4^2}}} \qquad (4\text{-}21)$$

for $e_+ = e_3 + e_4$

$e_- = e_3 - e_4$

e_3, e_4 = fluctuating voltage across each wire

Wire calibrations were made for each set of runs from which the turbulence and the correlation data were obtained. The results of the measurements are given in Figures 4-19 and 4-20. The spectral density of the stream-wise fluctuation at $\theta = 10°$ was obtained by use of a hot wire attached to the micrometer probe. The spectra data were obtained both internal ($y/\delta = .5$) and external ($y/\delta = 2$) to the boundary layer at Reynolds numbers of both 30,000 and 60,000, corresponding to $U_o = 20$ ft/sec and $U_o = 40$ ft/sec. The boundary layer thickness, δ, was taken from the theory given in Reference 23. The spectra data obtained are given in Figures 4-21 and 4-22. The procedures for obtaining and reducing the data are as described in Section 4.1.4.

Oscillograms of the streamwise velocity fluctuations in the boundary layer $(y/\delta = 0.05)$ and at angles of $\theta = 0°$, 20°, 40°, and 60° were obtained at $R_{e_D} = 240{,}000$ with the clear tunnel and with 5% free stream turbulence at the leading edge of the cylinder. These results were obtained with a hot wire, an oscilloscope and a Polaroid Land camera and are shown in Figures 4-23 and 4-24.

5.0 DISCUSSION OF RESULTS

The discussion of results cannot be effectively categorized since part of the intent of the discussion is to bring the results together in a coherent manner. Nevertheless, the previous categorization will be maintained with the headings now referring only to the main theme of the discussions.

5.1 Flat Plate-Basic Data

This paragraph summarizes the important results to be discussed in this section. These are the influence of the free stream turbulence on the boundary layer mean velocity profile, on the velocity fluctuations in the boundary layer and on the heat transfer. The heat transfer coefficient in the region preceding transition is measurably increased by free stream turbulence of about 6%, measured at the leading edge of the plate. This increase in heat transfer is accompanied by irregular low frequency velocity fluctuations in the boundary layer and by a measurable increase in the slope of the mean velocity profile at the wall. In addition, the transition of the boundary layer to turbulent flow occurs at a small Reynolds number of less than 300,000. A region of laminar flow exists, extending back from the leading edge of the plate, in which there is no effect of large free stream turbulence on the heat transfer.

5.1.1 Heat Transfer

The flat plate results with the clear tunnel are shown in Figure 4-2, in comparison with Eckert's constant heat transfer theory, Reference 24, and in Figure 5-1 in comparison with the constant temperature theory. The procedure for reduction to the constant temperature case is

given in Appendix 7.6. The data show close correlation with theory in each case. As noted in Section 4.1.1, the data taken from the top and bottom of the plate were within 2%, indicating symmetrical flow conditions. In addition, hot wire probes placed in the boundary layer about 12" from the leading edge and at a distance from the plate of $y/\delta = 0.2$ showed negligible velocity fluctuations. Thus significant tunnel or leading edge disturbances were not present in the flow. The results with the grid installed are shown in Figures 4-3, 4-4, and 4-5. From these data, the ratio of the Nusselt number with high free stream turbulence to that with low turbulence can be obtained. This ratio is plotted in Figure 5-2. The data show that a laminar region exists in which the effect of the free stream turbulence on the heat transfer is negligible. It is evident from the figure that in the region where the Nusselt number ratio is appreciably greater than 1.0, the ratio does not depend upon the free stream turbulence level and the plate Reynolds number alone. Thus, it is implied that another Reynolds number effect is present, possibly a grid mesh or a leading edge radius Reynolds number. The data show a higher Nusselt number ratio at the lower speeds with a given Reynolds number, R_{e_x}, and free stream turbulence level. Further tests in which the grid mesh size and the leading edge radius are varied, all other variables being held constant, should segregate the effects of the grid mesh and the leading edge radius.

The tendency of the data in Figure 5-2 to coalesce at the higher Reynolds numbers is due to an integration effect in heat transfer phenomena occurring in convective flow. This is the tendency for upstream

variations in the heat transfer coefficient to average out to common values in the downstream turbulent flow region for either constant heat transfer or constant temperature plates. This effect has been previously noted in Reference 25.

The data of Wang (Reference 3) reproduced in Figure 2-5 and discussed in Section 2.1, show an effect of free stream turbulence on the heat transfer coefficient similar to that noted in the preceding paragraphs. However, as shown in Figure 2-5, transition occurs at an appreciably lower Reynolds number in his case, and with a lower value of free stream turbulence. This figure also shows that his transition Reynolds number is lower than the transition Reynolds numbers obtained by Schubauer (Reference 30). This lower transition Reynolds number is possibly due to a leading edge disturbance interacting with the free stream turbulence.

5.1.2 Static Pressure

The results of the static pressure measurements on the flat plate, given in Section 4.1.2, show that the velocity gradient over the heated portion of the plate is negligible.

5.1.3 Hot Wire Mean Velocity

The results of the mean velocity measurements are given in Table 4-1 and Figure 4-6. Figure 4-6 shows the mean velocity profiles at a Reynolds number of about 130,000 with the grid installed and with the clear tunnel. These were obtained at a speed of about 20 ft/sec and so correspond with the heat transfer data taken under these conditions. The clear tunnel velocity profile is the Blasius profile while the profile

occurring with free stream turbulence of about 6% at the leading edge of the plate has a greater value of $\partial U/\partial y$ at the wall than does the Blasius profile. The increase in $\partial U/\partial Y$ at the wall amounts to about 35%. The corresponding increase in the heat transfer coefficient is about 30%. The difference of 5% between these two increases of 30% and 35% is well within the experimental error. It may be noted that the difference between the velocity profiles is rather small in comparison with experimental error usually accompanying such measurements.

Several previous investigations of the effect of free stream turbulence on the laminar boundary layer velocity profile have been made. Wang (Reference 3) obtained data with about 3% free stream turbulence showing a modification of the Blasius profile similar to that shown in Figure 4-6. This data is reproduced in Figure 2-4. Dryden (Reference 18) obtained data at a higher Reynolds number per foot than at present. In this case, transition took place within a short distance of a few tenths of an inch in the stream-wise direction. Thus, the effect of the free stream turbulence on the velocity profile near the transition was not detected, and the data obtained showed only the Blasius profile and the turbulent profile.

5.1.4 Velocity Fluctuations

The results of measurements of the stream-wise component of the velocity fluctuations in the boundary layer are given in Table 4-1 and in Figure 4-7. In addition, oscillograms of fluctuations were obtained at two locations and are given in Figure 4-8. The data were obtained at a distance from the plate of about $y/\delta = 0.20$.

The data of Table 4-1 show that the magnitude of the fluctuations at a distance of about 12" from the leading edge of the plate, corresponding with a Reynolds number of about 125,000 at a free stream speed of 20 ft/sec, was less than 0.4%. When a grid was installed giving about 6% free stream turbulence at the leading edge of the plate, this value was increased to about 25%. It is noted that these percentages are based on the local velocity which can be obtained from Table 4-1. The high value of 25% corresponds with the increased heat transfer and velocity slope at the wall, discussed in Sections 5.1.1 and 5.1.3. Data were also obtained at a tunnel speed of 40 ft/sec at this location. In this case the turbulence level was about 10% and the heat transfer coefficient corresponded approximately with Eckert's theoretical value for turbulent flow. As noted in Table 4-1, oscilloscope observations at this location on the plate showed irregular velocity fluctuations and steady turbulence respectively for tunnel speeds of 20 ft/sec and 40 ft/sec and a free stream turbulence level of 6% at the leading edge of the plate. Additional data for the conditions U_o = 20 ft/sec ; x = 8" , R_{e_x} = 80,000; u'_o = 6% at the leading edge, and y/δ = .3 showed irregular velocity fluctuations of about 20% magnitude. It is interesting to note that these low Reynolds number, high free stream turbulence tests result in somewhat higher magnitudes of the stream-wise velocity fluctuations in the boundary layer than reported by Dryden (Reference 18).

Oscillograms of the fluctuations were also taken at a tunnel speed of 20 ft/sec, at distances of 8" and 12" from the leading edge of

the plate and with 6% turbulence as previously noted. These are shown in Figure 4-8 and indicate the difference between the free stream turbulence at these locations and the irregular velocity fluctuations in the boundary layer.

Additional data on the velocity fluctuations both inside and outside the boundary layer were obtained by spectral measurements of the stream-wise fluctuation component. These results are given in Figure 4-7. Figure 4-7 shows the very low level of turbulence in the boundary layer when the tunnel is clear. The figure also shows the increased level of the fluctuations at $x = 12"$ over that at $x = 8"$. It is interesting to note from Figure 4-7 that the spectral density of the fluctuations at 8" at $y/\delta = 0.5$ have a larger magnitude at frequencies higher than about 30 cps than do the measurements at $y/\delta = 0.25$. This result is reversed at frequencies lower than 30 cps. Figure 4-7 shows that the boundary layer fluctuations have low frequency components that are a factor of 10 higher in magnitude than those of the free stream turbulence. However, at the higher frequencies the magnitude of the boundary layer fluctuations is only about 25% of the magnitude of the free stream turbulence fluctuations. The division point between low and high frequency in this case is about 100 cps.

The grid generated free stream turbulence generates lower frequency oscillations in the boundary layer. These oscillations increase in magnitude as the distance from the leading edge is increased. As one proceeds downstream, these oscillations are accompanied by increased skin friction and heat transfer. With 6% free stream turbulence, data taken

where the u' oscillations at $y/\delta = 0.2$ amounted to 26% of the local mean velocity showed about a 30% increase in both the skin friction and the heat transfer of the boundary layer. This location on the plate corresponded with a Reynolds number of about 125,000. Heat transfer data, taken at greater distances from the leading edge under the same flow conditions, showed that the location for which the Reynolds number was 125,000 marked the initial phases of transition of the boundary layer. It is noted that no turbulent bursts were observed at this location at the Reynolds number of 125,000.

5.2 Circular Cylinder-Basic Data

This paragraph contains a brief summary of the discussion of the circular cylinder results. The detailed discussion is given in the following sections. The results show that the free stream turbulence increases the heat transfer in the laminar flow region near the stagnation point. This increase is larger at larger Reynolds numbers and is approximately linear with the magnitude of the free stream turbulence up to about 6% turbulence. Increased heat transfer coefficients up to about 70% larger than the laminar flow values were obtained at free stream turbulence levels of 5% and a Reynolds number of 240,000. The slope at the wall of the mean velocity profile in the boundary layer of the cylinder showed a comparable increase, but at the condition of $R_{e_D} = 240{,}000$ and 5% free stream turbulence, the increase in the slope of the mean velocity at the wall was only about 45% larger than the clear tunnel value. Turbulence measurements and oscillogram pictures showed that the free stream turbulence resulted in turbulent fluctuations within the boundary layer of the cylinder

that were of higher frequency than those in the flat plate boundary layer for the same free stream turbulence conditions.

5.2.1 Heat Transfer

The primary heat transfer results with the circular cylinder are summarized in Table 4-2 and Figure 4-9. Figure 4-9 shows the approximately linear relation between the stagnation point Nusselt number and the free stream turbulence level for a constant Reynolds number. It is evident that the slope of the curves is increasing with Reynolds number, indicating that the effect of the free stream turbulence increases with Reynolds number. The data were not all taken at fixed free stream turbulence levels, due to noise and other turbulent sources in the 5' x 7' tunnel with the grid installed. Thus, a crossplot was obtained from the lines faired through the data of Figure 4-9. This crossplot is given in Figure 5-3 showing the Nusselt number - Reynolds number relation for constant free stream turbulence levels. It may be noted that the faired relation shown for zero free stream turbulence is:

$$N_{u_D} = \sqrt{R_{e_D}} \quad . \tag{5-1}$$

This correlates well with the data and with the theory of Squire given in Reference 26. The zero free stream turbulence level is only an approximation as a turbulence level of about 0.1% exists in the clear tunnels. The faired data and the data points are shown in Figure 5-4, along with a theoretical relation derived in Appendix 7.8. The variables have been selected as $N_{u_D}/\sqrt{R_{e_D}}$ and $u'_o\sqrt{R_{e_D}}$. It may be noted that a highly accurate correlation of the data can be obtained by using the relation:

$$\frac{\frac{N_{uD}}{\sqrt{R_{e_D}}} - 1}{\frac{u'_o}{} \sqrt{R_{e_D}}} = A(1 - e^{-BR_{e_D}}). \qquad (5\text{-}2)$$

where $A = 0.0277$ and $B = 2.90 \times 10^{-5}$.

The necessity for the exponential term on the righthand side of the equation becomes evident from examination of Figure 5-5. This figure shows that the low Reynolds number data does not fall on the same correlation curve as the high Reynolds number data. Thus, the right-hand term, which is zero at $R_{e_D} = 0$, and the constant A at $R_{e_D} = \infty$, provides the correction for the low Reynolds numbers. This term is shown in Figure 5-6 in comparison with the faired experimental data.

Figure 5-4 also contains the results of some measurements made by other investigators. These results are discussed in Section 2.0 Historical Account of Related Work. The figure shows the large amount of scatter in the data. Some of this scatter can probably be attributed to errors in measuring the free stream turbulence, as noted in Section 7.1.2. However, for the most part, satisfactory explanations are not evident.

5.2.2 Static Pressure

The static pressure data is presented in Figure 4-15. These results show that some deviation from potential theory occurs at the low Reynolds number of 60,000. This is due to the effects of viscosity. The deviation is much less at the higher Reynolds number of 240,000.

The ratio of the mean velocity, derived from the static pressure measurements, with about 6% free stream turbulence to that with the clear

tunnel is given in Figure 4-16. These data show that at a Reynolds number of 60,000 the average ratio of mean velocity with turbulence to mean velocity without turbulence is about 0.94. At the Reynolds number of 240,000 the average ratio is about 1.08. However, considering the difficulties of measuring the small pressure difference, the differences between these values appear to be within the experimental errors. This conjecture is based, in part, on the results of hot wire measurements of the mean velocity in the vicinity of the stagnation point, also shown in Figure 4-16. These show a minor effect of the free stream turbulence on the mean velocity. It may be noted that Fage (Reference 27) measured no appreciable static pressure differences near the stagnation point of the circular cylinder with and without free stream turbulence of about 3%. Giedt (Reference 10) and Seban (Reference 11) also obtained no significant changes for turbulence levels of about 4%.

5.2.3 Hot Wire Mean Velocity

The results of mean velocity measurements at Reynolds numbers of 30,000 and 240,000, made with the hot wire cemented to the surface of the cylinder, are given in Figure 4-17. The regular oscillations of the flow due to the cylinder vortex street resulted in an rms value of the velocity fluctuations at $\theta = 0°$ with no free stream turbulence. Thus, it is the ratio of these rms velocity fluctuations with and without free stream turbulence that is plotted at $\theta = 0°$. It is noted that this ratio does not have the same meaning as the ratio of the mean velocities with and without the grid at angles of θ large enough so that a mean flow appreciably greater than the fluctuations exists. In the

latter instance, the ratio is proportional to the mean skin friction while in the former instance it is not. The heat transfer associated with the velocity ratio is also plotted in Figure 4-17. This shows that the Reynolds analogy does not quite account for the increase in the heat transfer; i.e., the increase in the skin friction, proportional to the ratio U_g/U_c plotted in the figure, is not quite as large as the increase in the heat transfer. It is evident that the Reynolds analogy is not applicable at $\theta = 0°$ since the average skin friction is zero due to the plus and minus oscillations. These data were taken for a free stream turbulence level of about 5%.

It is possible that the high value of U_g/U_c at $\theta = 0$ had a larger effect on the heat transfer than is shown in Figure 4-17. The distance represented by the angle from $\theta = 0$ to $\theta = 5°$ is only a few tenths of an inch. Thus, it might be expected that longitudinal conduction in the heating ribbon at the stagnation point would effectively "smear out" the heat transfer. However, the data of Figure 7-12 show that at least some temperature gradient can exist in the vicinity of the stagnation point with non-uniform flow conditions. Thus, a question remains concerning the relation between the values of U_g/U_c and N_{u_g}/N_{u_c} in the immediate vicinity of $\theta = 0°$. Therefore, the faired curve of the velocity ratio, shown in Figure 4-17 is not extended to values of θ less than 10°.

It is noted that Fage and Falkner (Reference 27) using a Stanton tube, measured no increase in skin friction at angles from $\theta = 0°$ to $\theta = 20°$ with about 3% free stream turbulence. Giedt (Reference 10) also did not detect an increase in the skin friction by similar measurements with about 4% free stream turbulence. The reason for the disagreement between their results and the present results is not known.

It is interesting to note that at the low Reynolds number of 30,000 the effect of the turbulence on the mean velocity near the wall dies out as the angle θ is increased, while at the Reynolds number of 240,000 the effect is almost constant until a sudden increase occurs near $\theta = 70°$. This latter effect can be attributed to transition in the boundary layer. It is noted that a corresponding relative increase in the heat transfer coefficient also occurs near $\theta = 70°$ at the higher Reynolds numbers.

The relative velocity over the surface of the cylinder can be used as a check on the results of the measurements made with the hot wire cemented to the surface. Thus, the theory and data of Thom, Reference 28 and Green, Reference 36, are compared with present results in Figure 5-7. This comparison is satisfactory.

Additional mean velocity measurements were attempted at a Reynolds number of 30,000 with the micrometer probe mounted inside the cylinder. These attempts to measure the mean velocity profile in the boundary layer were not satisfactory due primarily to the fact that the boundary layer thickness was only about 0.02".

5.2.4 Velocity Fluctuations

The u', v', and $\overline{uv}$ measurements made with the X wire near the stagnation point provide the data given in Table 4-3. These data, taken at about three boundary layer thicknesses from the surface of the cylinder, show that the vortex street of the cylinder causes u' velocity fluctuations at $\theta = 10°$ and $\theta = 20°$ of about 3% of the free stream velocity. The corresponding v' fluctuations are about 0.3% of the free stream velocity and the corresponding $\overline{uv}$ correlation coefficient is about 0.7.

The most significant result of the X wire measurements with 6% free stream turbulence is that the u' and v' fluctuations are each about 6% of the free stream velocity at the distance of $y/\delta = 3$ from the surface of the cylinder. Thus, the flow apparently carries the free stream turbulence up to the cylinder without appreciable change in magnitude. The turbulence reduces the positive $\overline{uv}$ correlation from 0.70 to 0.10. It is noted that the correlation coefficient and the fluctuation magnitudes are both slightly higher at $\theta = 10°$ than at $\theta = 20°$.

Considerably more data are given in Table 4-3 for the case of the cylinder with combinations of a tail and a splitter plate. These results are discussed in Appendix 7.1.

Correlation and velocity fluctuation measurements made with hot wires at $\theta = \pm 10°$ provided the data given in Figures 4-19 and 4-20. These data show correlation coefficients of about -1.0 for the clear tunnel case. The implication of this data is that in the clear tunnel the regular shedding of vortices from the rear of the cylinder causes the velocity fluctuations at the forward portion of the cylinder. This effect of the vortex street is further implied by the results of measurements with the cylinder and the tail. These show a much lower fluctuation magnitude and a correlation coefficient of about -0.5 when the tail is present. Thus, the tail effectively eliminates the vortex street. The magnitude of the fluctuations varies only slightly from about 12% to 15% of the local mean velocity with no grid and with 6% free stream turbulence, respectively. However, the regular velocity fluctuations existing with no grid tend to become random fluctuations with 6% free stream turbulence and the correlation coefficient is reduced to about -0.5.

The details of the spectral measurements and the associated magnitudes of the u' fluctuations are given in Figures 4-21 and 4-22, and the spectral density is plotted in these figures. The salient features of the spectral data are the peaks at the frequencies associated with the Strouhal number. These are:

$$S = 5 = \frac{U_o}{nD} \qquad \text{(Reference 29)}$$

or

$$n = \frac{20}{5 \cdot \frac{1}{4}} = 16 \text{ cps for } U_o = 20 \text{ ft/sec}$$

$$= 32 \text{ cps for } U_o = 40 \text{ ft/sec.}$$

It is also very evident that the irregular velocity fluctuations associated with the cylinder vortex street have negligible higher frequency components in comparison with those of the fluctuations associated with free stream turbulence of 6%. It is interesting to note that at the Reynolds numbers of 30,000 (U_o = 20 ft/sec), the higher frequency ($f > 100$ cps) spectral density magnitudes of the fluctuations in the boundary layer in high turbulence, are about 0.15 of those of the fluctuations in the boundary layer of the flat plate at a location where about the same heat transfer increase with 6% free stream turbulence is realized. On the other hand, the spectral density magnitudes at these frequencies and a Reynolds number of 60,000 are about equal to those obtained on the flat plate. Since the heat transfer coefficient increase due to free stream turbulence is only about 10% higher at a Reynolds number of 60,000 than at a Reynolds number of 30,000 it is apparent that high frequency stream-wise fluctuation components alone are not sufficient to strongly influence the heat transfer.

It is seen from the oscillograms, Figures 4-23 and 4-24 that at a Reynolds number of 240,000 with free stream turbulence, the traces of the stream-wise velocity fluctuations in the boundary layer are similar in appearance to the traces of the stream-wise velocity fluctuations in the free stream. However, the oscillograms of the stream-wise velocity fluctuations in the boundary layer of the flat plate, Figure 4-8, show only low frequency oscillations in comparison with the free stream turbulence. The oscillograms, Figure 4-23, also show the more or less regular oscillations present in the boundary layer of the cylinder and also external to the cylinder when in the clear tunnel. These oscillations are caused by the vortex street of the cylinder.

6.0 SUMMARY AND CONCLUSIONS

This section contains a summary of the results of the study, and the conclusions drawn therefrom. Some of the conclusions given here are based upon the results reported in Appendix 7.1 Supplementary Experimental Data and Observations.

6.1 Flat Plate

The discussion here is divided into two parts 6.1.1 Sharp Leading Edge and 6.1.2 Hemicylindrical Leading Edge.

6.1.1 Sharp Leading Edge

The results show that the free stream turbulence induces large streamwise velocity fluctuations in the laminar boundary layer. These fluctuations increase with downstream distance along the plate, and have a value of about 25% of the local mean velocity at a distance from the wall of $y/\delta = 0.2$ for a Reynolds number of about 125,000 and for 6% free stream turbulence at the leading edge of the plate. Under these conditions they are accompanied by approximately equal increases of 35% in the local skin friction and the local heat transfer coefficients. This is shown in Table 4-1 and Figures 4-6 and 5-2.

The transition Reynolds number is reduced by the free stream turbulence. The transition region occurs at Reynolds numbers from about 100,000 to 200,000 with 6% free stream turbulence. This result is in agreement with the results of other investigators.

6.1.2 Hemicylindrical Leading Edge

The results show that if the flat plate has a leading edge of 3/8" radius, (radius Reynolds number = 3900) large velocity

fluctuations exist in the laminar boundary layer. Despite these fluctuations a nominally laminar mean velocity profile and laminar heat transfer can exist in a region before transition occurs. However, when free stream turbulence is large, transition occurs very near the leading edge and turbulent heat transfer and velocity profiles prevail. Under these conditions, a magnitude of turbulence of about 17% of the local mean velocity occurs at $y/\delta = 0.16$ and $R_{e_x} = 82{,}000$ with 4% free stream turbulence at the leading edge.

6.2 Circular Cylinder

This discussion is divided into three parts, 6.2.1 Heat Transfer, 6.2.2 Mean Velocity and 6.2.3 Velocity Fluctuations.

6.2.1 Heat Transfer

The free stream turbulence has a large effect on the heat transfer from the cylinder near the stagnation point. A linear proportionality exists between the Nusselt number and the free stream turbulence for Reynolds numbers up to 240,000 and turbulence levels up to 6%. The proportionality constant increases with the Reynolds number. This effect of the free stream turbulence on the heat transfer can be correlated at the higher Reynolds numbers in the form $N_{uD}/\sqrt{R_{e_D}}$ vs $u'_o R_{e_D}$. This correlation is derivable theoretically using the momentum and energy equations for the stagnation point flow, a semi-empirical representation of the turbulence, and one undetermined constant obtained from the data.

The free stream turbulence increases the heat transfer around the forward portion of the cylinder approximately the same amount as at the stagnation point.

6.2.2 Mean Velocity

The mean velocity external to the boundary layer around the cylinder is not appreciably affected by the free stream turbulence, and variations in it do not cause the increased heat transfer.

The mean velocity near the wall of the cylinder, in the boundary layer, is increased by the free stream turbulence. This increase in the slope of the mean velocity at the wall is about 70% of the increase in the heat transfer coefficient.

6.2.3 Velocity Fluctuations

The free stream turbulence fluctuations persist, undiminished, up to the outer edge of the boundary layer at the stagnation point. The u and the v components are comparable in magnitude. Within the boundary layer itself, even as close as 0.001" from the wall, relatively high frequency fluctuations exist. These are amplified at large Reynolds numbers as one goes around the cylinder. They decay at the lower Reynolds numbers.

Regular velocity fluctuations exist at all points in the boundary layer, even at the stagnation point, in the clear tunnel. These are due to the vortex street shed from the cylinder. These fluctuations have no measurable effect on the heat transfer.

6.3 General

The scale of the free stream turbulence does not have a large effect on the increase in the heat transfer from the circular cylinder within the range of the present measurements. This effect with the 1" mesh, 2" mesh and 0.06" mesh is shown in Figure 7-10. It is noted that

the structure of the turbulence was that of turbulence generated by round rod, square mesh grids. The integral scale of the turbulence in the present experiments was always several times larger than the boundary layer thickness.

Significant local heat transfer variations in the vicinity of the stagnation point can result from inducing local small scale flow disturbances in the mean flow approaching the cylinder. Wind tunnel noise, vibration and flow disturbances can cause free stream turbulence that significantly influences the heat transfer from the cylinder in the stagnation point region. These influences can be present and add to those of the free stream turbulence generated by a grid.

A pressure gradient on a flat plate with no leading edge disturbance does not seem to enhance the effectiveness of the free stream turbulence in increasing the heat transfer. Thus, it is concluded that the pressure gradient alone does not cause the phenomenon occurring with the circular cylinder. However, it is noted that although a dynamic pressure increase of a factor of 4 over a distance of 6" was obtained with the plate and tunnel bump configuration, the average value of $\partial P/\partial X$ over the 6" distance was only about 3% of the $\partial P/\partial X$ near the stagnation point of the circular cylinder at the Reynolds number of 30,000. This test is described in Appendix 7.1.

In summarizing the results of this study it is evident that a detailed "explanation" of the phenomenon cannot be made, based on the information presently available. In particular, the reason why the free stream turbulence can "penetrate" the circular cylinder boundary layer

and influence the heat transfer, but cannot do the same in the case of the flat plate boundary layer is not clear. The reason probably rests on the fact that near the stagnation point of the circular cylinder, just outside the boundary layer, the mean velocity has been reduced to a value comparable to that of the fluctuating velocities, while in the case of the flat plate, just outside the boundary layer, the turbulence is an order of magnitude smaller than the mean velocity. It might be hoped that a theoretical study along the lines of that reported in Reference 31 would bear fruit in this area.

The present results also do not yield any information concerning the role of Taylor-Goertler vortices near the stagnation point in influencing the heat transfer. It might be expected that these vortices could not exist in a steady state in the presence of the large random turbulent velocity fluctuations. On the other hand, transient selective amplification of the fluctuation components due to the stretching of the vortex lines can be anticipated.

7.0 APPENDICES

7.1 Supplementary Experimental Data and Observations

This appendix contains discussions of the results obtained with the flat plate with the hemicylindrical leading edge, with the flat plate with vortex generators, and with the circular cylinder with a tail fairing and with rods, wires and small dimension screens a short distance in front of the cylinder. In addition, cylinder data were obtained with turbulence generated by a screen of mesh .06" x .01" and by a grid of mesh 2" x 1/2". Also, flat plate data were obtained with a pressure gradient over the plate, and with thermocouples located very near the leading edge. Finally, one set of temperature profile data on the flat plate was obtained. The discussion is given in three parts, 7.1.1 Flat Plate Data, 7.1.2 Circular Cylinder Data and 7.1.3 Evaluation of Results.

7.1.1 Flat Plate Data

This section contains the results of the supplementary measurements made with the flat plate. These results are difficult to summarize because of the variety of test conditions. Thus, advantage will be taken of the relatively short descriptions of the results and no summary will be given here.

The procedure in obtaining the heat transfer data was basically the same as that noted in Section 4.1.1 and the data were reduced in a similar way. The data in Figure 7-1 were obtained with the sharp nosed plate with vortex generators on the upper portion of the leading edge. The vortex generators were a line of 1/32" x 1/32" x 1/8" pieces of balsa wood mounted upright 1-1/2" to the rear of the leading edge and spaced

1/16" apart. This line spanned the heating section of the plate. The data in Figure 7-2 show the effect of the hemicylindrical leading edge on the heat transfer in the clear tunnel. The data in Figures 7-3 and 7-4 show the effect of the splitter plate and about 4% free stream turbulence at the leading edge of the plate, respectively.

Temperature profiles in the boundary layer were obtained with the sharp leading edge plate for the case of the clear tunnel and with 6% free stream turbulence at the leading edge. These profiles were obtained with an iron-constantan thermocouple junction mounted on the micrometer probe. The results of these measurements are shown in Figure 7-5. The data were not corrected for radiation to the probe near the wall.

The mean velocity data consisted of hot wire probe measurements. These data were obtained with the micrometer boundary layer probe and were reduced by conventional methods. The results of the measurements are given in Table 4-1 and Figures 7-6 and 7-7.

The velocity fluctuation data was obtained by use of a hot wire bug placed at two x locations and one y location in the boundary layer. These data were obtained and reduced by the methods discussed in Section 4.1.4. The results are given in Table 4-1.

7.1.2 Circular Cylinder Data

This section contains the results of the supplementary measurements and observations made using the circular cylinder. The summary of these results is given in Section 7.1.3

The cylinder heat transfer measurements were made using basically the same procedure as previously noted in Section 4.2.1. The data reduction was identical to that previously noted in Section 4.2.1.

One heat transfer test was made at a Reynolds number of 30,000 with twice the temperature difference between the heating ribbon and the free stream as in the other runs. This result is shown in Figure 4-10. In a second test, heat transfer data were taken with a tail on the cylinder at Reynolds numbers of 30,000 and 60,000. The procedure was to obtain data without the tail, remove the cylinder from the tunnel, attach the tail with masking tape, replace the cylinder with tail in the tunnel and make the next test. This took only a few minutes. These results are given in Figure 7-8. The tail was a symmetrical NACA 0020 section approximately 11" long. Several exploratory heat transfer tests were made using rods, wires and small dimension screens to disturb the flow. In addition, runs were made with splitter plates attached to the leading edge of the cylinder. The procedure in these tests was to make a "standard" run, attach the local flow disturbance devices and then make the following run. The configuration change took only a few minutes. Finally, a screen of .06" x .01 mesh and a 2" x 1/2" grid, both spanning the tunnel, were used. The large mesh grid was placed at 15 mesh lengths, or 30" from the leading edge of the cylinder, and the screen was placed at distances of 1", 5-3/4" and 15" from the leading edge of the cylinder. The results of these measurements are given in Table 7-1 and Figure 7-9 through 7-12. All of these heat transfer data are given in terms of the ratio $N_{u_D}/\sqrt{R_{e_D}}$ for convenience in interpreting the results.

Static pressure data, with the tail fairing, were obtained and reduced as noted in Section 4.2.2. The procedure was to make a "standard" run to insure proper equipment operation and then to remove the cylinder and attach the fairing. The cylinder was then replaced and the data with the fairing was obtained. These data with and without the tail are shown in Figure 4-15.

Mean velocity data external to the boundary layer at the stagnation point, with the tail attached to the cylinder, were obtained with the hot wire micrometer probe. The test procedure was as described in the preceding paragraph and the wire calibration was obtained from clear tunnel data and potential theory. The measurements showed no effect of the tail on the mean flow at $\theta = 0°$ and $y = 0.13"$.

Extensive data were taken to determine the u', v' and $\overline{uv}$ values in the vicinity of the stagnation point with the tail, splitter and tail plus splitter attached. In addition, stream-wise correlations and u' data were obtained at $\theta = \pm 10°$. All of these data were obtained at a distance from the cylinder of about $y/\delta = 3$. The data reduction procedure was similar to that previously discussed in Section 4.2.4. These results are given in Table 4-3 and Figures 4-19 and 4-20.

Free stream turbulence measurements made in the 5' x 7' tunnel in support of the circular cylinder heat transfer measurements showed that the free stream turbulence did not decay according to the law represented by the results given in Figure 4-1. The turbulence level at any location behind the grid was a function of the tunnel speed. The effect of increasing tunnel speed was to increase the turbulence level.

In addition, increasing tunnel vibrations and noises were observed with increasing speed when the grid was installed. The results of the turbulence measurements are given in Figure 7-13 and were used in the evaluation of the heat transfer data.

7.1.3 Evaluation of Results

This paragraph contains a summary of the discussion, to be presented in this section, of the supplementary data obtained with the flat plate and the circular cylinder. This supplementary data serves to indicate the effect of free stream turbulence on the heat transfer within 1/2" of the leading edge of the plate, the effect with a longitudinal pressure gradient, and the effect with leading edge disturbances (hemicylindrical nose and vortex generators). In addition, mean velocity boundary layer profiles were obtained with the hemicylindrical nose which served to show the laminar and turbulent flow conditions associated with the heat transfer. The cylinder data showed that local flow disturbances ahead of the stagnation point can affect the local heat transfer and that the tail does not affect the local heat transfer, but does affect the velocity fluctuations caused by the cylinder vortex street. In addition, tests with grid mesh sizes of .06" and 2" gave an indication of the effect of the integral scale of the turbulence on the heat transfer.

The heat transfer results given in Figure 7-1, obtained with the sharp leading edge, show that the vortex generators cause heat transfer coefficients that are approximately the same as coefficients calculated by Eckert for turbulent flow. Thus, it is evident that sufficiently strong disturbances can be introduced into the boundary layer to cause effectively

turbulent heat transfer, even at the low Reynolds number of 10^5/ft used for these tests.

Exploratory information on heat transfer was obtained with the sharp leading edge with a heating ribbon folded over the leading edge and running back to the juncture with the main body of the plate. Thermocouples were placed on the top and bottom of the leading edge, under the heating ribbon, at a distance of $x = 1/2"$. Heat transfer data obtained with these two thermocouples showed no effect of 6% free stream turbulence at this location on the plate.

It is noted that heat transfer data taken with the hemicylindrical nose showed that the grid generated turbulence caused a large increase in the heat transfer at a distance of 1/2" to the rear of the juncture of the nose and the plate. This is shown by comparison of the data in Figure 7-2 and 7-4. This increase in heat transfer was probably caused either by the interaction of the free stream turbulence with the leading edge disturbance produced by the hemicylindrical nose, or by the enhancement of the effect of the free stream turbulence by the strong adverse pressure gradient associated with the hemicylindrical nose. In the case of the sharp leading edge, only a weak adverse pressure gradient existed and there was no leading edge disturbance present.

Further exploratory information on heat transfer was obtained by placing two symmetric "bumps" in the tunnel, one above and one below the plate. These were placed so that the forward portion formed a quarter cylinder, with a linear taper at 10° towards the rear of the tunnel. The average velocity gradient was about 40 ft/sec per foot in the converging

flow region. Heat transfer measurements were made over the forward portion of the plate back to the point of minimum tunnel flow cross-section. These measurements showed that the effect of 6% free stream turbulence on the heat transfer coefficient was not enhanced by accelerating the flow. It is noted that the heat transfer was identical on the top and bottom of the plate, so that an appreciable leading edge disturbance probably did not exist. Hot wire measurements at $y = 0.05"$, $x = 8"$, showed irregular oscillations with no grid present. These had an amplitude of about 3% of the free stream velocity and were probably due to flow oscillations at the juncture of the forward portion of the bump and the tunnel. Since irregular flow oscillation in the boundary layer of magnitude up to 10% did not affect the heat transfer appreciably in the experiments with the sharp leading edge with no pressure gradient (Table 4-1 and Figures 4-2 and 4-4), it is believed that the low level irregular fluctuations of 3% induced by the external flow did not influence the heat transfer results with the pressure gradient.

The results of tests with the hemicylindrical nose, Figures 7-2, 7-3, and 7-4 showed that the effect of 4% free stream turbulence was to cause turbulent heat transfer almost from the leading edge of the heating. In the clear tunnel a dissymmetry existed resulting in an appreciable length of nearly laminar heat transfer on the top of the plate and effectively turbulent heat transfer on the bottom of the plate. The effect of the splitter plate on the hemicylindrical nose was to cause both the top and the bottom of the plate to have an appreciable length of nearly laminar heat transfer.

Several boundary layer mean velocity profile and turbulence measurements were made on the plate with the hemicylindrical nose. These results are given in Table 4-1 and Figure 7-6 and 7-7. The results show that 4% free stream turbulence with the hemicylindrical nose produces a turbulent mean velocity profile. The turbulence level is about 17% of the local velocity at a Reynolds number of about 80,000 and a distance from the wall of $y/\delta = 0.16$. A laminar profile results without the grid, although the velocity fluctuations are as large as 19% of the local velocity at a Reynolds number of 80,000 and a $y/\delta = 0.29$. It was evident from oscilloscope traces, as noted in Table 4-1, that there was considerable qualitative difference between the boundary layer velocity fluctuations with and without free stream turbulence.

The following paragraphs describe the results of supplementary tests on the circular cylinder. The nomenclature for the figures displaying the data is given in Table 7-1.

The results of the heat transfer test on the circular cylinder at twice the temperature difference between the ribbon and the free stream, Figure 4-10, show that the effect of the temperature rise on the data was negligible.

The results of the heat transfer runs with the tail in place on the cylinder, Figure 7-8, show that the effect of the cylinder vortex street on the cylinder heat transfer is negligible.

The results of the tests with the 2" x 1/2" mesh grid, Figure 7-10, show that the effect of the free stream turbulence on the heat transfer is unchanged by increasing the integral scale of the turbulence by a

factor of 2. The results with the .06" x .01" mesh screen, Figure 7-10, show about a 50% increase in the heat transfer coefficient compared with a 20% increase with the 1" grid, both at the same number of grid mesh lengths from the cylinder. Some effect of the screen this close to the cylinder (one inch upstream of the leading edge) may be expected on the mean flow about the cylinder. However, static pressure data did not show an appreciable effect. Thus, it is likely that the smaller scale of the turbulence from the .06" screen as compared with that from the 1" grid is the cause of the enhanced effect on the heat transfer coefficient. It is recalled that the cylinder laminar flow boundary layer thickness for these tests is about 0.02". Thus, a higher percentage of the energy of the turbulence has a scale comparable to the boundary layer thickness.

The results of the tests with the splitter plates, Figure 7-11, show that the presence of the splitter plate attached to the cylinder at the stagnation point reduced the heat transfer. This probably results in part from the finite width of the plate and its emplacement over the heating ribbon. At angles larger than about $\theta = 20^\circ$ there is almost no effect of the splitter plate on the heat transfer either with the clear tunnel or with 6% free stream turbulence.

The results of tests with the rods, wires, and small dimension screens, Figures 7-9 and 7-12 show that local flow disturbances can increase the local heat transfer coefficient by about the same magnitude as does free stream turbulence. These results are further evidence that it is unlikely that variations in the mean flow about the cylinder appreciably contribute to the increased heat transfer.

The results of the static pressure measurements at a Reynolds number of 60,000 with the tail on the cylinder, plotted in Figure 7-15, are significant in that they show that the tail does not appreciably affect the static pressure distribution over the forward portion of the cylinder. Thus, the lack of effect of the tail on the heat transfer cannot be attributed to its influence on the mean flow about the cylinder. Further evidence of the lack of influence of the tail on the mean velocity near the stagnation point was obtained from the hot wire measurements. These data showed no effect of the tail on the mean velocity outside the boundary layer at $\theta = 0°$ with 6% free stream turbulence.

The u', v' and uv correlation results, Table 4-3 obtained with the tail, splitter and tail plus splitter show that in the clear tunnel the tail does not affect the correlation coefficient appreciably, but reduces the u' fluctuations by a factor of about 0.1 at $\theta = 10°$ and 20°, and the v' fluctuations by a factor of about 0.25 at $\theta = 10°$ and a factor of 0.05 at $\theta = 20°$. With the tail and 6% free stream turbulence the correlation coefficient is reduced to about 0.03, while the u' and v' magnitudes are approximately equal to the values without the tail. With the splitter plate and the clear tunnel, the correlation coefficient at $\theta = 10°$ is about -0.5 and at $\theta = 20°$ is about +0.2. The negative value can be attributed to the fixing of the stagnation point by the splitter plate and the subsequent fluctuation in the direction of the streamlines due to the cylinder vortex street. This fixing of the stagnation point by the splitter plate also results in an increase in v' at $\theta = 10°$ by a factor of 10 and a decrease in u' by a factor of 0.5. With 6% free stream turbulence, the values of u' and

v' are not appreciably affected by the splitter plate, but the correlation coefficient at $\theta = 20°$ has a negative value of about -0.1. With the tail and the splitter on the cylinder, and with a clear tunnel, both u' and v' at the location of the X wire are only a few tenths of a percent. The associated correlation coefficients approximate those obtained with the splitter plate alone. With 6% turbulence the correlation coefficients are about the same as those obtained with the splitter plate alone, while the values of u' and v' are about 10% less than those obtained with the cylinder alone.

One primary result of these measurements is that the values of u' and v', with the grid and outside the boundary layer, are approximately equal to their values in the free stream, independent of the influence of the splitter plate or the tail. Thus, the ratios u'/U and v'/U, based upon the local velocity U, increase as the cylinder is approached. These values are about 0.14 and 0.10 respectively at $y/\delta = 4$. A secondary result is the further demonstration that the vortex street of the cylinder causes the velocity fluctuations near the stagnation point with a clear tunnel. Finally, the free stream turbulence effectively reduces the large positive correlation between the u and the v velocity components caused by the cylinder vortex street.

Further evidence of the effect of the tail on the velocity fluctuations near the stagnation point of the cylinder is given in Figures 4-19 and 4-20. These results show the stream-wise fluctuation correlations and magnitudes for $\theta = \pm 10°$. The results without the tail or grid generated free stream turbulence show a correlation coefficient of about -1.0 and a magnitude of $u'/U = 0.11$. With the tail, large reductions of

both these values occur, to about -0.5 and 0.01 respectively. The scatter of the correlation data with the tail is due to slight misalignments of the tail during removal and replacement for the various runs.

Comparison of the heat transfer and the fluctuation data with the tail on the cylinder shows that the type of oscillation induced by the vortex street does not influence the stagnation point heat transfer appreciably. This result compares well with the results of theoretical studies of the effect of free stream or cylinder oscillations on heat transfer, References 4, 5 and 6.

7.2 Plate and Cylinder Conduction Errors

Estimates of the conduction of heat away from the thermocouple junctions by the material of the plate can be made using the simplified representation of Figures 7-14. This figure shows a homogeneous plate with an infinitely thin heat source and heat transfer through only two walls of the control element. This problem has been solved in Reference 32. The solution is:

$$\theta = 2h'\theta_o \sum \frac{\cos \alpha_n y \cosh \alpha_n (a/2 - x)}{\left[(\alpha_n^2 + h'^2)\frac{b}{2} + h'\right] \cos \alpha_n \frac{b}{2} \cosh \alpha_n \frac{a}{2}} \qquad (7\text{-}1)$$

where:

$$\theta = -(T - T_o - \quad) \qquad (7\text{-}2)$$

q = heat generation density.

The boundary conditions are:

$$\begin{aligned} &x = 0 \; ; \quad T = T_o && x = \frac{a}{2} \; ; \quad \frac{\partial T}{\partial x} = 0 \\ &y = 0 \; ; \quad \frac{\partial T}{\partial y} = 0 && y = \frac{b}{2} \; ; \quad k\frac{\partial \theta}{\partial y} + h\theta = 0 \end{aligned} \qquad (7\text{-}3)$$

The α_n are roots of:

$$\tan \alpha \frac{b}{2} = h' \quad \text{for} \quad h' = \frac{h}{k} . \tag{7-4}$$

The solution is obtained as a function of x for the conditions:

$$y = \frac{b}{2} = 0.375"$$

$$k = 3 \times 10^{-5} \frac{\text{BTU}}{\text{sec ft}^2 \text{ °F/ft}} \tag{7-5}$$

$$h = 5 \times 10^{-4} \frac{\text{BTU}}{\text{sec ft}^2 \text{ °F}} \quad \text{(minimum expected for the flat plate)}$$

The roots are

$$\alpha_1 = 21.12 ; \quad \alpha_2 = 105.8 ; \quad \alpha_3 = 203.8 ; \quad \alpha_4 = 303.8$$
$$\alpha_5 = 403.8 ; \quad \alpha_6 = 504.5 . \tag{7-6}$$

Under these conditions, the heat flux at $x = 0$ is:

$$\left(\frac{k\partial\theta}{\partial x}\right)_{x=0} = - 2h'\theta_4 \sum \frac{\cos \alpha_n \; y \sinh \alpha_n (a/2)}{\left[(a_n^2 + h'^2) \frac{b}{2} + h'\right] \cos \alpha_n \frac{b}{2} \cosh \alpha_n \frac{a}{2}} . \tag{7-7}$$

The maximum value occurs for $y = b/2$ so that:

$$\left(h \frac{\partial\theta}{\partial x}\right)_{\substack{\text{average} \\ x=0}} < - 2 \frac{h}{k} \frac{q}{h} = .056q \tag{7-8}$$

The amount of heat transferred from the center section will be proportional to the ratio of the thickness $b/2$ to the length $a/2$. Thus:

$$\left(k \frac{\partial\theta}{\partial x}\right)_{\substack{\text{average} \\ x=0}} < .056q \frac{b}{a} = 0.008q \tag{7-9}$$

Since this is a "worst case" analysis, and the results show that less than 1% of the heat generated at the thermocouple junction is conducted away by the plate, no correction was made for this effect.

The temperature distribution for $y = b/2$ was calculated from Equation (7-1) and is plotted in non-dimensional form in Figure 7-16. This result will be used in Appendix 7.3 Thermocouple Conduction Error.

The average heat transferred out of the control element of Figure 7-14 can be used to estimate the error in determining the heating ribbon surface temperature due to locating the thermocouple beneath the heating ribbon. To do this, consider Figure 7-15. Here it is assumed that no heat flow occurs across the boundaries A or B. The heat generated in the ribbon is q, and the heat flow from the bottom is αq. Thus, the centerline is taken as a heat sink with capacity αq. The value of α can be taken conservatively as 0.008, from the previous result.

The problem is taken as one dimensional with the equation:

$$k_R \frac{\partial^2 T}{\partial y^2} = - Q_R \quad \text{for } Q_R = \text{the heat generated per unit volume in the ribbon} \tag{7-10}$$

The boundary conditions are:

$$\begin{aligned} T &= T_2 \; ; \quad y = y_2 \\ T &= T_3 \; ; \quad y = y_3 \\ q_2 &= h(T_2 - T_o) = -k_R \left(\frac{\partial T}{\partial y}\right)_{y_2} \\ (y_2 - y_3)\, \alpha\, Q_R &= - k_R \left(\frac{\partial T}{\partial y}\right)_{y_3} \end{aligned} \tag{7-11}$$

Integrating and applying the first two conditions yields:

$$T = \frac{Q_R}{2k_R}\left[y_2^2 - y^2 - (y_2 + y_3)(y_2 - y)\right] + T_2\left[1 - \frac{y_2 - y}{y_2 - y_3}\right] + T_3 \frac{y_2 - y}{y_2 - y_3} \tag{7-12}$$

Then:

$$k_R \left(\frac{\partial T}{\partial y}\right)_{y=y_2} = -\frac{Q_R}{2}(y_2 - y_3) + k_R \frac{T_2 - T_3}{y_2 - y_3} = -q_2 \tag{7-13}$$

The heat transferred out of the bottom of the ribbon is:

$$q_3 = -\alpha Q_R (y_2 - y_3) = -k_R \left(\frac{\partial T}{\partial y}\right)_{y_3} = -\frac{Q_R}{2}(y_2 - y_3) - k_R \frac{T_2 - T_3}{y_2 - y_3} \tag{7-14}$$

So:

$$-\alpha Q_R (y_2 - y_3) = -q_2 - 2k_R \frac{T_2 - T_3}{y_2 - y_3}$$

$$= -h(T_2 - T_o) - 2k_R \frac{(T_2 - T_o - (T_3 - T_o))}{y_2 - y_3}$$

Thus:

$$\frac{T_3 - T_o}{T_2 - T_o} = 1 - \frac{Q_R (y_2 - y_3)(1 - 2\alpha)}{2k_R (T_2 - T_o)} \tag{7-15}$$

The numerical values are:

$$Q_R (y_2 - y_3) = 1.4 \times 10^{-2} \frac{\text{BTU}}{\text{sec ft}^2}$$

$$y_2 - y_3 = \frac{.002}{12} = 1.67 \times 10^{-4} \text{ ft}$$

$$k_R = 2 \times 10^{-3} \frac{\text{BTU}}{\text{sec ft}^2 \text{ °F/ft}} \tag{7-16}$$

$$T_2 - T_o = 30°\text{F}$$

So:

$$\frac{T_3 - T_o}{T_2 - T_o} = 1 - .00004 \tag{7-17}$$

Thus, the temperature correction can be considered to be negligible. A similar result can be expected in the case of the circular cylinder.

The cylinder configurations tested, shown in Figure 3-3 have a smaller ratio of b/a. In addition, the value of h is larger by almost an order of magnitude. Both these effects reduce the percentage of heat transferred out the ends of the cylinder. Thus, the loss of heat was treated as negligible in the data reduction for the circular cylinder.

7.3 Thermocouple Conduction Error

This effect will be calculated by treating the thermocouple wire as a heat sink similar to the case of the heated turbine blade discussed in Reference 33. It is presumed that the thermocouple wires lie beneath the heating ribbon from $x = 0$ to $x = a/2$. In this position, they are assumed to experience the temperature distribution near their surface given by Figure 7-16, obtained from Equation (7-1). It will be assumed that the thermocouple temperature at $x = 0$ is T_o. It is further assumed that the heat transfer to the thermocouple wire is equal, at each station x, to the value that would occur for a thin section taken at x, of width dx and of circular dimension extending to infinity. This is sketched in Figure 7-18. There is no temperature dependence on ϕ, and T_b is the temperature occurring for the wire absent, as given by Figure 7-16.

The preceding simplified problem is discussed in a similar form in Reference 33. This discussion is followed below.

The elemental heat transfer around the circumference is:

$$dq_r = - k \frac{dT}{dr} r d\phi \ . \tag{7-18}$$

So:

$$q_r = - 2\pi r k \frac{dT}{dr} = \text{constant radial heat flux} \tag{7-19}$$

and:

$$\frac{-2\pi k T}{q_r} = \ln r + \ln c_1 \ . \tag{7-20}$$

Let

$$T = T_b \ ; \quad r = r_b \ ; \quad \frac{-2\pi k T_b}{q_r} = \ln r_b + \ln c_1 \ ;$$

$$\ln c_1 = \frac{-2\pi k T_b}{q_r} - \ln r_b \tag{7-21}$$

So:

$$T - T_b = \frac{q_r}{-2\pi k} \ln \frac{r}{r_b} \tag{7-22}$$

At any section, x, the heat transfer into the wire is:

$$dQ_w = - q_r dx = \frac{+2\pi k (T_w - T_b)}{\ln \frac{r_w}{r_b}} dx \quad \text{for} \quad r_w = \text{wire radius} \tag{7-23}$$

From Reference 33, the heat transfer equations is:

$$k_w A_w \frac{d^2 T_w}{dx^2} = \frac{dQ_w}{dx} = + \frac{2\pi k (T_w - T_b)}{\ln \frac{r_w}{r_b}} \tag{7-24}$$

Or:

$$\frac{d^2 T_w}{dx^2} = M^2 (T_w - T_b) \quad \text{for} \quad M^2 = \frac{2\pi k}{A k \ln \frac{r_w}{r_b}} \tag{7-25}$$

A conservative estimate of the conduction error can be obtained by approximating the temperature distribution T_b by:

$$T_b = T_o + (T_{b_o} - T_o)(1 - Bx'^3) \text{ for } T_{b_o} = T_b \ (x = 0) \qquad (7\text{-}26)$$

$$B = 1.48.$$

This is shown in non-dimensioanl form in Figure 7-16. Then Equation (7-25) becomes:

$$\frac{d^2T'_w}{dx'^2} = M^2 (T'_w - T'_b) \quad \text{for} \quad T'_w = \frac{T_w - T_o}{T_{b_o} - T_o}$$

$$T'_b = \frac{T_b - T_o}{T_{b_o} - T_o} \qquad (7\text{-}27)$$

$$x' = a/2 - x$$

The solution is:

$$T'_w = C_1 e^{-Mx'} + C_2 e^{+Mx'} + 1 - Bx'^3 - \frac{6Bx'}{M^2} \qquad (7\text{-}28)$$

The boundary conditions are:

$$k \frac{dT'_w}{dx'} = 0 \ ; \quad x' = 0 \qquad (7\text{-}29)$$

$$T'_w = 0 \ ; \quad x' = a/2 \qquad (7\text{-}30)$$

The values of $M \frac{a}{2}$ and thus $e^{M \frac{a}{2}}$ are very large in the present case. Taking advantage of this fact produces the simple result:

$$T'_w = 1 - \frac{6B}{M^3} . \qquad (7\text{-}31)$$

Using:

$$h = 3 \times 10^{-5} \frac{\text{BTU}}{\text{sec ft}^2 \ ^\circ\text{F/ft}} \ ; \quad k_w = 2 \times 10^{-3} \frac{\text{BTU}}{\text{sec ft}^2 \ ^\circ\text{F/ft}}$$

$$r_b = 0.01"$$

gives M = 64.0.

Calculation then yields the ratio of the temperature difference at $x' = 0$ with and without the thermocouple wire present as:

$$T'_w = 0.99993 .$$

This amounts to about 0.001°F and is considered negligible.

A similar result can be expected in the case of the circular cylinder, due to the similarity in construction.

7.4 Alternating Current Heating Error

This section contains an estimate of the maximum temperature fluctuation to be expected in the ribbon as a result of using an alternating current for heating the ribbon. The result shows the maximum temperature difference to be within 1/2% of the average temperature difference. This result holds approximately for both the plate and the cylinder and is considered to have a negligible effect on the heat transfer coefficient.

Consider the length of ribbon shown in Figure 7-17.

The heat generated in an element of volume is:

$$dq = i^2 r \, dv \quad \text{for } r = \text{resistivity per unit volume.} \tag{7-33}$$

Assume no heat is transferred in the x, y or negative z direction. Then all the heat must leave the surface at $z = t$. Also, assume that the ribbon thermal conductivity is so large with respect to the heat convection at $z = t$, that the element is at uniform temperature throughout, although time varying. Assume that r = constant. Then a heat balance yields:

$$\rho c \, wtl \frac{dT}{d\tau} = i^2 \, rwtl - h \, (T - T_o) \, wl \tag{7-34}$$

for τ = time; ρ = ribbon density; c = specific heat

T = temperature; T_o = air temperature;

h = heat transfer coefficient.

The heat transfer coefficient will be a function of time, but it will be assumed constant here as a first approximation.

Let $\theta = T - T_o$, so: (7-35)

$$\rho ct \frac{d\theta}{d\tau} = i^2 rt - h\theta \tag{7-36}$$

$$\frac{d\theta}{d\tau} + \frac{h\theta}{\rho ct} = \frac{i^2 r}{\rho c}$$

Let: $i = i_m \sin \omega\tau$, so:

$$\frac{d\theta}{d\tau} + a_1\theta = b_1 \sin^2 \omega\tau \quad \text{for} \quad a_1 = \frac{h}{\rho ct}, \quad b_1 = \frac{i_m^2 r}{\rho c} \tag{7-37}$$

The solution of (7-37) is:

$$\theta = \left[\frac{b_1}{4 + (\frac{a_1}{\omega})^2}\right]\left[\frac{\sin \omega\tau}{\omega}\left(\frac{a_1}{\omega}(\sin \omega\tau - 2 \cos \omega\tau) + \frac{2}{a_1}(1 - e^{-a_1\tau})\right)\right] \tag{7-38}$$

The steady state solution is:

$$\theta' = \frac{\theta}{\frac{b_1/a_1}{4 + (\frac{a_1}{\omega})^2}} = 2 + \frac{a_1}{\omega} \sin \omega\tau \left(\frac{a_1}{\omega} \sin \omega\tau - 2 \cos \omega\tau\right) \tag{7-39}$$

Averaging over one cycle yields:

$$\theta'_{ave} = \frac{1}{2}\left[4 + \left(\frac{a_1}{\omega}\right)^2\right] . \tag{7-40}$$

The value of θ'_{max} occurs at values of $\omega\tau$ for which $d\theta'/d\omega\tau = 0$.

Taking the derivative and solving for θ'_{max} yields:

$$\frac{\theta_m}{\theta_{ave}} = \frac{2 + \frac{a_1}{\omega}\sin\frac{1}{2}\tan^{-1}\frac{2\omega}{a_1}\left(\frac{a_1}{\omega}\sin\frac{1}{2}\tan^{-1}\frac{2\omega}{a_1} - 2\cos\frac{1}{2}\tan^{-1}\frac{2\omega}{a_1}\right)}{\frac{1}{2}\left[4 + \left(\frac{a_1}{\omega}\right)^2\right]} \tag{7-41}$$

If $\omega \to \infty$: $\frac{\theta_m}{\theta_{ave}} \to 1$; if $f = 60$ cps, then:

$$\frac{\theta_m}{\theta_{ave}} = 0.995 . \tag{7-42}$$

The conclusion is that the maximum temperature difference fluctuation is about 1/2%.

7.5 Thermocouple Resistance Corrections

All the thermocouple readings were corrected for the voltage drop in the thermocouple wires. The resistance of the two wires in series was 48 ohms per foot and the input impedance of the electronic galvonometer driven by the thermocouples was 10^4 ohms. Thus, the corrected thermocouple readings were:

$$\begin{aligned} TC_{corr.} &= 1.096\ T.C. \quad \text{flat plate} \\ TC_{corr.} &= 1.024\ T.C. \quad 3" \text{ cylinder} \\ TC_{corr.} &= 1.106\ T.C. \quad 8" \text{ cylinder} \end{aligned} \tag{7-43}$$

These corrections were applied to all the data.

7.6 Eckert Flat Plate Theory

The Eckert theory for laminar and turbulent flow over a flat plate, Reference 25, is based upon the rigorous expression:

$$q(x) = \int_0^x h(x,\zeta)\left(\frac{d\upsilon_w}{d\zeta}\right) d\zeta + \sum_i h\,(x,\zeta)\left[\upsilon_w\,(\zeta_i^+) - \upsilon_w\,(\zeta_i^-)\right] \qquad (7\text{-}44)$$

where $q(x)$ is the local heat transfer rate at x, $h\,(x,\zeta)$ is the local heat transfer coefficient, υ_w is the difference between the wall temperature and the recovery temperature and ζ is the distance along the plate to the position of the heating. This relation is a direct result of the linearity of the differential equation for the temperature in the boundary layer. The value of $h(x,\zeta)$ is given by:

$$h(x,\zeta) = h_{isothermal}\,[1 - (\zeta/x)^{\alpha}]^{\beta}$$

$$h_{isothermal} = C(k/x)R_{e_x}^{n} P_r^{p} \; ; \quad P_r = \text{Prandtl number} .$$

The relations have been established for some time (Reference 34) and the values of α, β, C, n and p used by Eckert for his numerical calculations are given in Reference 25. His results for stepwise constant heat transfer rate are:

Laminar:
$$N_u(x,\zeta) = \frac{1.600\, P_r^{1/3}\, R_{e_x}^{1/2}}{P(1)-P(\zeta/x)} \; ; \quad P(1) = 3.534 \qquad (7\text{-}45)$$

$$N_u(x) = 0.453\, P_r^{1/3}\, R_{e_x}^{1/2} \; ; \; \zeta/x = 0 . \qquad (7\text{-}46)$$

Turbulent:
$$N_u(x,\zeta) = \frac{0.302\, P_r^{1/3} R_{e_x}^{0.8}}{P(1) - P(\zeta/x)} \; ; \quad P(1) = 9.827 \qquad (7\text{-}47)$$

$$N_u(x) = 0.0308\, P_r^{1/3}\, R_{e_x}^{0.8} \quad ; \quad \zeta/x = 0 \tag{7-48}$$

where

P_r = Prandtl number of fluid

ζ = distance from plate leading edge to start of heating ribbon

The function $P(\zeta/x)$ has been obtained by numerical integration and is tabulated in Reference 25.

For a P_r of 0.70 these are:

Laminar:

$$N_u(x,\zeta) = \frac{1.421\, R_{e_x}^{1/2}}{3.534 - P(\zeta/x)} \tag{7-49}$$

Turbulent:

$$N_u(x,\zeta) = \frac{0.2681\, R_{e_x}^{0.8}}{9.827 - P(\zeta/x)} \tag{7-50}$$

The form of Eckert's theory implies that curves of N_{u_x} versus R_{e_x} for constant ζ/x can be drawn. However, the experimental data were not obtained by fixing a value of ζ/x and varying the free stream velocity and thus the Reynolds number. Rather, the free stream velocity was fixed and data were obtained at several values of x, and thus ζ/x and R_{e_x}. The theory is plotted for the specific experiments performed for direct comparison with the data. This type of plot results in the dependence of the Nusselt number on both U_o and R_{e_x} and the shape of the curves such as shown in Figure 4-2.

In order that a comparison of some of the data with other work be facilitated, the heat transfer data for constant heat transfer can be reduced to the case of a constant temperature flat plate. Following

Reference 25:

$$\upsilon_w(x) = \int_0^x g(x,\zeta)\, q\,(\zeta)\, d\zeta\,, \qquad \upsilon_w = \text{temperature difference between plate and stream}$$

$$q(\zeta) = \text{heat transfer rate} \qquad (7\text{-}51)$$

The value of $g(x,\zeta)$ is:

$$g(x,\zeta) = g^* \left[1 - (\zeta/x)^{\alpha'}\right]^{\beta'} \qquad (7\text{-}52)$$

For constant heat transfer rate:

$$\upsilon_w(x) = g^* x \left[P(1) - P(\zeta/x)\right] \qquad (7\text{-}53)$$

for

$$P(\zeta/x) = \int_0^{\zeta/x} \frac{g(x,\zeta)}{g^*}\, d\left(\frac{\zeta}{x}\right) \qquad (7\text{-}54)$$

for

ζ = start of heating

x = distance from the leading edge.

The $P(\zeta/x)$ are tabulated in Reference 25.

Then:

$$h(x,\zeta)_{\substack{\text{laminar}\\ \text{flow}}} = \frac{q(x,\zeta)}{\upsilon_w(x,\zeta)} = \frac{k}{x}\, \frac{R_{e_x}^{1/2}\, P_r^{1/3}\, 1.600}{\left[P(1)-P(\zeta/x)\right]} \qquad (7\text{-}55)$$

When $\zeta = 0$, $P(1) = 3.534$ so:

$$h(x,\zeta) = \frac{k}{x} R_{e_x}^{1/2}\, P_r^{1/3}\, 0.453. \qquad (7\text{-}56)$$

(It is noted that other calculations give a different constant, e.g., 0.420 from Reference 35.) The correction factor to be applied to the data is:

$$h_{isothermal} = \frac{h(x,\zeta)_{data}}{\frac{1.26}{\left[1 - (\zeta/x)^{3/4}\right]^{1/3}}} \quad \text{Laminar flow.} \tag{7-52}$$

This relation was used to reduce the data plotted in Figure 5-1. It is noted that a similar relation is also developed in Reference 25 for the case of turbulent flow.

7.7 Eckert Circular Cylinder Theory

In the case of the circular cylinder, $\zeta = 0$. Thus, Equation (7-51) becomes:

$$g(x,\zeta) = g^* \tag{7-58}$$

For the circular cylinder Eckert (Reference 25) gives:

$$g^* = \frac{0.776}{k} R_{e_x}^{-1/2} P_r^{-.362} . \tag{7-59}$$

Thus:

$$v_w(x) = qg^*[x][P(1) - P(\zeta/x)]\, x = qg^*(x)\ 2.21\ x \tag{7-60}$$

(from Reference 25).

Then:

$$h(x) = \frac{q}{v(x)} = \frac{1}{2.21 g^*[x]} = \frac{k\, R_{e_x}^{1/2}\, P_r^{0.362}}{2.21\ 0.776\ x} \tag{7-61}$$

Also:

$$h_{isothermal} = 0.583 \frac{k}{x} R_{e_x}^{1/2} P_r^{0.362} \tag{7-62}$$

So:

$$\frac{h}{h_{isothermal}} = 1.0 \text{ , and the heat transfer data can} \tag{7-63}$$

be compared directly with constant temperature theory if desired.

An example of data reduction is as follows:

$$T_o = 544.4$$

$$\Delta T = \mu v/30 = \frac{1.024}{30}(215 - 5) = 7.17$$

$$T = T_o + \Delta T = 551.6$$

$$\frac{T}{T_o} = 1.014$$

$$\left(\frac{T}{T_o}\right)^4 - 1 = 0.058$$

$$q_R = 4.3 \times 10^{-4} \frac{BTU}{ft^2\ sec} \quad \text{for} \quad \epsilon = 0.20$$

$$i = 2.70_{read} + 0.02_{calib} = 2.72 \text{ amp.}$$

$$q = 0.280 \times 10^{-2}\ i^2 \frac{BTU}{ft^2\ sec} = 2.09 \times 10^{-2} \frac{BTU}{ft^2\ sec}$$

$$q_N = 2.05 \times 10^{-2} \frac{BTU}{ft^2\ sec}$$

$$k = 4.23 \times 10^{-6} \frac{BTU}{sec\ ^\circ F\ ft}$$

$$\frac{D}{k} = 5.92 \times 10^5 \left(\frac{BTU}{sec\ ^\circ F}\right)^{-1}$$

$$h = \frac{q_N}{\Delta T} = 2.86 \frac{BTU}{ft^2\ sec\ ^\circ F}$$

$$N_u = \frac{hD}{k} = 170$$

In this case the constant 1.024 is associated with the length of the thermocouple wires used with the 3" cylinder.

7.8 Data Correlation Theory

This section contains a discussion of a solution of the boundary layer momentum and energy equations for the stagnation point flow of the circular cylinder. This solution is based on a form of the equations containing terms dependent upon the turbulent velocity fluctuations in the boundary layer. One constant, required by the theory, is determined from the experimental data. The results, obtained by computer calculation, show good agreement between theory and experiment for both the skin friction and the heat transfer in the vicinity of the stagnation point.

This discussion is divided into three parts 7.8.1 Boundary Layer Equations, 7.8.2 Analysis and 7.8.3 Results.

7.8.1 Boundary Layer Equations

The appropriate incompressible boundary layer equations, taken from Reference 27 are:

$$u \frac{\partial T}{\partial x} + v \frac{\partial T}{\partial y} = \frac{\partial}{\partial y} \left(\kappa \frac{\partial T}{\partial y} + \overline{Lv} \frac{\partial T}{\partial y} \right) \tag{7-64}$$

$$u \frac{\partial u}{\partial x} + v \frac{\partial u}{\partial y} = - \frac{1}{\rho} \frac{\partial \overline{p}}{\partial x} + \frac{\partial}{\partial y} \left(\upsilon \frac{\partial u}{\partial y} + \overline{Lv} \frac{\partial u}{\partial y} \right) \tag{7-65}$$

$$\frac{\partial u}{\partial x} + \frac{\partial v}{\partial y} = 0 \tag{7-66}$$

In these equations, the terms $\overline{Lv} \frac{\partial T}{\partial y}$ and $\overline{Lv} \frac{\partial u}{\partial y}$ represent the effect of the velocity fluctuations in the boundary layer on the temperature and the velocity fields, respectively. The nomenclature is conventional with u, v, T and $\overline{p}$ representing mean values.

7.8.2 Analysis

It is assumed that the turbulent fluctuations in the boundary layer at the stagnation point are proportional to the fluctuations external to the boundary layer and to the distance from the wall. Thus:

$$\overline{Lv} \sim u'y \tag{7-67}$$

Then, a proportionality constant K is defined by:

$$\overline{Lv} = K u'_o U_o y \; ; \qquad u'_o = \frac{u'}{U_o} \tag{7-68}$$

This representation using u' rather than v' is reasonable since u' and v' are approximately equal external to the boundary layer, and at least are proportional.

The classical change of variables, given in Reference 27, can be used with Equations (7-64) through (7-66) to obtain the ordinary differentail equations of the non-dimensional variables, f , η and Θ . The complete equations are:

$$u(\eta) = u_1 f'(\eta)$$

$$v(\eta) = - (\upsilon\beta_1)^{1/2} f(\eta)$$

$$\eta = (\frac{\beta_1}{\upsilon})^{1/2} y$$

$$\sigma = \frac{\upsilon}{\kappa} = 0.72$$

$$\kappa = k/\rho C_p$$

$$u_1 = \beta_1 x = \frac{4U_o x}{D} \text{ for cylinder .}$$

D = cylinder diameter

$$N_{u_D} = \alpha_3 (\sigma) \left(\frac{\beta_1 D^2}{\upsilon} \right)^{1/2}$$

$$\theta(\eta) = \frac{T_w - T(\eta)}{T_w - T_o}$$

$$a' = \frac{K}{2} u_o' R_{e_D}^{1/2}$$

$$\theta'' + \theta' \frac{(f + a')}{(\frac{1}{\sigma} + a'\eta)} = 0$$

$$f'^2 - f'' (f + a') = 1 + (1 + a'\eta) f'''$$

$$\alpha_3 (\sigma, a) = \left[\int_o^\infty \left[e^{-\left(\int_o^\eta \left(\frac{f+a'}{1/\sigma + a'\eta} \right) d\eta \right)} \right] d\eta \right]^{-1}$$

$$\theta(0) = f(0) = f'(0) = 0$$

$$\theta(\infty) = f'(\infty) = 1$$

When $a = 0$, this set of equations reduces to the classical equations given in Reference 27.

The computer calculations were performed by substituting $\eta = 6$ for $\eta = \infty$ in the boundary conditions. The value of $K = 0.164$ was determined as follows. First, the values of 10 for $u_o' \sqrt{R_{e_D}}$ and 0.643 for α_3 were selected from the faired experimental data shown in Figure 5-5. Second, a value of a' was estimated from hand calculations. Third, the value of f'' at the wall was varied until the condition $.9999 < f'(\eta = 6) < 1.0001$ was satisfied. Fourth, the value of α_3 was calculated and used in the test: Is: $(0.99 \cdot 0.643) < \alpha_3 < (1.01 \cdot 0.643)$? Fifth, the values of a' and thus f'' at the wall were varied until the

test was satisfied affirmatively. Sixth, the value of K was calculated from the definition of a'.

Once the value of K was determined, three other values of a' were calculated for selected values of $u_o' \sqrt{R_{e_D}}$. Values of f and its derivatives as well as θ and α_3 were then calculated.

7.8.3 Results

The results of the calculations are shown in Figures 7-19 through 7-22 and in Figure 5-4 in comparison with the experimental data. Figure 7-19 shows that the function $N_{u_D}/\sqrt{R_{e_D}}$ vs $u_o' R_{e_D}$ is linear over the range of the calculations. Figure 5-4 shows that the theory predicts the experimental values of $N_{u_D}/\sqrt{R_{e_D}}$ accurately as a function of $u_o' \sqrt{R_{e_D}}$. The ratio of the slope at the wall of the u velocity profile, $f''(0)$, with and without free stream turbulence, is nearly linear with $u_o' \sqrt{R_{e_D}}$. Figure 7-19 shows that the calculated values are comparable with the two sets of experimental values obtained.

The u and the v velocity profiles are shown in Figures 7-20 and 7-21 for the largest value of $u_o' \sqrt{R_{e_D}}$ used i.e., 28. These are compared with the values calculated for $a' = 0$, which are the same as those calculated by Howarth, (Reference 27).

Figure 7-22 shows the temperature profiles obtained for $a' = 0$ and for $u_o' \sqrt{R_{e_D}} = 28$. These profiles show that the value of $\eta = 6$ chosen to approximate $\eta = \infty$ was not quite large enough to permit an accurate calculation of $\theta(\eta)$ for $u_o' \sqrt{R_{e_D}} = 28$. This approximation does not have a significant effect on the important results of these calculations.

BIBLIOGRAPHY

1. Sugawara, S., and Sato, T., "Heat Transfer on the Surface of a Flat Plate in the Forced Convection," Memoirs of the Faculty of Engineering, Kyoto University, Japan, 14, No. 1, (1952) 21.

2. Edwards, A., and Furber, B. N., "The Influence of Free Stream Turbulence on Heat Transfer by Convection from an Isolated Region of a Plane Surface in Parallel Air Flow," Proc. Inst. Mech. Engin., 170, No. 28, (1956) 941.

3. Wang, Hung-En, The Influence of Free Stream Turbulence on the Local Coefficient of Heat Transfer from a Flat Plate, Ph.D. Thesis, Brown University, Division of Engineering, 1959.

4. Lighthill, M. J., "The Responses of Laminar Skin Friction and Heat Transfer to Fluctuations in the Stream Velocity," Proc. Roy. Soc. London, 224A, (1954) 1.

5. Lin, C. C., "Motion in the Boundary Layer with a Rapidly Oscillating External Flow," 9th International Congress of Applied Mechanics, Brussels, 1956.

6. Moore, F. K., and Ostrach, S., "Average Properties of Compressible Laminar Boundary Layer on Flat Plate with Unsteady Flight Velocity," NACA TN 3886, 1956.

7. Moore, F. K., "Unsteady Laminar Boundary-Layer Flow," NACA TN 2471, 1951.

8. Schmidt, E., and Wenner, K., "Heat Transfer over the Circumference of a Heated Cylinder in Transverse Flow," TM 1050, 1943.

9. Kestin, J., Maeder, P. F., and Sogin, H. H., "The Influence of Turbulence on the Transfer of Heat to Cylinders near the Stagnation Point," Z. Angew. Math. Phys., 12, 1961.

10. Giedt, W. H., "Investigation of Variation of Point Unit Heat Transfer Coefficient Around a Cylinder Normal to an Air Stream," Trans. ASME, 71, (1949) 375.

11. Seban, R. A., "The Effect of Free Stream Turbulence on the Heat Transfer from Cylinders," WADC TR 57-480, 1957.

12. Seban, R. A., "The Influence of Free Stream Turbulence on the Local Heat Transfer from Cylinders," Trans. of the ASME, May 1960.

13. Zapp, G. M., The Effect of Turbulence on Local Heat Transfer Coefficients Around a Cylinder Normal to an Air Stream, Masters Thesis, Oregon State College, Corvallis, Oregon, 1950.

14. Schnautz, J. A., Effect of Turbulence Intensity on Mass Transfer from Plates, Cylinders and Spheres in Air Streams," Ph.D. Thesis, Oregon State College, Chemical Engineering Dept., 1958.

15. Glauert, M. B., "The Laminar Boundary Layer on Oscillating Plates and Cylinders," J. of Fluid Mech., Vol. I, Pt. I, May 1956.

16. Watson, J., "The Two-Dimensional Laminar Flow Near the Stagnation Point of a Cylinder which has an Arbitrary Transverse Motion," Quart. J. Mech. and Appl. Math., Vol. XII, Pt. 2, 1959.

17. Sutera, S. P., Maeder, P. F., and Kestin, J., "On the Sensitivity of Heat Transfer in the Stagnation Point Boundary Layer to Free-Stream Vorticity," J. of Fluid Mech., 16, Pt. 4, Aug. 1963.

18. Dryden, H. L., "Air Flow in the Boundary Layer Near a Plate," NACA Report 562, 1936.

19. Dryden, H. L., Schubauer, G. B., Moch, W. C. Jr., and Skramstad, H. K., "Measurements of Intensity and Scale of Wind Tunnel Turbulence and Their Relation to the Critical Reynolds Number of Spheres," NACA Report 581, 1937.

20. Schubauer, G. B., "Air Flow in the Boundary Layer of an Elliptic Cylinder," NACA Report 652, 1939.

21. Fage, A., and Falkner, V., "The Flow Around a Circular Cylinder," R and M 1369, Feb. 1931.

22. Short, W. W., Brown, R. A. S., and Sage, B. H., "Thermal Transfer in Turbulent Gas Streams. Effect of Turbulence on Local Transport from Spheres," J. of Appl. Mech., Sept. 1960.

23. Schlichting, H., Boundary Layer Theory, McGraw-Hill, 1955.

24. Eckert, E., Hartnett, J., and Birkebak, R., "Calculation of Convection Heat Transfer to Non-Isothermal Surfaces Exposed to a Fluid Stream with Wedge Type Surface Pressure Gradient," WADC Tech. Report, 57-753, July 1958.

25. Reynolds, W. C., Kays, W. M , Kline, S. J., "A Summary of Experiments on Turbulent Heat Transfer from a Non-Isothermal Flat Plate," J. of Heat Transfer, ASME, Nov. 1960.

26. Goldstein, S., Modern Developments in Fluid Mechanics, Oxford Press, 1957.

27. Fage, A., and Falkner, V., "The Flow Around a Circular Cylinder," R and M 1369, 1931.

28. Thom, A., "The Boundary Layer of the Front Portion of a Cylinder," R and M 1176, 1928.

29. Kuethe, A. M., and Schetzer, J. D., Foundations of Aerodynamics, Wiley, 1950.

30. Gazley, C., "Boundary Layer Stability and Transition in Subsonic and Supersonic Flow, J.A.S., 20, No. 1, 1953.

31. Sternberg, J., "A Theory for the Viscous Sublayer of a Turbulent Flow," J. of Fluid Mech., 13, p. 241.

32. Carslow, H., and Jaeger, J., Conduction of Heat in Solids, Oxford University Press, 1959.

33. Schneider, P. J., Conduction Heat Transfer, Addison Co., 1955.

34. Chapman, D. R., and Rubesin, M. W., "Temperature and Velocity Profiles in the Compressible Laminar Boundary Layer with Arbitrary Distribution of Surface Temperature," J.A.S., Sept. 1949.

35. Klein, J., and Tribus, M., "Forced Convection from Non-Isothermal Surfaces," Heat Transfer Symposium, Engr. Res., Inst., U. of Michigan, Aug. 1952.

36. Green, J. J., "Viscous Layer Associated with a Circular Cylinder," R and M 1313, April 1930.

37. Piercy, N., Richardson, E., and Winny, H., "On the Convection of Heat from a Wire Moving Through Air Close to a Cooling Surface," Proc. Phys. Soc. London, 69, Sect. B., (1956) 731.

TABLE 1-1

SYMBOLS

English Alphabet

e, de	Voltage across hot wire
f	Frequency
h_d	Heat transfer coefficient from data
i	Heating current
k	Thermal conductivity
n	Frequency
q	Net heating power
u	Streamwise velocity fluctuation
v	Velocity fluctuation normal to the streamwise direction and lying in a plane either normal to the plate or normal to the axis of the cylinder.
u'	$\sqrt{\overline{u^2}}$
u'_o	$\sqrt{\overline{u^2}}/U_o$
v'	$\sqrt{\overline{v^2}}$
x	Streamwise direction
y	Normal to the streamwise direction and to the surface of the body
A	Correlation constant
B	Correlation constant
C_l	Thermocouple reading correction factor
C_p	Pressure coefficient
D	Cylinder diameter
E	Spectral density

TABLE 1-1 (CONT'D)

H	Dynamic head
K	Hot wire sensitivity
N_{u_D}	Local cylinder Nusselt number
N_{u_x}	Local flat plate Nusselt number
Q_R	Ribbon heating power
R_{e_x}	Reynolds number based upon distance x
R_{e_D}	Reynolds number based upon cylinder diameter
R_{uv}	Correlation coefficient for u , v fluctuations
S	Strouhal number
T	Temperature
U_o	Mean free stream velocity
U	Mean local streamwise velocity
U_g	Mean local streamwise velocity with grid in tunnel
U_c	Mean local streamwise velocity in clear tunnel

Greek Alphabet

α_i	Coefficients in calculating correlations
α	Angle of flow to the direction of the surface
δ	Boundary layer thickness
ϵ	Emissivity of heating ribbon
θ	Angle around cylinder from forward stagnation point
μ	Viscosity of fluid
μv	Thermocouple output in microvolts
υ	Kinematic viscosity of fluid
σ	Stephan-Boltzman Constant

TABLE 1-1 (CONT'D)

Subscripts

c	Clear tunnel
d	Data
D	Cylinder
g	With grid in tunnel
N	Convective heat transferred
o	Free stream
R	Radiant heat
x	Distance from leading edge of flat plate

NOTE: Symbols defined in the appendix are not listed here.

TABLE 4-1

FLAT PLATE MEAN VELOCITY AND VELOCITY FLUCTUATION DATA

Figure	Symbol	Free Stream Speed, U_o	Configuration	Probe Location x	Probe Location y	Reynolds Number, R_{e_x}	Flow Condition	Boundary Layer Thickness δ_{theory}	Boundary Layer Thickness approx. δ_{data}	Hot Wire y/δ_{test}	$\frac{U}{U_o}$ test	$\frac{u'}{U}$	Experimental Equipment	Comments
7-6	⊙	20.1 l/sec	hemicylindrical nose	8.1"	-	82,000	clear	$\delta_{lam.} = 0.159"$ $\delta_{turb.} = 0.294"$	$\delta_d = 0.160"$	-	-	-	hot wire mean velocity probe	
7-7	●	20.6 l/sec	hemicylindrical nose	8.1"	-	84,900	1" grid @ 20"	$\delta_{lam.} = 0.159"$ $\delta_{turb.} = 0.294"$	$\delta_d = 0.300"$	-	-	-	hot wire mean velocity probe	
7-6	◈	20.1 l/sec	hemicylindrical nose	8.1"	-	82,000	clear	$\delta_{lam.} = 0.159"$ $\delta_{turb.} = 0.294"$	$\delta_d = 0.160"$	-	-	-	hot wire mean velocity probe	
-	+	20.2 l/sec	hemicylindrical nose	8.1"	0.047"	82,200	clear	-	-	0.290	0.53	.198	hot wire bug	
-	-	20.2 l/sec	hemicylindrical nose	8.1"	0.047"	82,200	1" grid @ 20"	-	-	0.156	0.73	.167	hot wire bug	scope trace: turbulent fluctuations
-	-	20.5 l/sec	hemicylindrical nose	8.1"	0.047"	83,500	clear	-	-	0.290	0.53	.194	hot wire bug	scope trace: irregular non-turbulent fluctuations
-	-	20.8 l/sec	hemicylindrical nose	8.1"	0.047"	84,500	1" grid @ 20"	-	-	0.156	0.73	.167	hot wire bug	
-	-	20.2 l/sec	hemicylindrical nose	3.6"	0.047"	36,500	1" grid @ 20"	$\delta_{turb.} = 0.153"$	-	0.307*	0.83	.107	hot wire bug	
-	-	20.2 l/sec	hemicylindrical nose	3.6"	0.047"	36,500	clear	$\delta_{lam.} = 0.106"$	-	0.444*	0.76	.0095	hot wire bug	scope trace: irregular non-turbulent fluctuations
-	-	20.1 l/sec	sharp nose	12.4"	0.047"	126,000	clear	$\delta_{turb.} = 0.199"$	-	0.235	0.38	.0038	hot wire bug	
-	-	20.1 l/sec	sharp nose	12.4"	0.047"	126,000	1" grid @ 15-1/2"	$\delta_{turb.} = 0.415"$	-	0.196	0.49	.261	hot wire bug	scope trace: irregular non-turbulent fluctuations
-	-	40.1 l/sec	sharp nose	12.4"	0.047"	251,000	1" grid @ 15-1/2"	$\delta_{turb.} = 0.477"$	-	0.099*	0.69*	.109	hot wire bug	scope trace: steady turbulent fluctuations
-	-	20.1 l/sec	sharp nose	7.9"	0.047"	80,300	1" grid @ 15-1/2"	$\delta_{lam.} = 0.164"$	-	0.286*	0.53*	.195	hot wire bug	scope trace: irregular non-turbulent fluctuations
4-6	○	20.8 l/sec	sharp nose	12.4"		130,000	clear	$\delta_{lam.} = 0.199"$	$\delta_d = 0.200"$	-	-	-	hot wire mean velocity probe	
4-6	●	20.5 l/sec	sharp nose	12.4"		129,000	1" grid @ 15-1/2"	$\delta_{turb.} = 0.415"$	$\delta_d = 0.240$	-	-	-	hot wire mean velocity probe	

* theory

TABLE 4-2

CYLINDER NUSSELT NUMBER DATA

Units and Factors for Table 4-2

	θ	μv_c	ΔT	q_R	q_N	h	N_{u_D}	$\frac{N_{u_D}}{\sqrt{Re_D}^{1/2}}$
Units	degrees	micro-volts	°R	$\frac{BTU}{sec\ ft^2}$	$\frac{BTU}{sec\ ft^2}$	$\frac{BTU}{sec\ ft^2\ °R}$	dimension-less	dimension-less
Factors	x1	x1	x1	$x10^{-3}$	x1	$x10^{-3}$	x1	x1

Note: Each number in the table should be multiplied by the appropriate factor.

4-2a R = 60,000; i = 4.13 amperes; T_o = 494°R; x = clear tunnel

80	1732	57.7	3.30	.0444	.769	132	.539
60	1154	38.5	2.03	.0457	1.187	205	.837
40	1043	34.8	1.85	.0459	1.319	227	.926
20	1020	34.0	1.85	.0459	1.350	233	.951
10	1004	33.5	1.79	.0459	1.370	236	.963
0	1004	33.5	1.79	.0459	1.370	236	.963
-10	1004	33.5	1.79	.0459	1.370	236	.963
-20	1020	34.0	1.85	.0459	1.350	233	.951
-40	1061	35.4	1.85	.0459	1.297	224	.914
-60	1072	35.7	1.90	.0458	1.283	221	.902
-80	1844	61.5	3.15	.0445	.724	125	.510

4-2b R = 120,000; i = 4.92 amperes; T_o = 494°R; x = clear tunnel

80	2160	72.0	3.22	.0646	.897	155	.447
60	1154	38.5	2.03	.0658	1.709	295	.851
40	1042	34.7	1.85	.0660	1.902	329	.959
20	1005	33.5	1.78	.0660	1.970	340	.981
10	988	32.9	1.75	.0660	2.006	346	.998
0	977	32.6	1.75	.0660	2.024	349	1.007
-10	977	32.6	1.75	.0660	2.024	349	1.007
-20	998	33.3	1.75	.0660	1.981	342	.987
-40	1048	34.9	1.85	.0660	1.891	327	.944
-60	1142	38.1	2.03	.0658	1.727	298	.860
-80	2060	68.6	3.20	.0646	.942	162	.468

4-2c R_{eD}= 240,000; i = 5.87 amperes; T_o = 494°R; x = clear tunnel

80	2202	73.4	3.22	.0933	1.271	2.9	.447
60	1152	38.4	2.03	.0945	2.461	425	.867
40	1057	35.2	1.85	.0947	2.690	464	.947
20	1017	33.9	1.78	.0947	2.794	482	.984
10	1001	33.4	1.75	.0947	2.835	489	.998
0	979	32.6	1.75	.0947	2.905	501	1.022
-10	979	32.6	1.75	.0947	2.905	501	1.022
-20	1006	33.5	1.78	.0947	2.827	489	.998
-40	1062	35.4	1.85	.0947	2.675	462	.943
-60	1175	39.2	2.09	.0944	2.408	416	.849
-80	2115	70.5	3.21	.0933	1.323	228	.465

4-2d R_{eD}= 60,000; i = 4.67 amperes; T_o = 490°R; x = 15-1/2 inches

80	1554	51.8	2.72	.0584	1.127	195	.796
60	1177	39.2	1.95	.0591	1.508	261	1.065
40	1053	35.1	1.73	.0594	1.692	293	1.196
20	982	32.7	1.63	.0595	1.820	316	1.290
10	970	32.3	1.58	.0595	1.742	319	1.302
0	970	32.3	1.58	.0595	1.842	319	1.302
-10	994	33.1	1.63	.0595	1.800	312	1.273
-20	1024	34.1	1.68	.0594	1.742	302	1.232
-40	1099	36.6	1.84	.0593	1.620	281	1.147
-60	1224	40.8	2.06	.0590	1.446	251	1.024
-80	1658	55.3	3.09	.0580	1.049	182	.743

4-2e R_{eD} = 120,000; i = 6.23 amperes; T_o = 490°R; x = 15-1/2 inches

80	1558	51.9	2.72	.1060	2.042	354	1.022
60	1360	45.3	2.34	.1053	2.349	407	1.175
40	1150	38.3	1.90	.1068	2.788	484	1.397
20	1128	37.5	1.90	.1068	2.848	494	1.426
10	1078	35.9	1.90	.1068	2.978	516	1.489
0	1068	35.6	1.80	.1069	3.002	520	1.501
-10	1068	35.6	1.84	.1069	3.003	520	1.501
-20	1106	36.9	1.84	.1069	2.897	503	1.452
-40	1150	38.3	1.90	.1068	2.788	484	1.397
-60	1420	47.3	2.45	.1063	2.247	390	1.126
-80	1718	57.3	2.99	.1057	1.856	320	.924

4-2f R_{eD} = 240,000; i = 5.90 amperes; T_o = 490°R; x = 15-1/2 inches

80	950	31.7	1.58	.0959	3.025	515	1.051
60	797	26.6	1.31	.0962	3.616	627	1.280
40	713	238	1.15	.0963	4.046	702	1.433
20	658	21.9	1.05	.0965	4.406	764	1.559
10	643	21.4	1.00	.0965	4.509	782	1.596
0	598	19.9	.952	.0965	4.849	836	1.706
-10	621	20.7	1.00	.0965	4.662	808	1.649
-20	664	22.1	1.05	.0965	4.366	757	1.545
-40	736	24.5	1.15	.0963	3.931	682	1.392
-60	817	27.2	1.31	.0962	3.537	614	1.253
-80	993	33.1	1.63	.0959	2.897	503	1.027

4-2g R_{eD} = 60,000; i = 4.68 amperes; T_o = 490°R; x = 24 inches

80	1800	60.0	3.44	.0579	.965	164	.669
60	1100	36.7	2.97	.0583	1.588	271	1.106
40	1041	34.7	1.87	.0594	1.711	292	1.192
20	992	33.1	1.70	.0596	1.801	307	1.253
10	978	32.6	1.70	.0596	1.828	312	1.275
0	970	32.3	1.70	.0596	1.845	314	1.282
-10	982	32.7	1.72	.0596	1.823	311	1.270
-20	996	33.2	1.72	.0596	1.795	306	1.249
-40	1014	33.8	1.78	.0595	1.760	300	1.225
-60	1100	36.7	2.97	.0583	1.588	271	1.106
-80	1800	60.0	3.44	.0579	.965	164	.669

4-2h R_{eD} = 120,000; i = 5.66 amperes; T_o = 490°R; x = 24 inches

80	1377	45.9	2.54	.0872	1.900	324	.935
60	1105	36.8	1.97	.0877	2.383	407	1.175
40	1042	34.7	1.91	.0878	2.530	432	1.247
20	1000	33.3	1.72	.0880	2.643	451	1.302
10	986	32.9	1.72	.0880	2.674	457	1.319
0	986	32.9	1.72	.0880	2.674	457	1.319
-10	996	33.2	1.72	.0880	2.651	453	1.308
-20	1025	34.2	1.81	.0879	2.570	439	1.267
-40	1087	36.2	1.91	.0878	2.425	414	1.195
-60	1148	38.3	2.05	.0877	2.290	391	1.129
-80	1486	49.5	2.79	.0869	1.756	300	.866

4-2i R_{eD} = 240,000; i = 7.12 amperes; T_o = 497°R; x = 24 inches

80	1360	45.3	2.42	.1394	3.077	524	1.069
60	1150	38.3	2.00	.1398	3.650	622	1.270
40	1050	35.0	1.81	.1400	4.000	682	1.392
20	1028	34.3	1.73	.1401	4.084	696	1.420
10	1017	33.9	1.73	.1401	4.133	704	1.437
0	1012	33.7	1.73	.1401	4.157	708	1.445
-10	1028	34.3	1.73	.1401	4.084	696	1.420
-20	1055	35.2	1.81	.1400	3.977	677	1.382
-40	1040	34.7	1.81	.1400	4.034	687	1.402
-60	1128	37.9	2.00	.1398	3.689	628	1.282
-80	1360	45.3	2.42	.1394	3.077	524	1.069

4-2j R_{eD} = 60,000; i = 4.47 amperes; T_o = 495°R; x = 38 inches

80	2040	68.0	3.98	.0519	.763	130	.531
60	1130	37.7	2.04	.0539	1.423	243	.992
40	1060	35.3	1.86	.0540	1.530	261	1.065
20	1012	33.7	1.78	.0541	1.605	274	1.118
10	1000	33.3	1.78	.0541	1.625	277	1.131
0	987	32.9	1.78	.0541	1.644	280	1.143
-10	1000	33.3	1.78	.0541	1.625	277	1.131
-20	1017	33.9	1.78	.0541	1.596	272	1.110
-40	1078	38.6	1.91	.0540	1.517	259	1.057
-60	1152	38.4	2.-4	.0539	1.404	239	.976
-80	2045	68.2	3.98	.0519	.761	130	.531

4-2k R_{eD} = 120,000; i = 4.53 amperes; T_o = 513°R; x = 38 inches

80	1032	34.4	1.93	.0555	1.613	268	.774
60	758	25.3	1.40	.0560	2.213	368	1.062
40	672	22,4	k,22	,9562	2,598	4k6	k,294
20	638	21.3	1.16	.0562	2.638	439	1.267
10	630	21.0	1.16	.0562	2.676	445	1.285
0	625	20.8	1.16	.0562	2.702	449	1.296
-10	636	21.2	1.16	.0562	2.651	441	1.273
-20	647	21.5	1.22	.0562	2.614	435	1.256
-40	698	23.3	1.28	.0561	2.408	400	1.155
-60	778	25.9	1.46	.0559	2.158	359	1.036
-80	1052	35.1	2.00	.0554	1.578	262	.756

4-2ℓ R_{eD} = 240,000; i = 6.65 amperes; T_o = 497°R; x = 38 inches

80	1292	43.1	2.36	.1214	2.817	481	.982
60	1102	36.7	1.97	.1218	3.319	567	1.157
40	1013	33.8	1.81	.1220	3.609	616	1.257
20	948	31.6	1.68	.1221	3.864	660	1.347
10	930	31.0	1.61	.1222	3.942	673	1.374
0	920	30.7	1.61	.1222	3.980	680	1.388
-10	908	30.3	1.58	.1222	4.033	689	1.406
-20	954	31.8	1.68	.1221	3.840	656	1.339
-40	1034	34.5	1.81	.1220	3.536	604	1.233
-60	1087	36.2	1.90	.1219	3.367	575	1.174
-80	1290	43.0	2.36	.1214	2.823	482	.984

4-2m R_{eD} = 30,000; i = 2.74 amperes; T_o = 544°R; x = clear tunnel

40	230	7.68	.43	.0206	2.68	158	.912
5	215	7.16	.43	.0206	2.88	170	.982
0	215	7.16	.43	.0206	2.88	170	.982
-5	215	7.16	.43	.0206	2.88	170	.982
-10	215	7.16	.43	.0206	2.88	170	.982
-20	215	7.16	.43	.0206	2.88	170	.982
-40	225	7.50	.43	.0206	2.75	162	.935

4-2n R_{eD} = 60,000; i = 3.34 amperes; T_o = 544°R; x = clear tunnel

40	225	7.51	.43	.0308	4.10	243	.992
5	215	7.16	.43	.0308	4.30	255	1.041
0	215	7.16	.43	.0308	4.30	255	1.041
-5	215	7.16	.43	.0308	4.30	255	1.041
-10	215	7.16	.43	.0308	4.30	255	1.041
-20	220	7.35	.43	.0308	4.19	248	1.012
-40	230	7.68	.43	.0308	4.01	238	.972

4-2o R_{eD} = 30,000; i = 2.76 amperes; T_o = 544°R; x = 15-1/2 inches

40	200	6.65	.35	.0209	3.14	186	1.074
5	180	5.97	.35	.0209	3.50	208	1.201
0	180	5.97	.35	.0209	3.50	208	1.201
-5	180	5.97	.35	.0209	3.50	208	1.201
-10	180	5.97	.35	.0209	3.50	208	1.201
-20	180	5.97	.35	.0209	3.50	208	1.201
-40	195	6.48	.35	.0209	3.22	192	1.109

4-2p R_{eD} = 60,000; i = 3.39 amperes; T_o = 537°R; x = 15-1/2 inches

40	195	6.49	.35	.0318	4.90	288	1.176
5	175	5.83	.35	.0318	5.45	320	1.306
0	175	5.83	.35	.0318	5.45	320	1.306
-5	180	5.99	.35	.0318	5.31	312	1.274
-10	180	5.99	.35	.0318	5.31	312	1.274
-20	180	5.99	.35	.0318	5.31	312	1.274
-40	195	6.49	.35	.0318	4.90	288	1.176

4-2q R_{eD} = 30,000; i = 2.74 amperes; T_o = 537°R; x = 24 inches

40	215	7.16	.42	.0206	2.88	171	.987
5	195	6.48	.42	.0206	3.18	189	1.091
0	195	6.48	.42	.0206	3.18	189	1.091
-5	195	6.48	.42	.0206	3.18	189	1.091
-10	195	6.48	.42	.0206	3.18	189	1.091
-20	200	6.65	.42	.0206	3.10	184	1.062
-40	215	7.16	.42	.0206	2.88	171	.987

4-2r R_{eD} = 60,000; i = 3.21 amperes; T_o = 537°R; x = 24 inches

40	185	6.15	.42	.0284	4.62	270	1.102
5	170	5.63	.42	.0284	5.04	295	1.204
0	170	5.63	.42	.0284	5.04	295	1.204
-5	170	5.63	.42	.0284	5.04	295	1.204
-10	170	5.63	.42	.0284	5.04	295	1.204
-20	170	5.63	.42	.0284	5.04	295	1.204
-40	185	6.15	.42	.0284	4.62	270	1.102

4-2s R_{eD} = 30,000; i = 2.76 amperes; T_o = 536°R; x = 38 inches

40	215	7.16	.42	.0209	2.92	175	1.010
5	205	6.82	.42	.0209	3.06	184	1.062
0	205	6.82	.42	.0209	3.06	184	1.062
-5	205	6.82	.42	.0209	3.06	184	1.062
-10	205	6.82	.42	.0209	3.06	184	1.062
-20	210	7.00	.42	.0209	2.98	179	1.034
-40	220	7.32	.42	.0209	2.86	172	.993

4-2t R_{eD} = 60,000; i = 3.22 amperes; T_o = 536°R; x = 38 inches

40	210	6.99	.42	.0286	4.09	238	.972
5	190	6.30	.42	.0286	4.54	264	1.078
0	190	6.30	.42	.0286	4.54	264	1.078
-5	190	6.30	.42	.0286	4.54	264	1.078
-10	185	6.13	.42	.0286	4.66	271	1.106
-20	190	6.30	.42	.0286	4.54	264	1.078
-40	200	6.65	.42	.0286	4.30	250	1.020

TABLE 4-3

CYLINDER X WIRE DATA

		$\frac{u'}{U}$	$\frac{u'}{U}$	$\frac{v'}{U}$	$\frac{v'}{U}$	R_{uv}	R_{uv}	$\frac{u'}{U_\theta}$	$\frac{u'}{U_\theta}$	$\frac{v'}{U_o}$	$\frac{v'}{U_o}$	Free Stream	
	θ =	20°	10°	20°	10°	20°	10°	20°	10°	20°	10°	$\frac{u'}{U_o}$	$\frac{v'}{U_o}$
Cylinder	Clear	.047	.070	.0028	.0074	.25	.75						
		.050	.072	.0043	.0087	.39	.75						
		.048	.072	.0046	.0078	1.10	.77						
	ave.	.048	.071	.0039	.0080	.58	.76	.032	.036	.0026	.0041	.001	.00053
Cylinder	Grid	.094	.139	.080	.125	.084	.17						
		.086	.136	.071	.125	.051	.14						
		.093	.135	.081	.120	.091	.14						
	ave.	.091	.137	.077	.123	.075	.15	.060	.070	.051	.063	.0574	.0495
Cylinder & Tail	Clear	.0074	.012	.00076	.0022	1.01	.90						
		.0072	.013	.00068	.0020	1.03	.72						
		.0069	.013	.00088	.0019	.72	.91						
	ave.	.0072	.013	.00077	.0020	.92	.84	.0047	.0065	.00051	.0010	.001	.00053
Cylinder & Tail	Grid	.095	.139	.092	.138	.10	-.010						
		.076	.139	.074	.138	.13	.043						
		.083	.138	.082	.137	.20	.060						
	ave.	.085	.139	.083	.138	.14	.031	.056	.071	.055	.070	.0574	.0495
Cylinder & Splitter	Clear	.036	.034	.0035	.086	.23	-.54						
		.037	.032	.0021	.077	.26	-.59						
		.036	.043	.0033	.074	.10	-.26						
	ave.	.036	.036	.0030	.079	.20	-.46	.024	.018	.0020	.040		
Cylinder & Splitter	Grid	.082	.110	.071	.093	-.060	-.58						
		.087	.120	.075	.110	-.080	-.69						
		.086	.125	.074	.104	-.13	-.47						
	ave.	.085	.118	.073	.102	-.090	-.58	.056	.060	.048	0.52		
Cylinder, Tail & Splitter	Clear	.0041	.0072	.00053	.0063	.060	-.55						
		.0044	.0060	.00053	.0054	-.14	-.78						
		.0044	.0059	.00053	.0054	.21	-.72						
	ave.	.0043	.0064	.00053	.0057	.043	-.68	.0028	.0032	.00035	.0029		
Cylinder, Tail & Splitter	Grid	.080	.117	.072	.089	.020	-.44						
		.082	.105	.074	.078	.020	-.60						
		.081	.110	.074	.080	.040	-.56						
	ave.	.081	.111	.073	.082	.027	-.53	.054	.057	.048	.042		

TABLE 7-1

SUPPLEMENTARY CYLINDER HEAT TRANSFER TESTS, Re_D = 30,000

Figure	Symbol	Configuration	Tunnel	Comments
7-8	⊕	cylinder and tail	clear	
	⊡	cylinder	std. grid	all cylinder - std.
	●	cylinder and tail	std. grid	grid runs listed are separate runs
7-9	▲	cylinder, screen 1" wide @ θ = 0°; y = 1"	clear	screen centered; 12" long
	⊡	cylinder	std. grid	
	◈	cylinder; 0.003" dia wire @ y = 0.06"	clear	wire centered approx.
7-10	⊙	cylinder	screen @ y = 1"	this screen has the dimensions of the tunnel crossection
	▲	cylinder	large grid	
	⊡	cylinder	std. grid	
	■	cylinder	std. grid	
	⊖	cylinder	screen @ 5-3/4"	
	⊙	cylinder	screen @ 15"	
7-11	⊡	cylinder & 1/32" x 1/4" splitter	std. grid	
	■	cylinder & 1/16" x 1/2" splitter	std. grid	
	◈	cylinder & 1/32" x 1/4" splitter	clear	
	◆	cylinder & 1/16" x 1/2" splitter	clear	
7-12	◆	cylinder; 3/16" wide screen @ θ = -20°; y = 1"	clear	the 3/16" wide screen is composed of a three wire strip of the window screen, 12" long.
	⊙	cylinder; 0.03" dia wire @ θ = 0°; y = 0.75"	clear	
	◈	cylinder; 3/16" wide screen @ θ = 20°; y = 1"	clear	
	▲	cylinder; 1/8" dowel @ θ = 0°, y = 0.75"	clear	

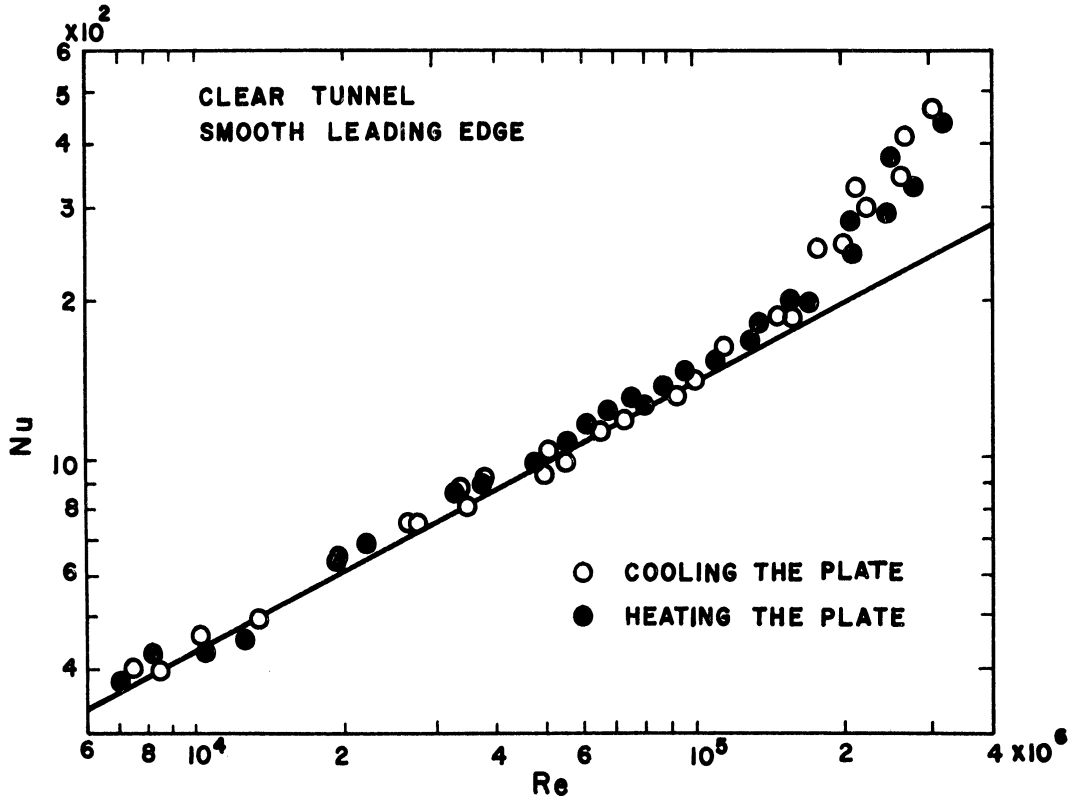

Figure 2-1. Laminar Heat Transfer From Sugawara and Sato.

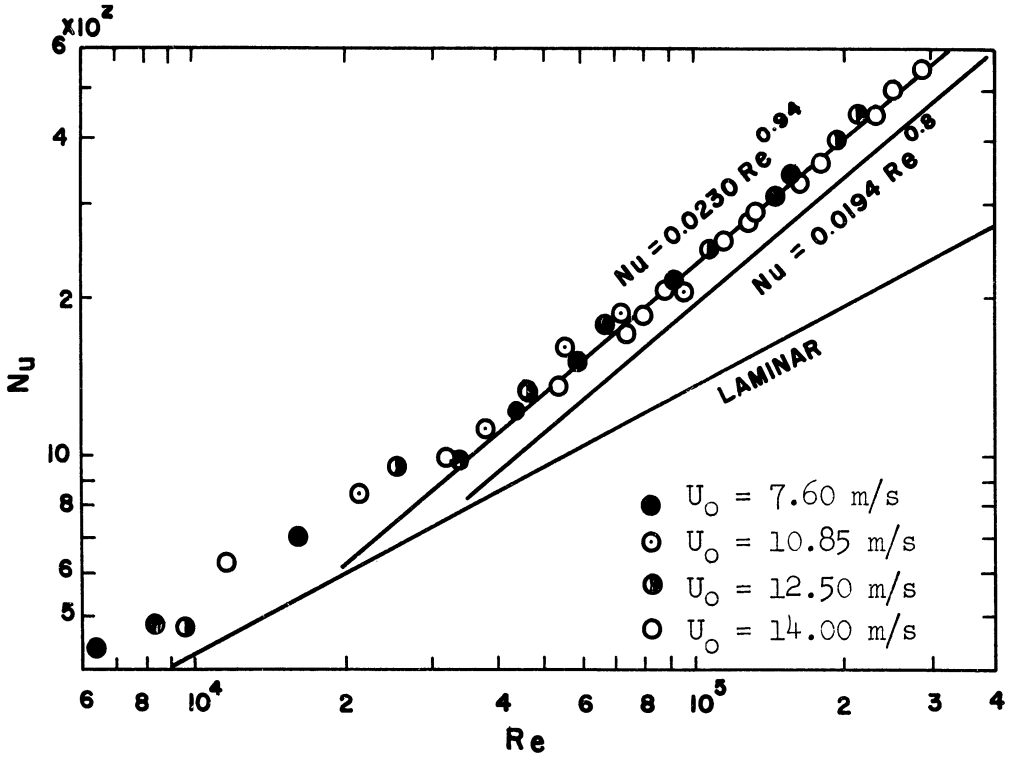

Figure 2-2. Turbulent Heat Transfer with Grid and Blunt Leading Edge.

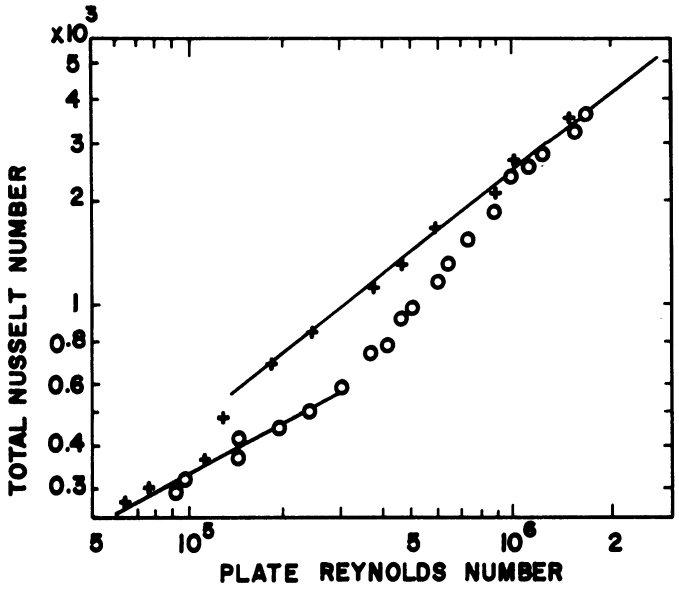

o No Turbulence Grid

+ Grid 2 $\bar{U}/U$ = 5.0 Per Cent

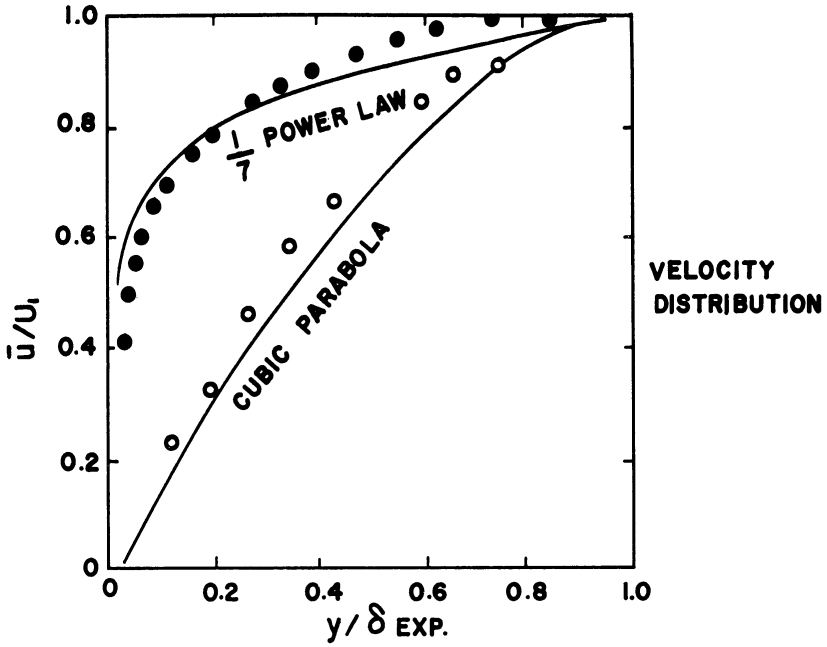

o 1.07 x 10^5 No Grid

● 2.03 x 10^5 Grid 5% Turbulence

Figure 2-3. Edwards and Furbers Results.

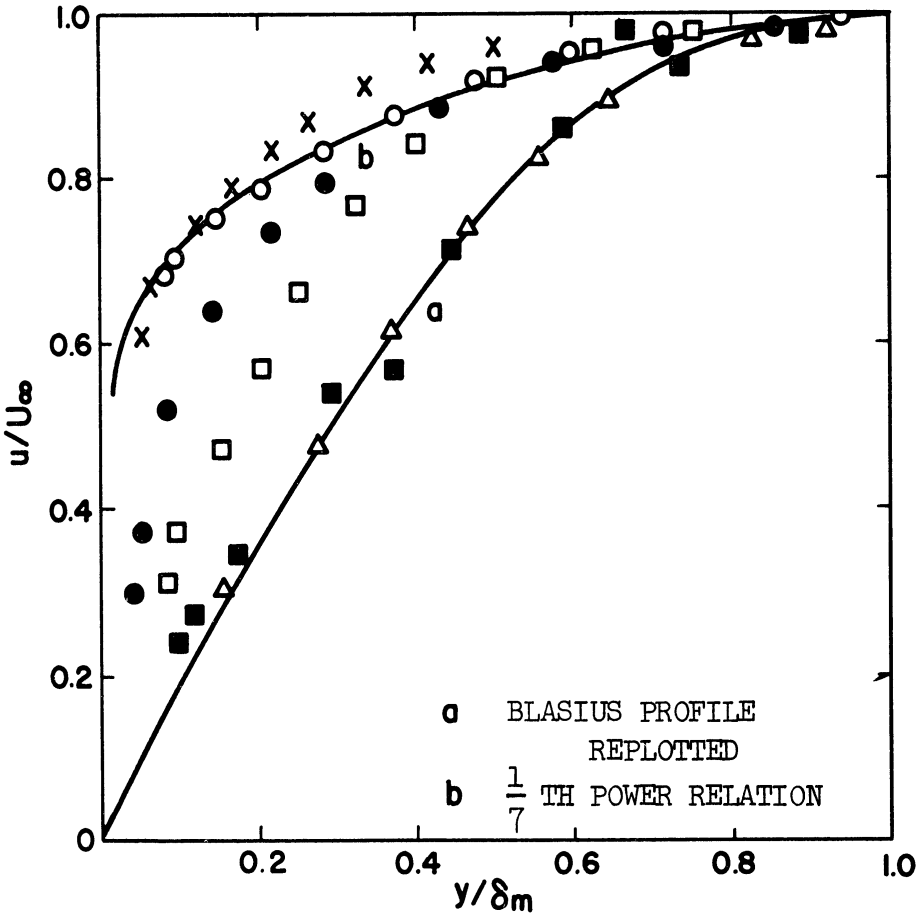

O	Re	=	289,000	with Screen
X	Re	=	552,000	no Screen
●	Re	=	123,000	with Screen
□	Re	=	247,000	no Screen
■	Re	=	42,900	with Screen
△	Re	=	123,000	no Screen

Figure 2-4. Velocity Profiles in Boundary Layer (Wang).

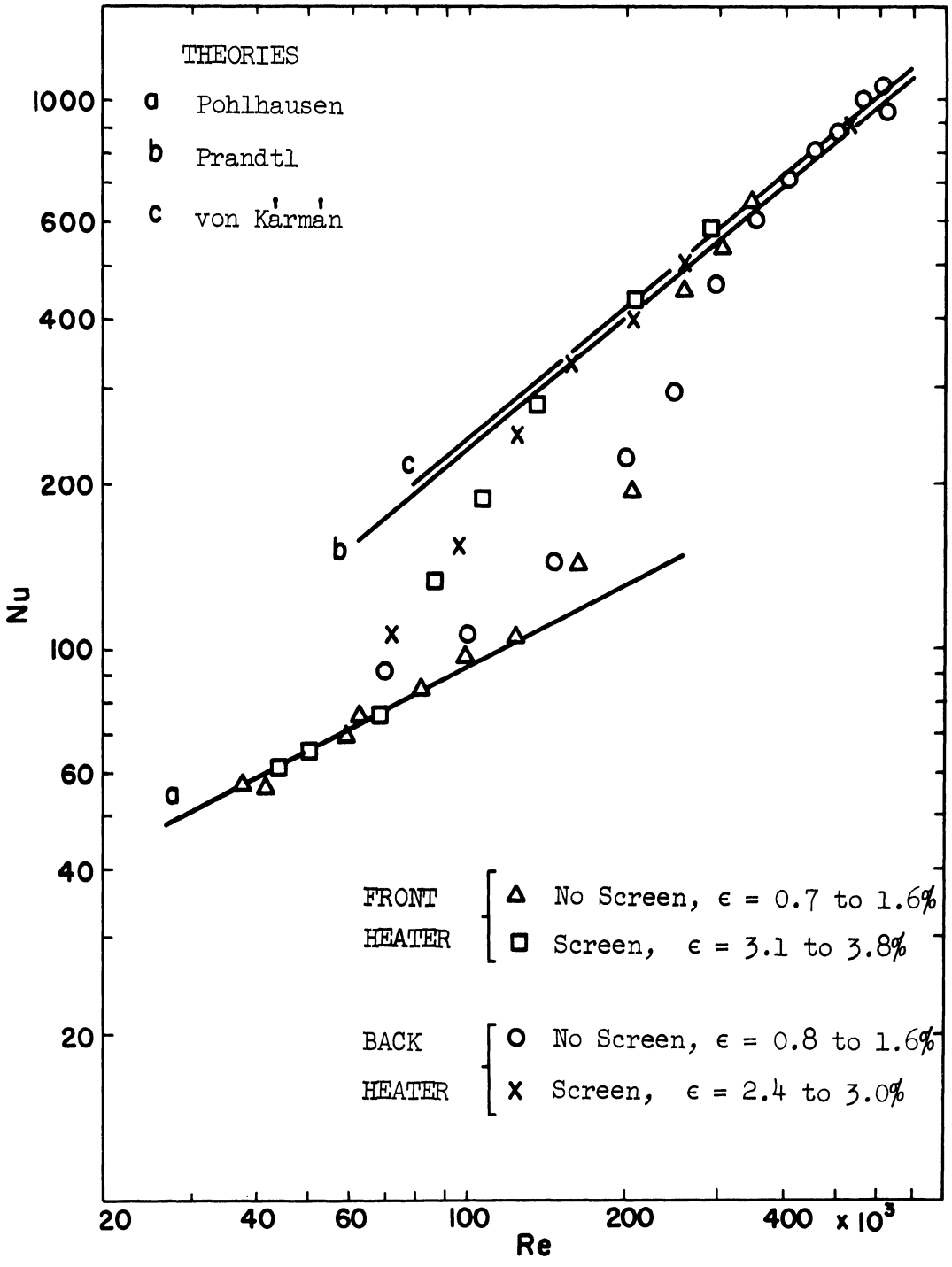

Figure 2-5. Local Heat Transfer from Flat Plate Negligible Pressure Gradient (Wang).

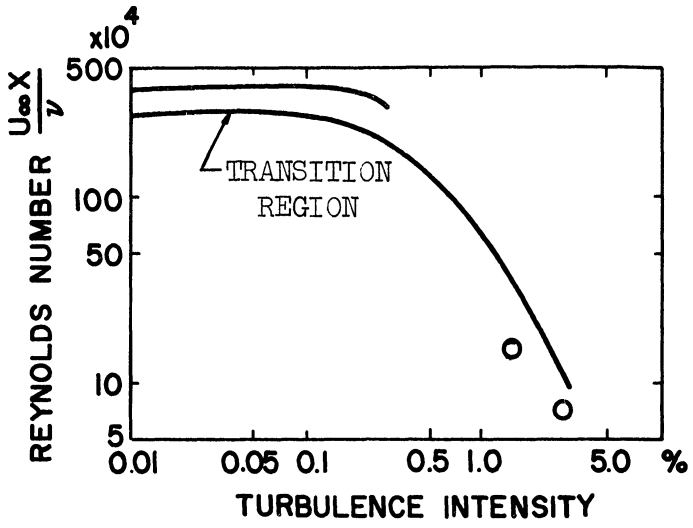

o Present Experimental Points

Figure 2-6. Effect of Free Stream Turbulence on Boundary Layer Transition, from Gazley (30) (Wang).

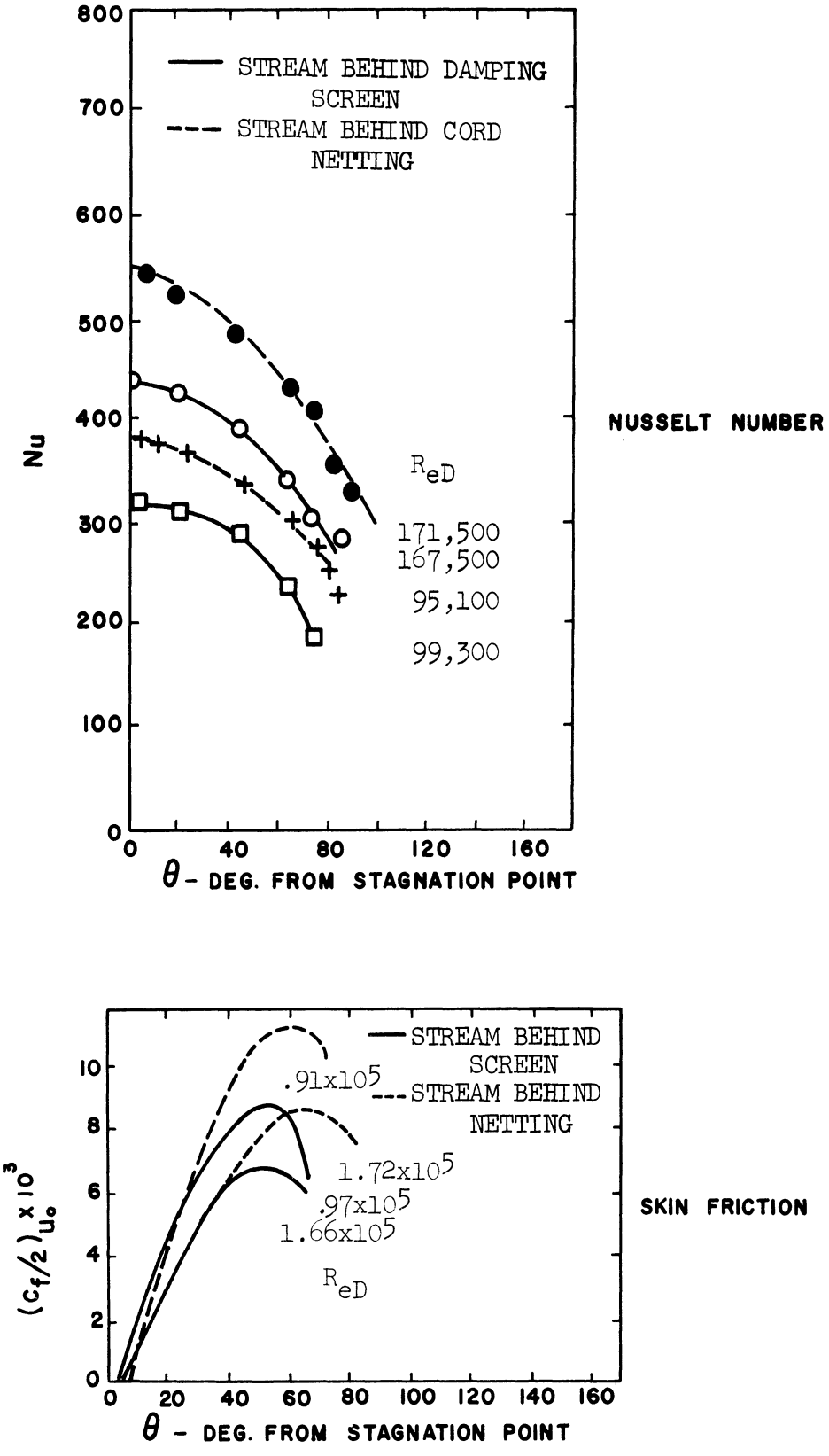

Figure 2-7. Giedts Results

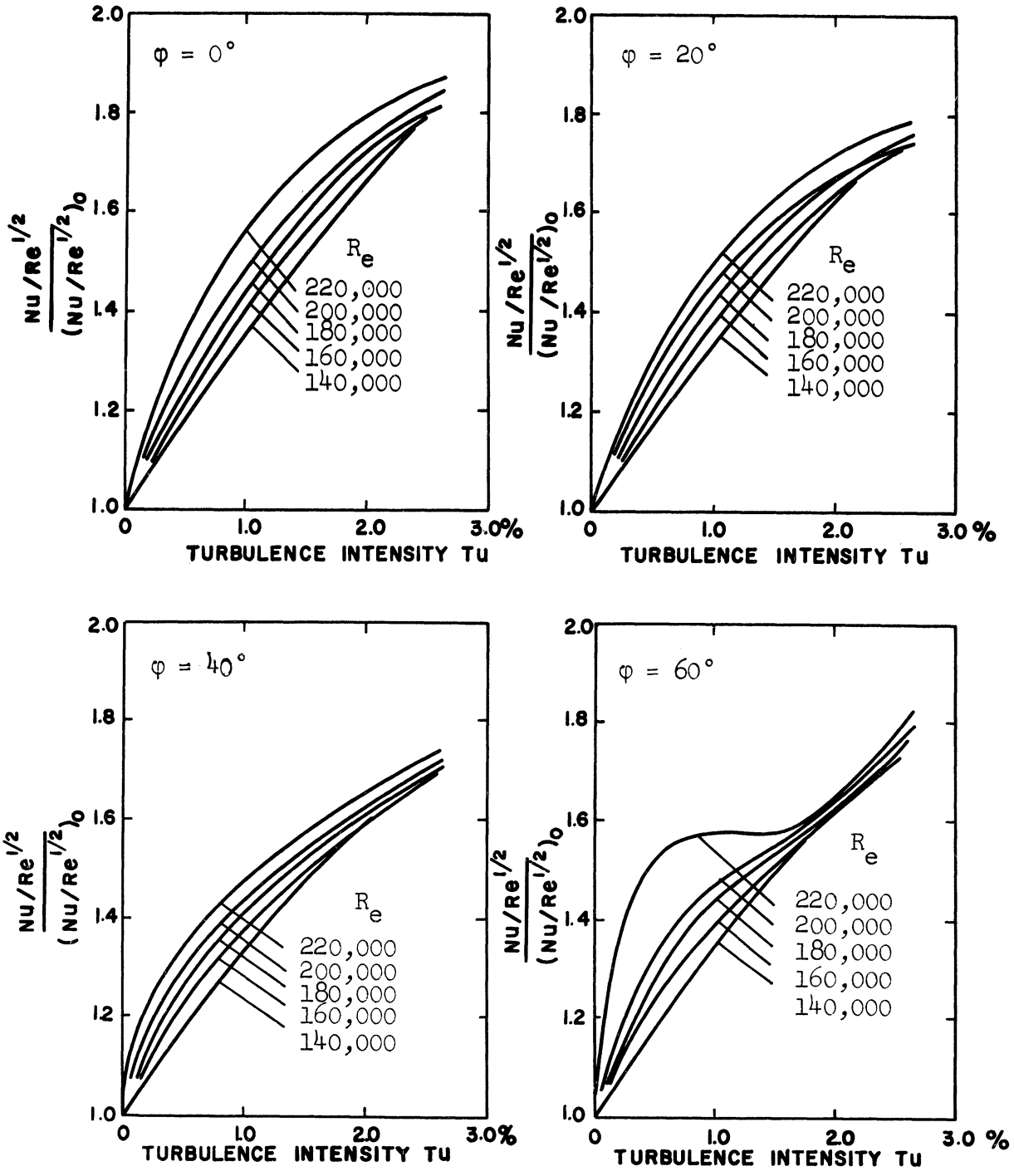

Figure 2-8. Kestins Results.

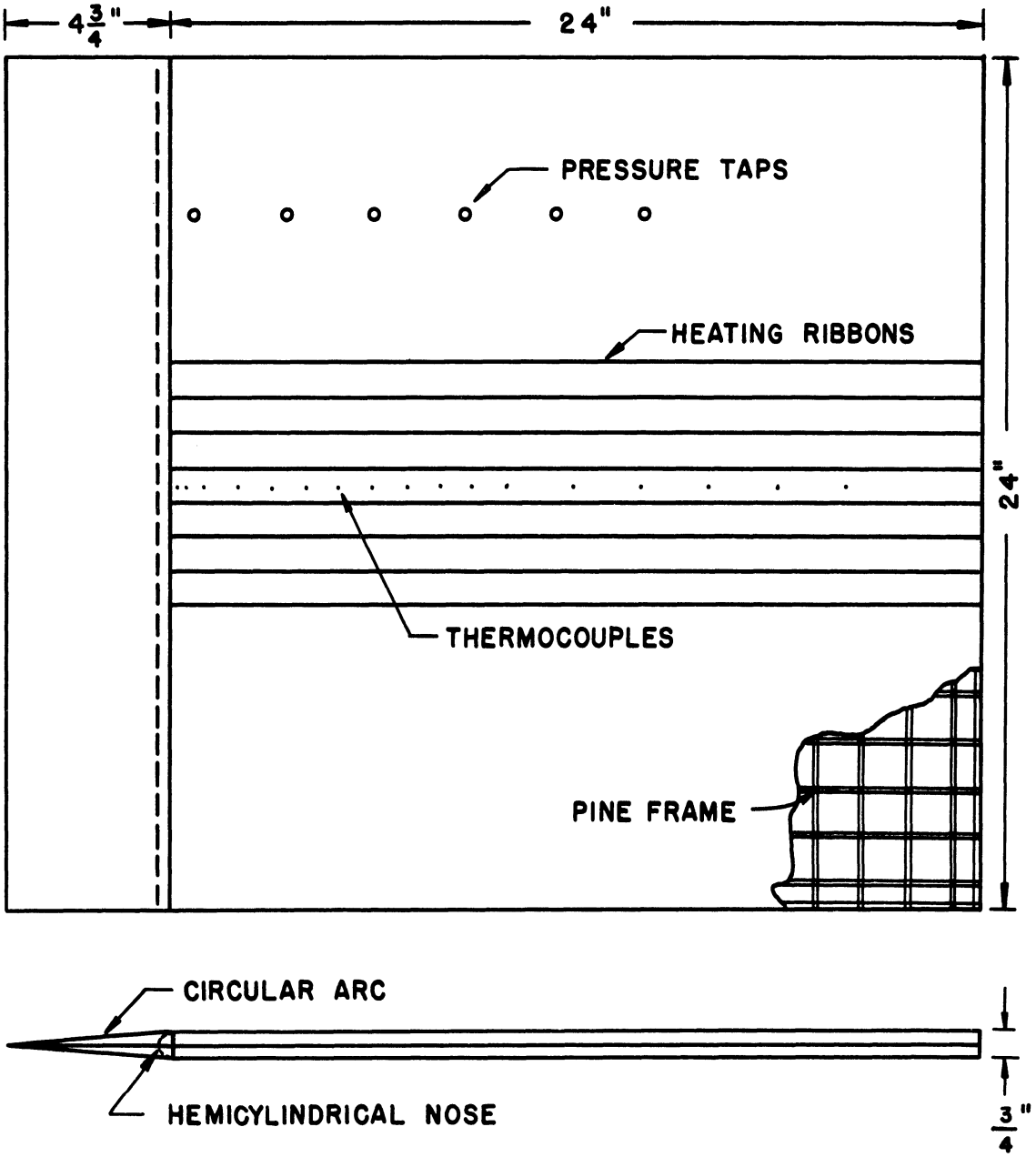

Figure 3-1. Flat Plate.

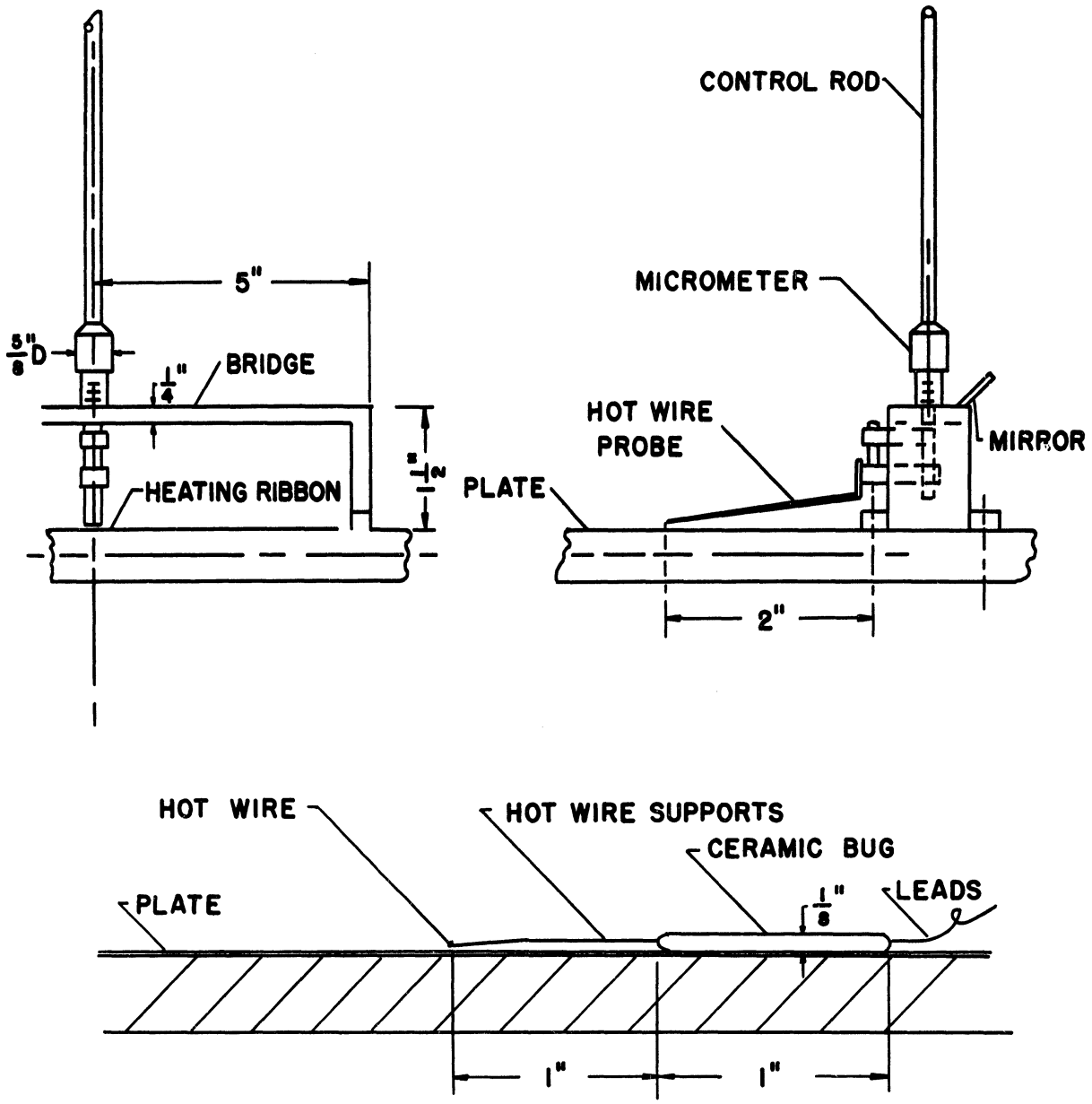

Figure 3-2. Plate Hot Wire Probe and Bug.

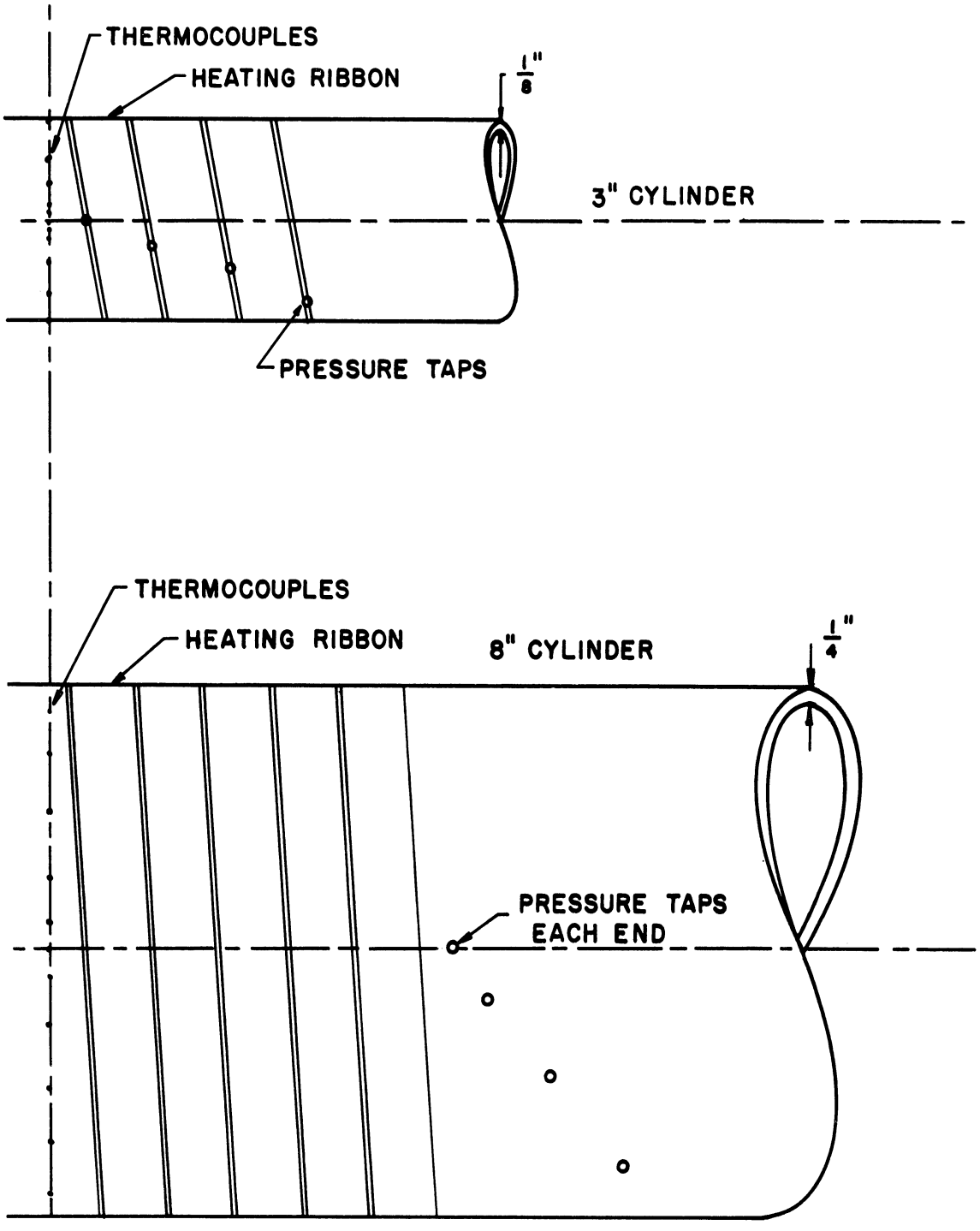

Figure 3-3. Heat Transfer Cylinders.

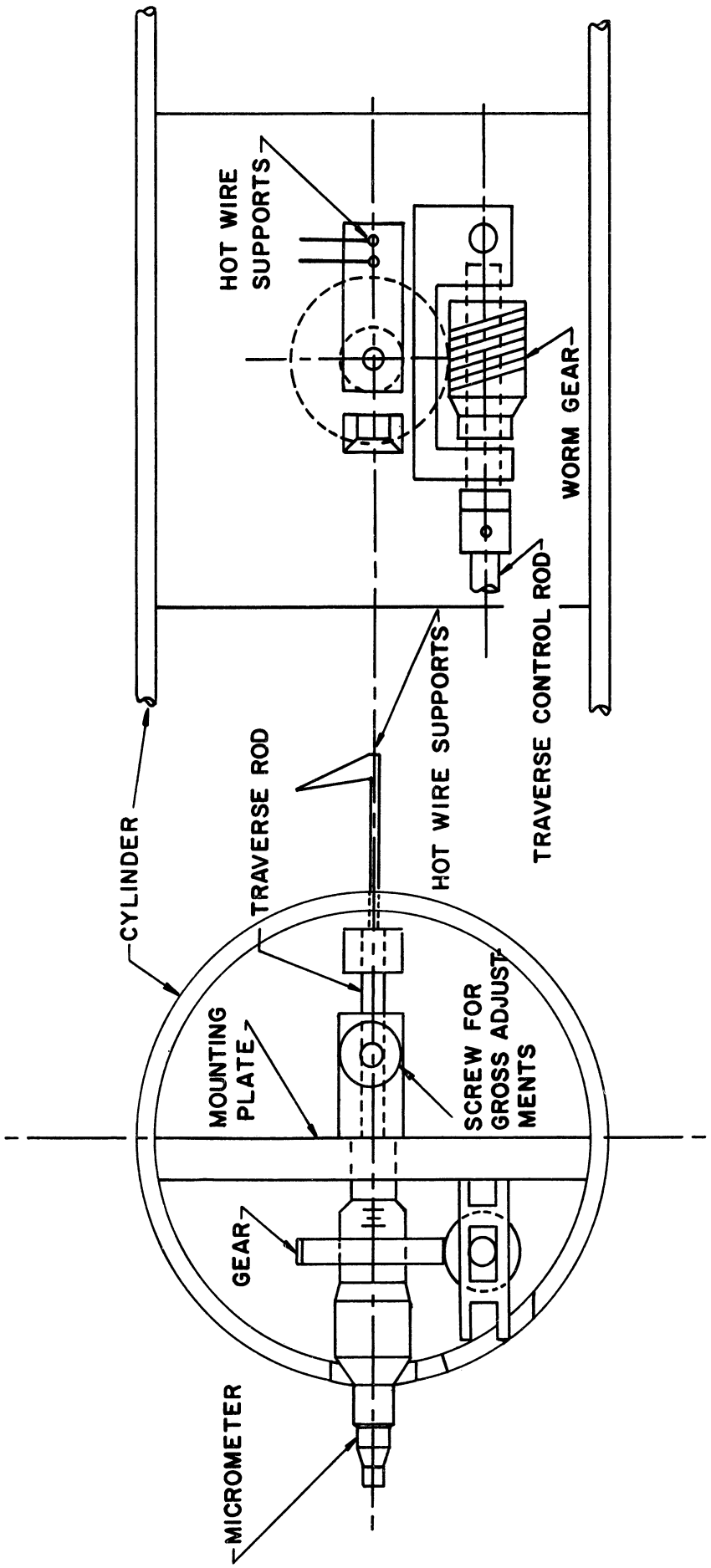

Figure 3-4. Cylinder Micrometer Probe Full Scale.

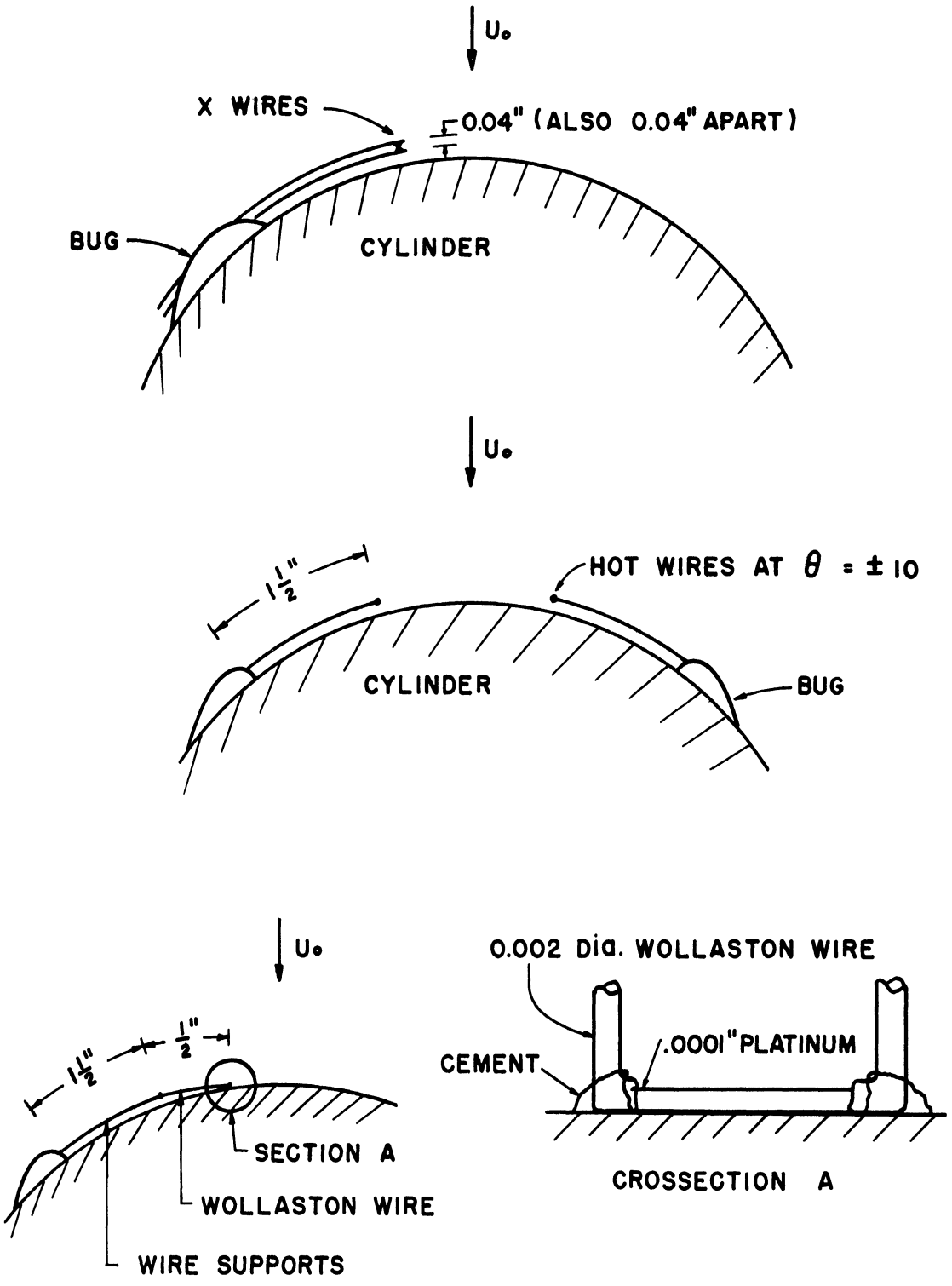

Figure 3-5. Cylinder Hot Wire Bugs.

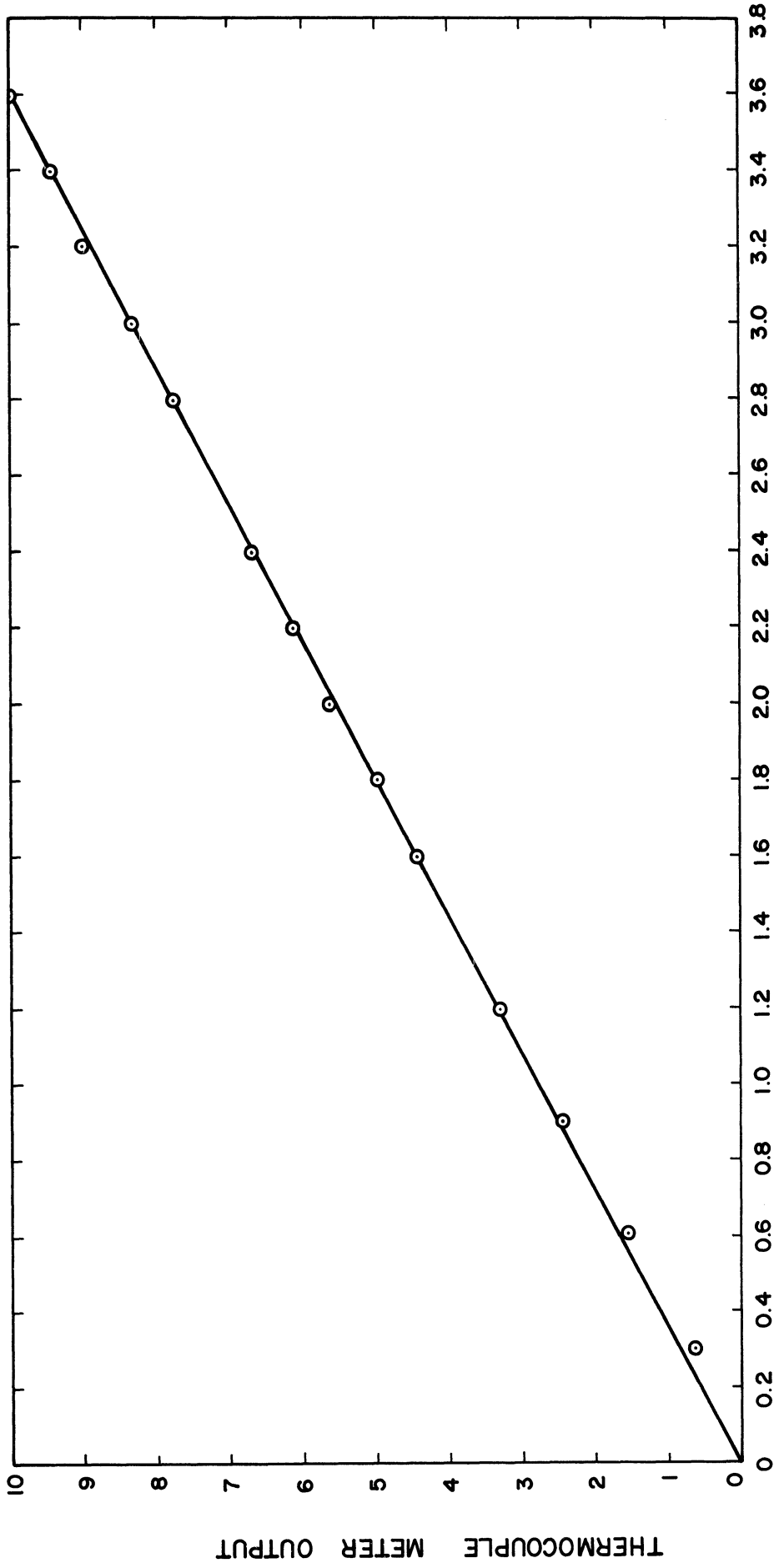

Figure 3-6. Hot Wire Amplifier Calibration.

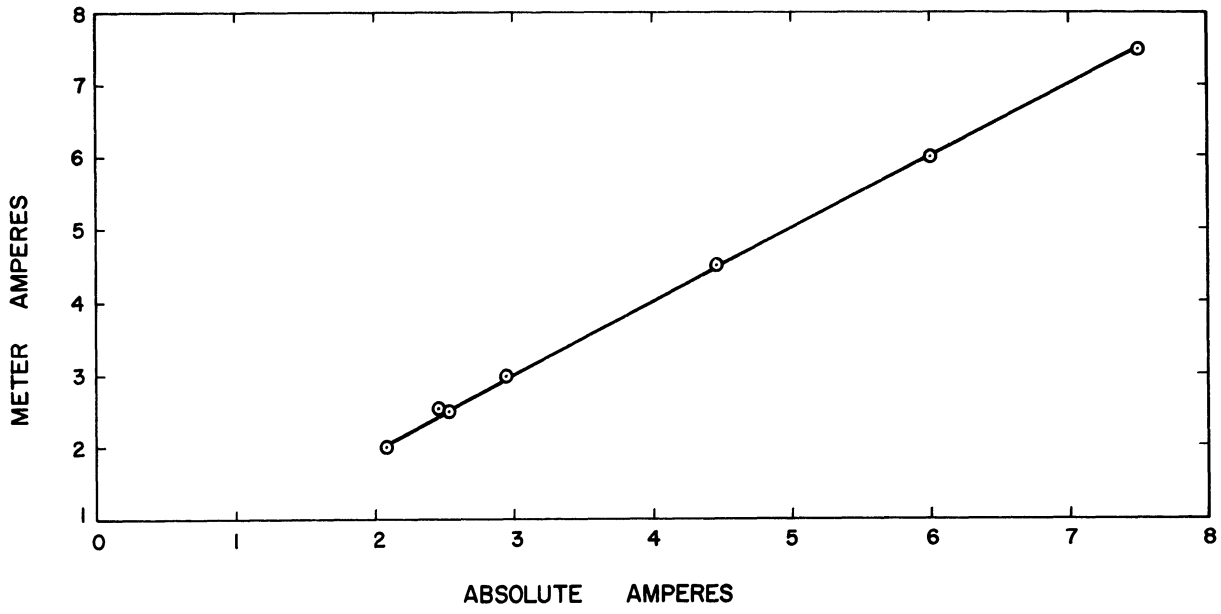

Figure 3-7. Ammeter Calibration.

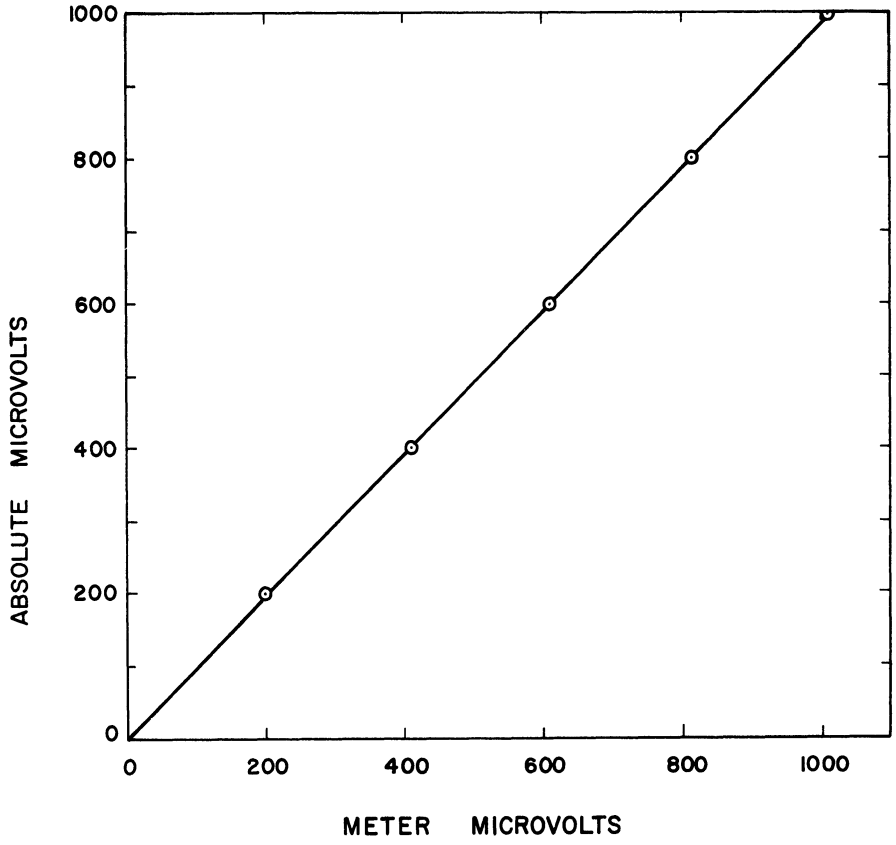

Figure 3-8. Galvanometer Calibration.

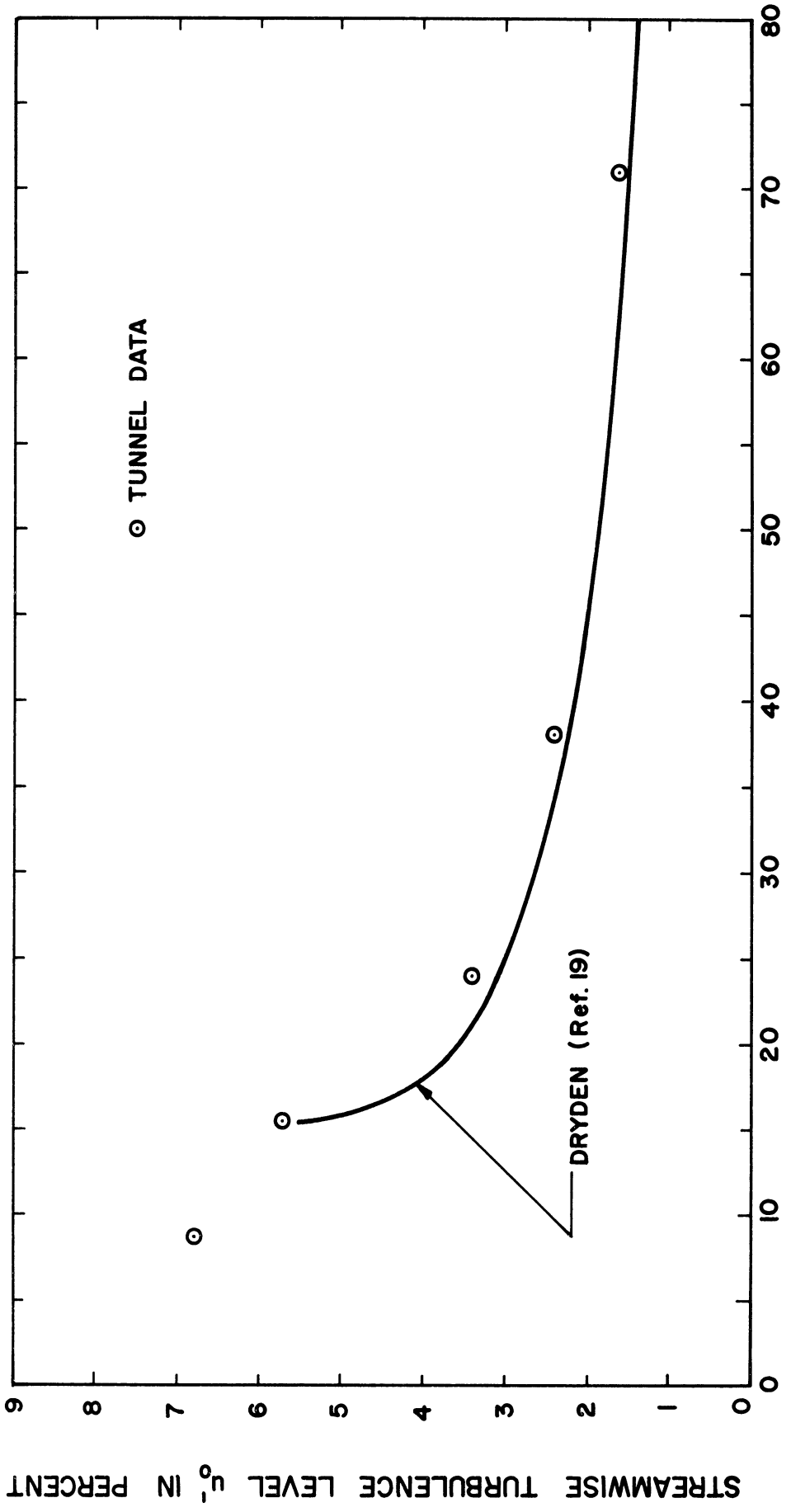

Figure 4-1. Freestream Turbulence in 2' x 2' Tunnel.

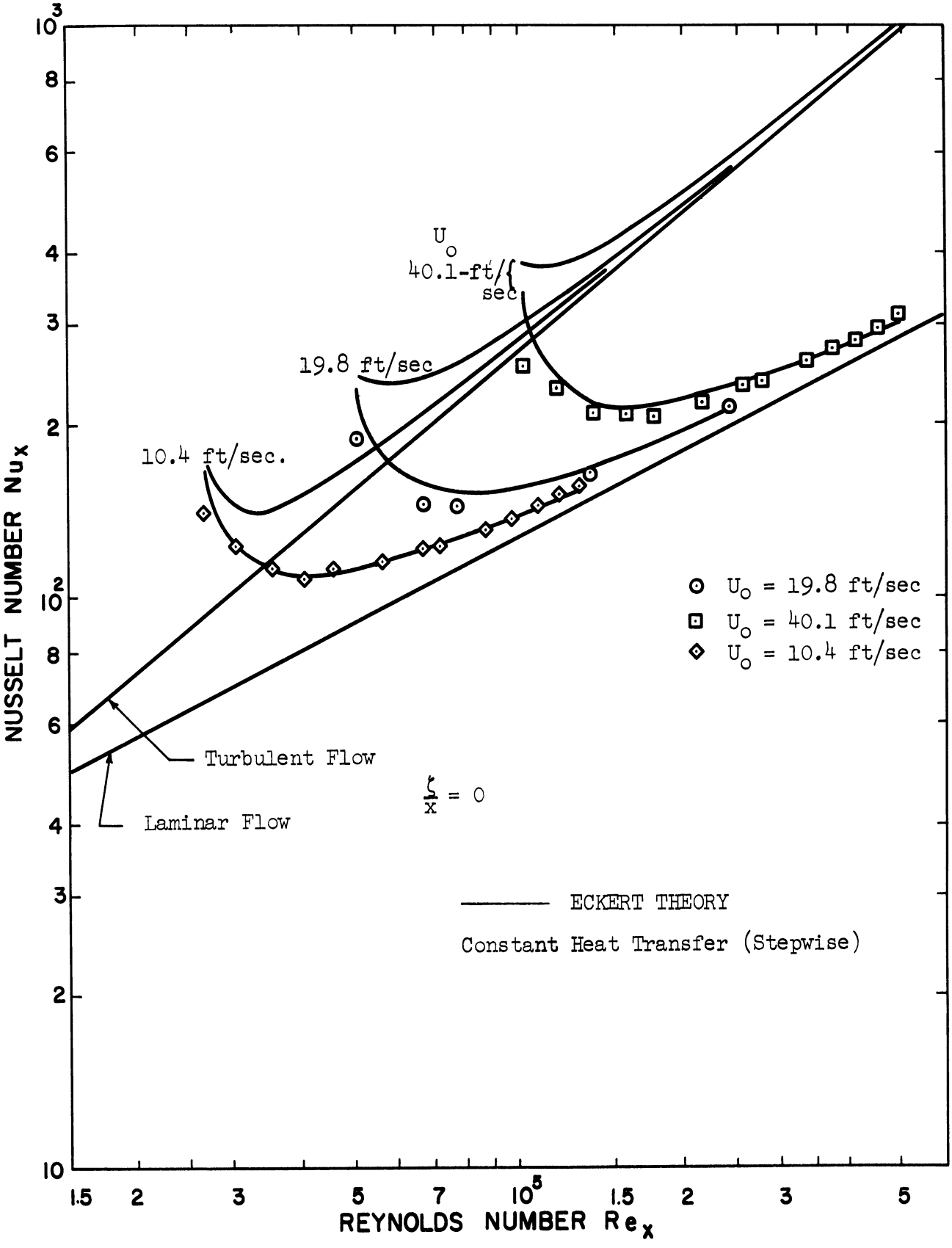

Figure 4-2. Clear Tunnel Flat Plate Nusselt Number.

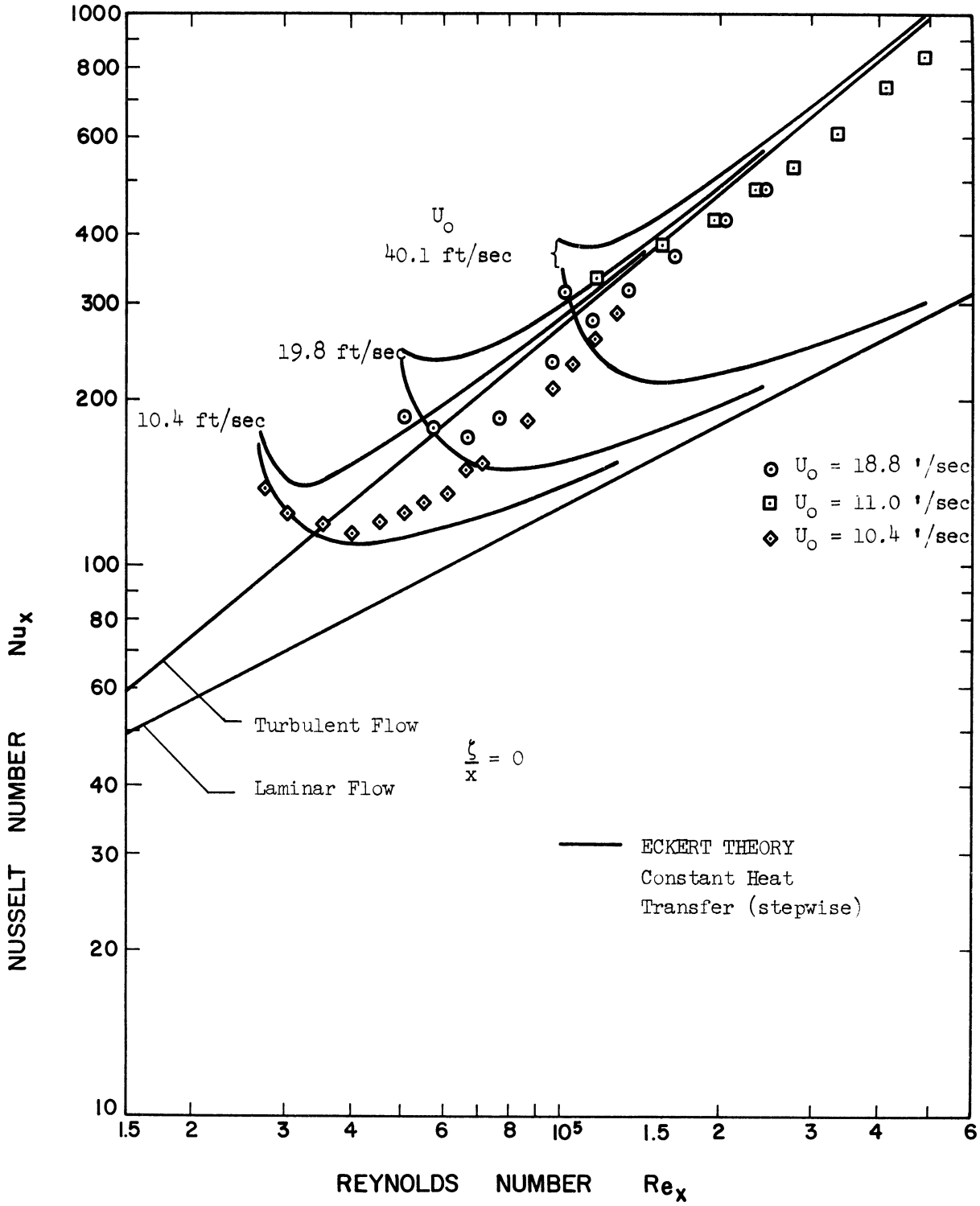

Figure 4-3. Flat Plate with Grid at 8-3/4 Inches.

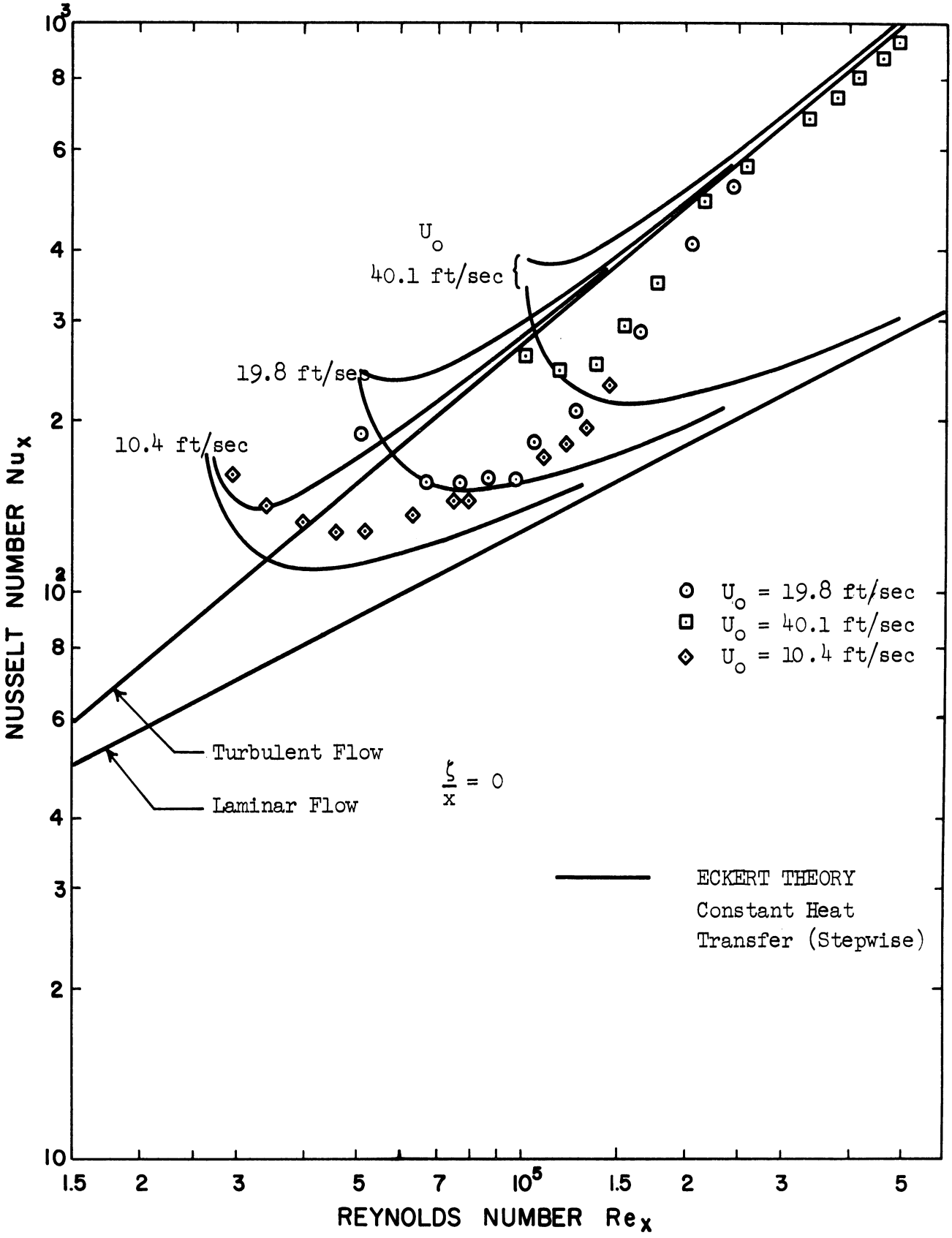

Figure 4-4. Flat Plate with Grid at 15-1/2 Inches.

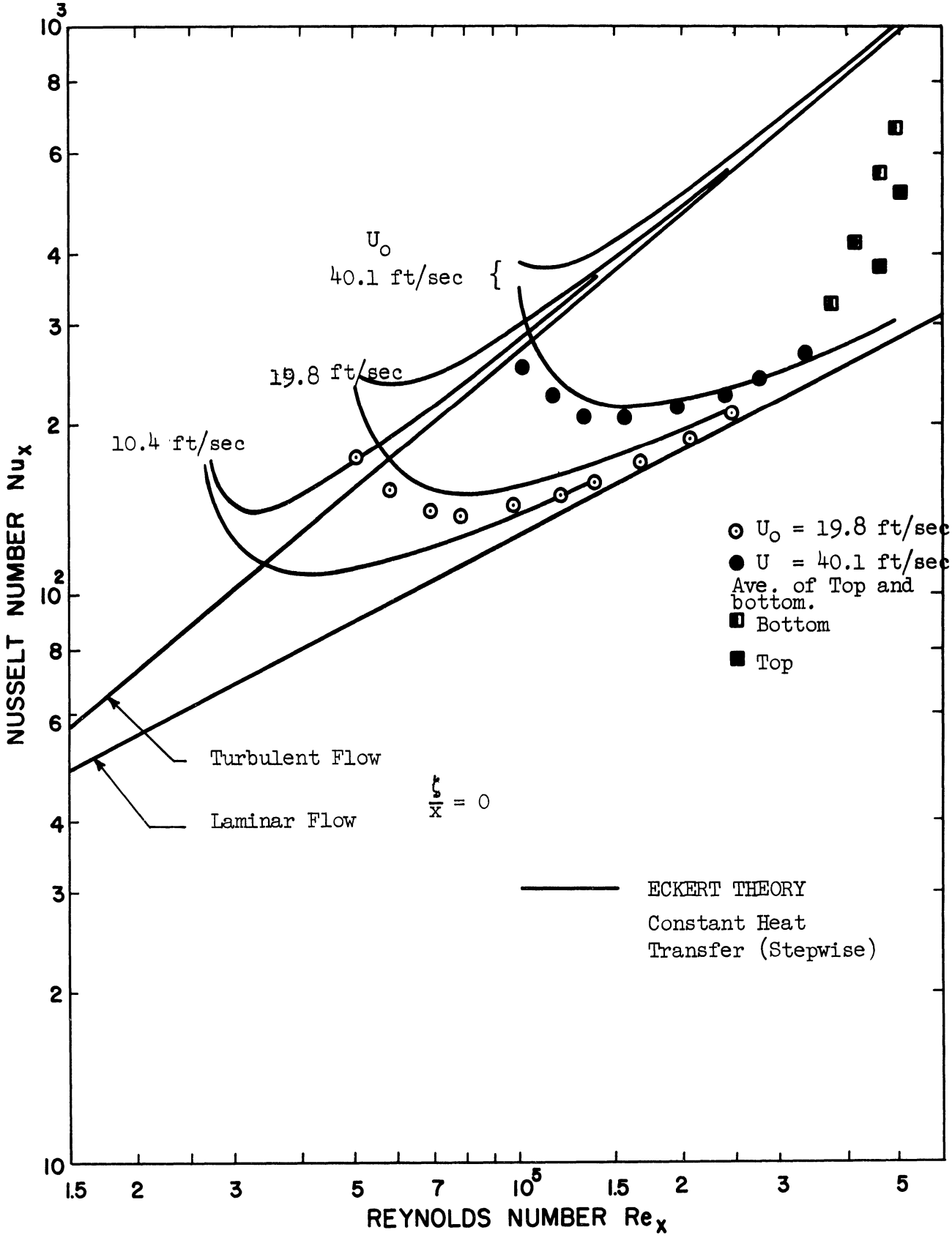

Figure 4-5. Flat Plate with Grid at 77 Inches.

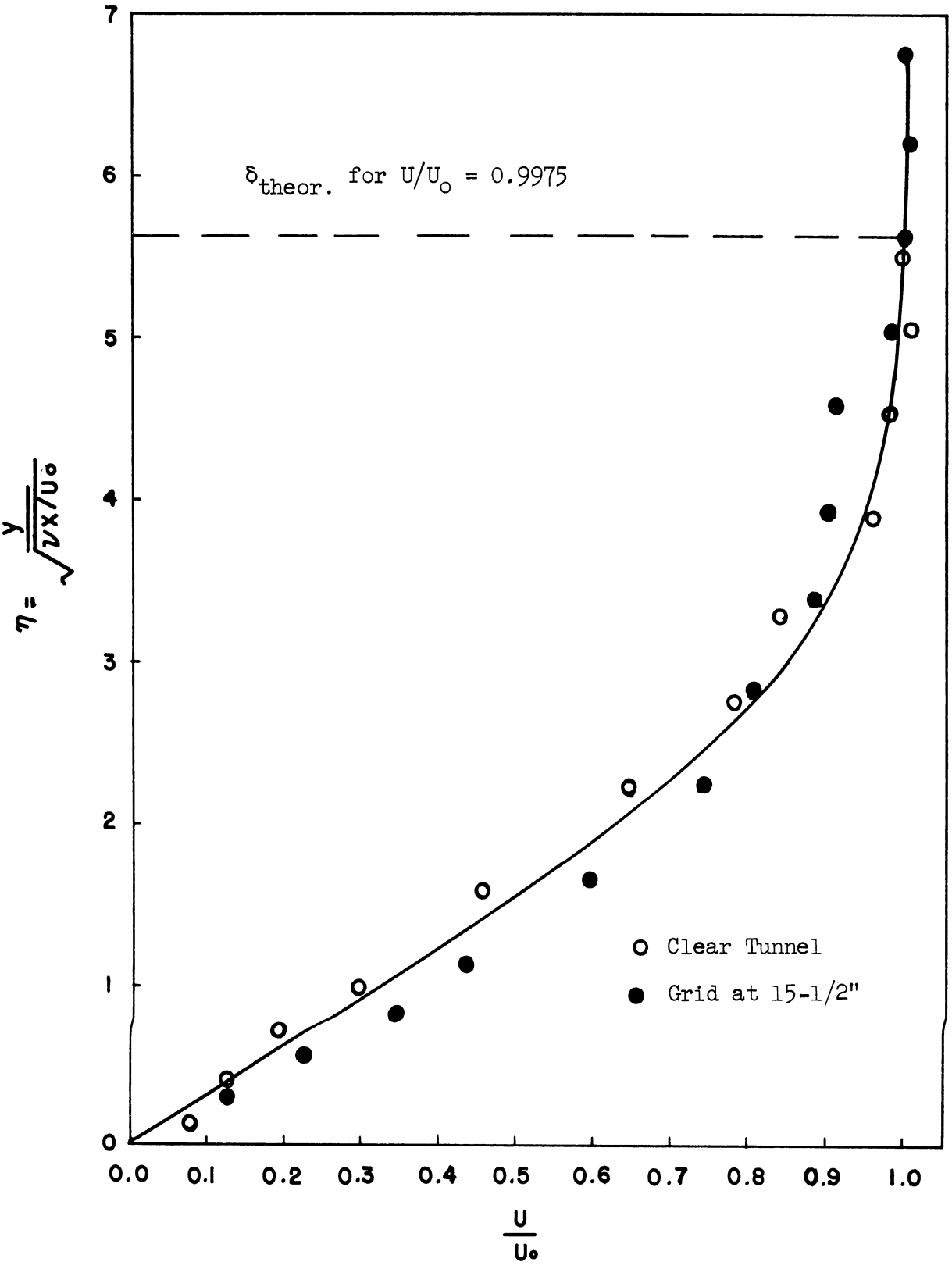

Figure 4-6. Flat Plate Velocity Profiles Sharp Leading Edge.

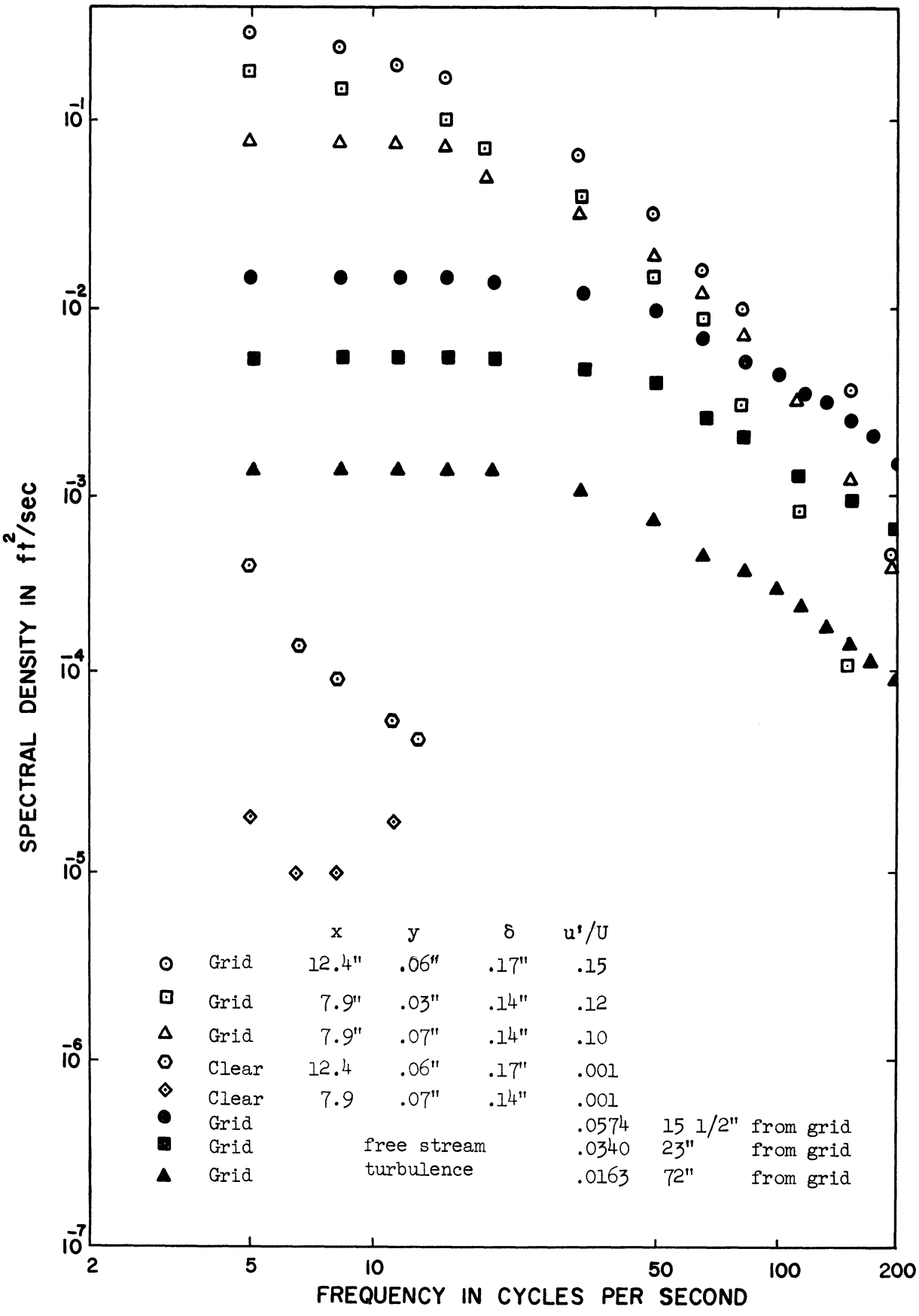

Figure 4-7. Plate and Free Stream Spectra.

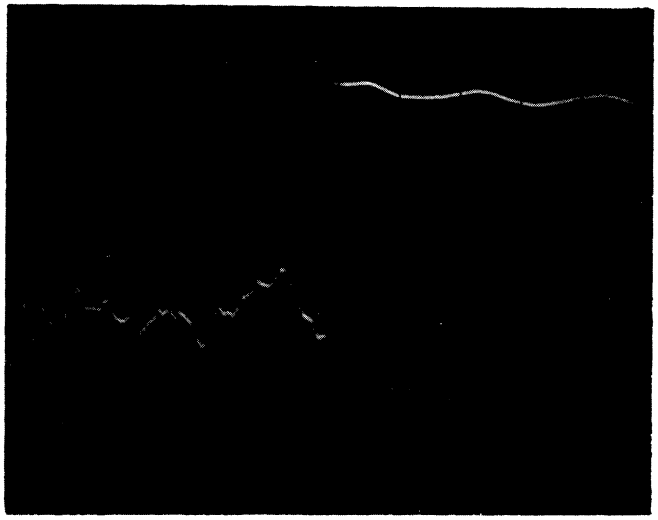

Tunnel	x	y	Sweep	Gain
Grid at 15-1/2"	8"	.02"	5 $\frac{\text{msec}}{\text{cm}}$	1
Grid at 15-1/2"	8"	.5" (outside B.L.)	5 $\frac{\text{msec}}{\text{cm}}$	10

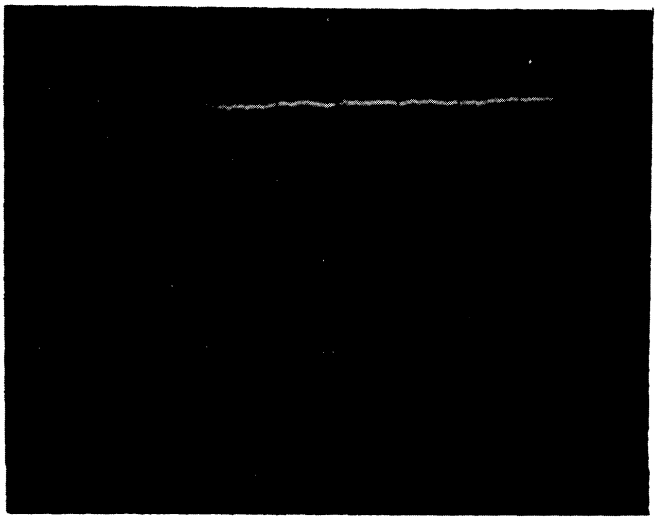

clear	8"	.02"	5 $\frac{\text{msec}}{\text{cm}}$	1

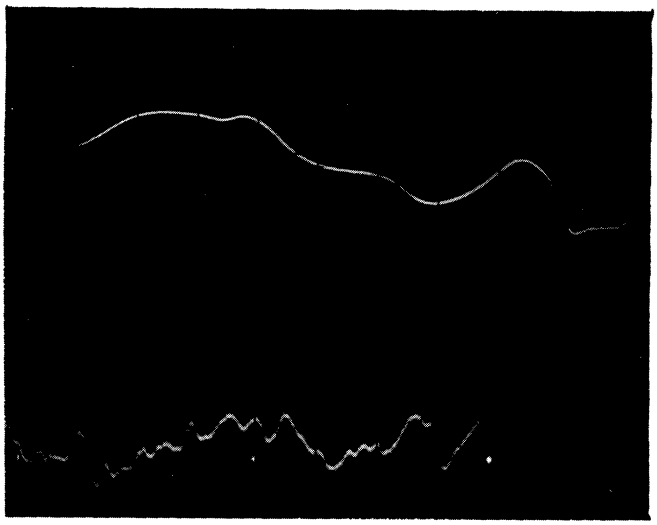

Grid at 15-1/2"	12"	.02"	5 $\frac{\text{msec}}{\text{cm}}$	1
Grid at 15-1/2"	12"	.5"	5 $\frac{\text{msec}}{\text{cm}}$	10

Figure 4-8. Flat Plate Oscillograms for U_o = 20 l/sec.

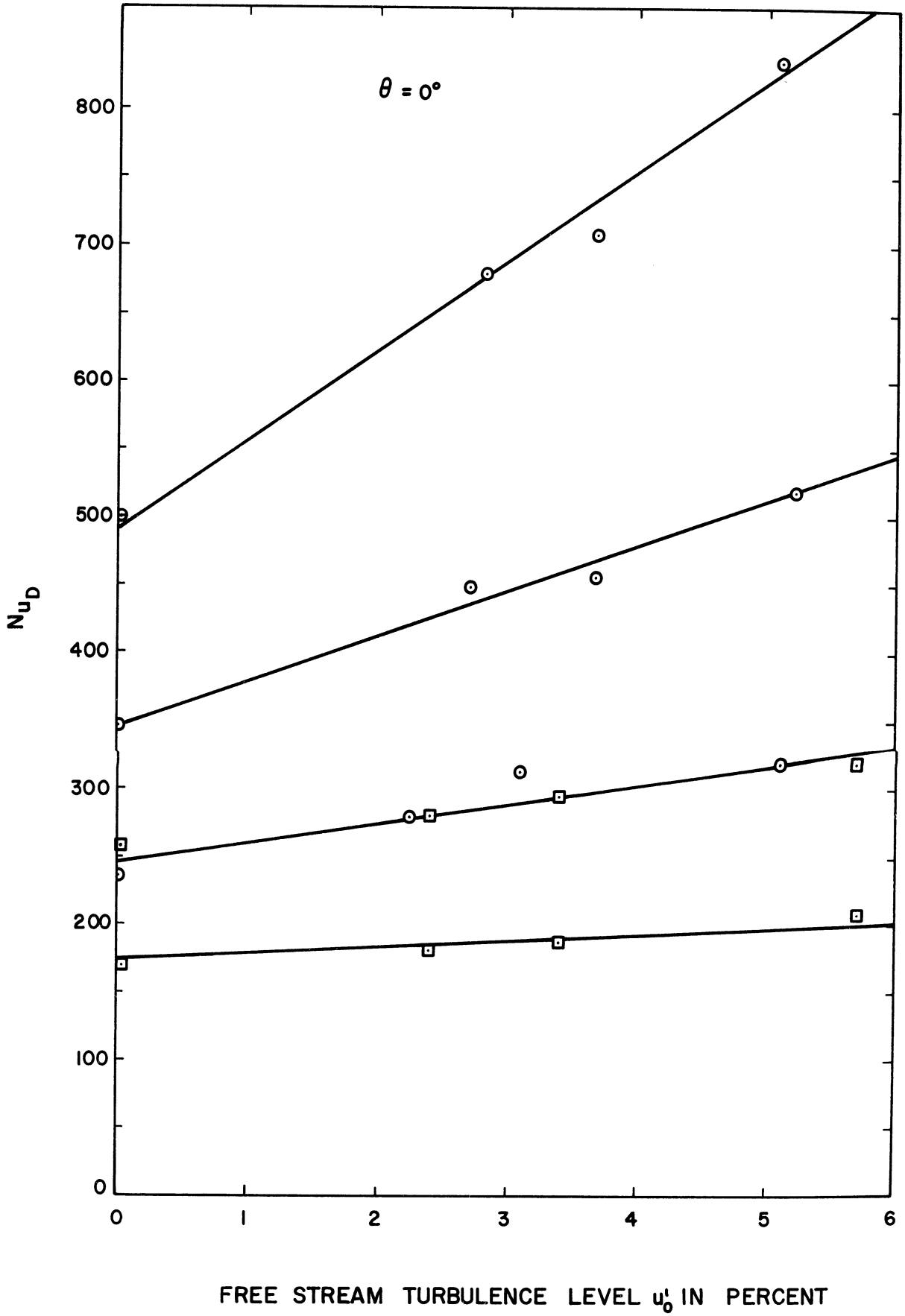

Figure 4-9. Cylinder Nusselt Number Data $\theta = 0°$.

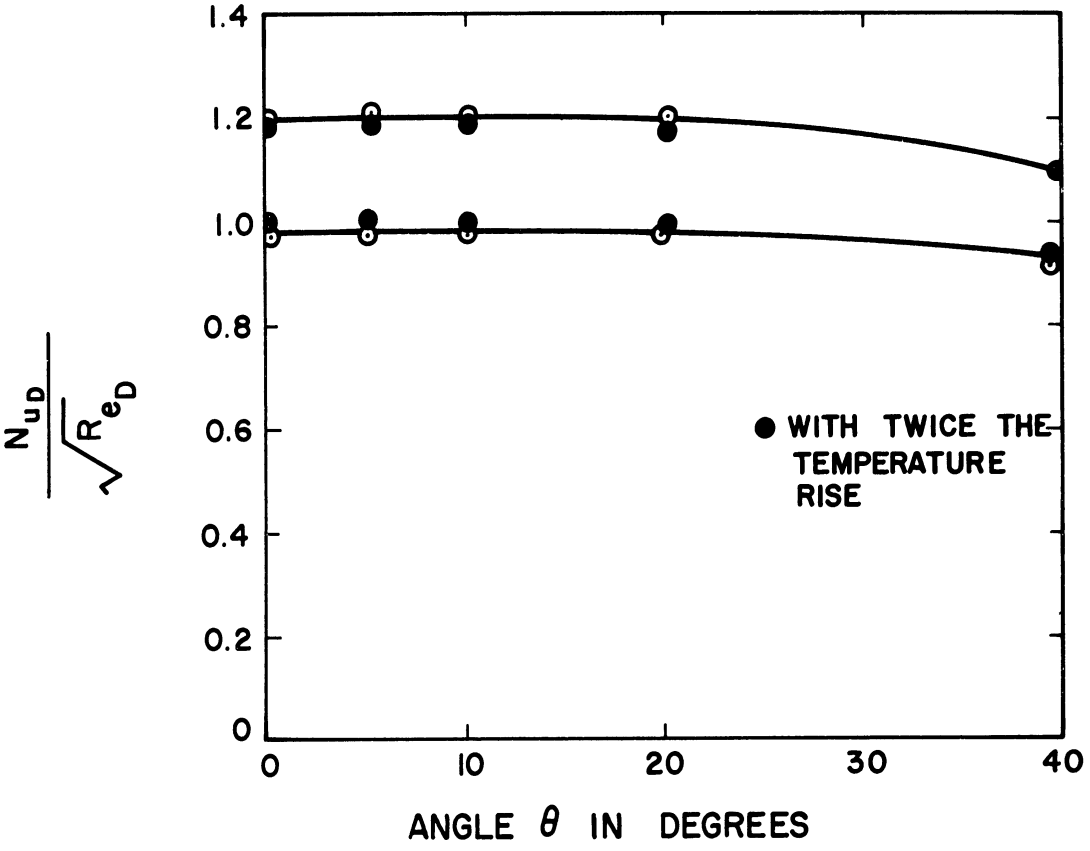

Figure 4-10. Heat Transfer Data with 3 Inch Cylinder, R_{e_D} = 30,000.

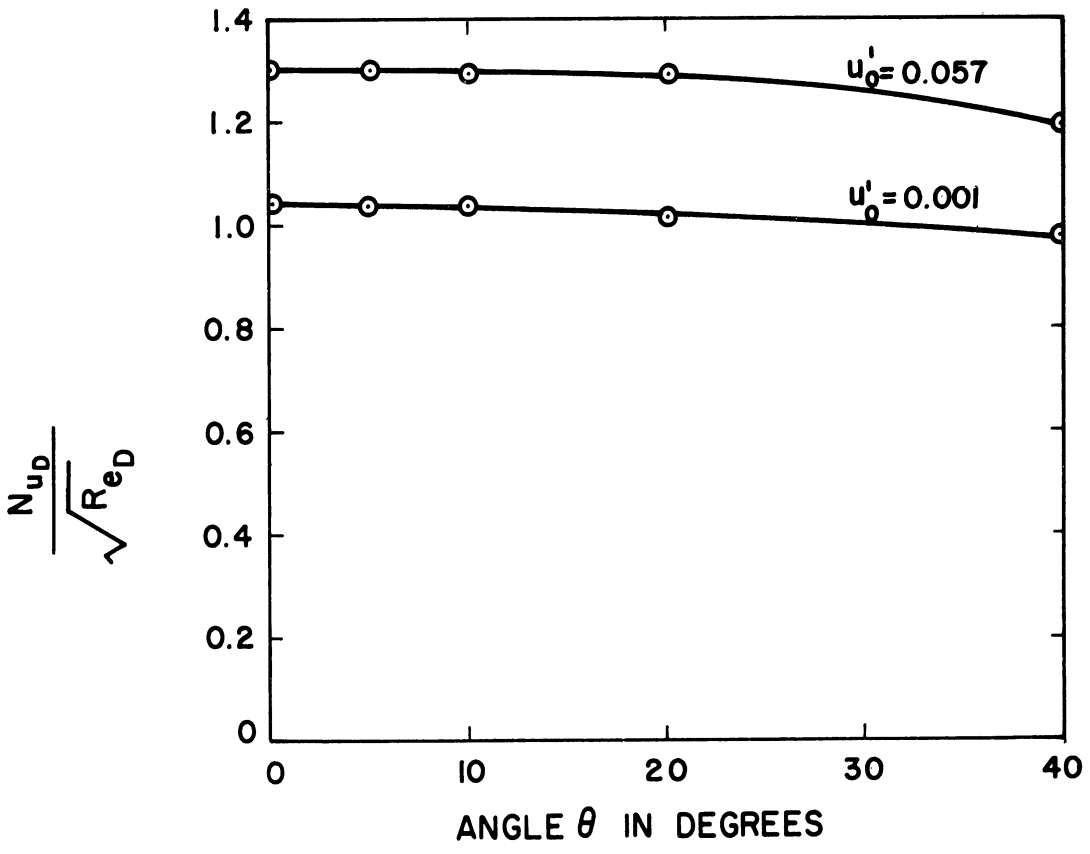

Figure 4-11. Heat Transfer Data with 3 Inch Cylinder, R_{e_D} = 60,000.

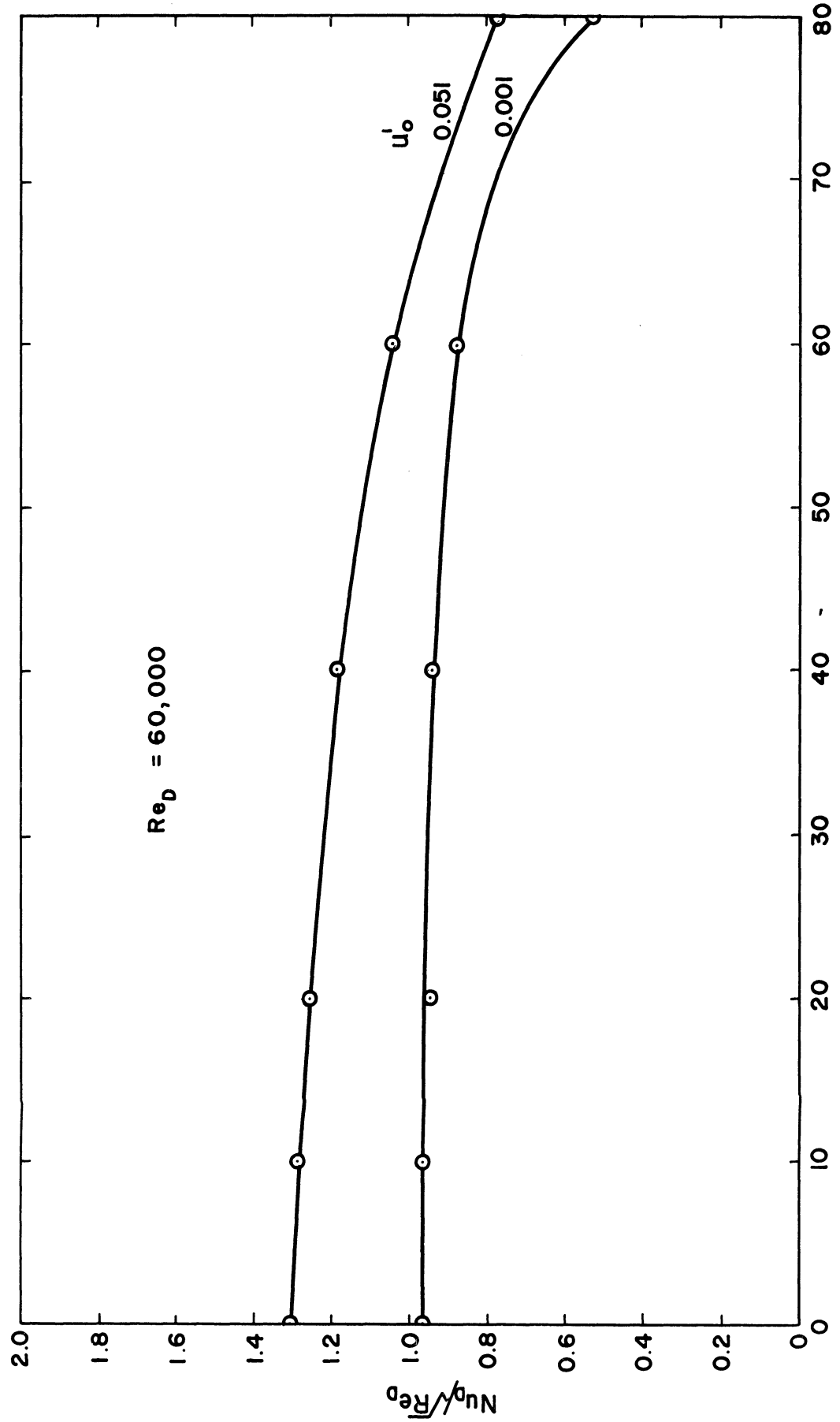

Figure 4-12. Heat Transfer Data with 8 Inch Cylinder, Re_D = 60,000 .

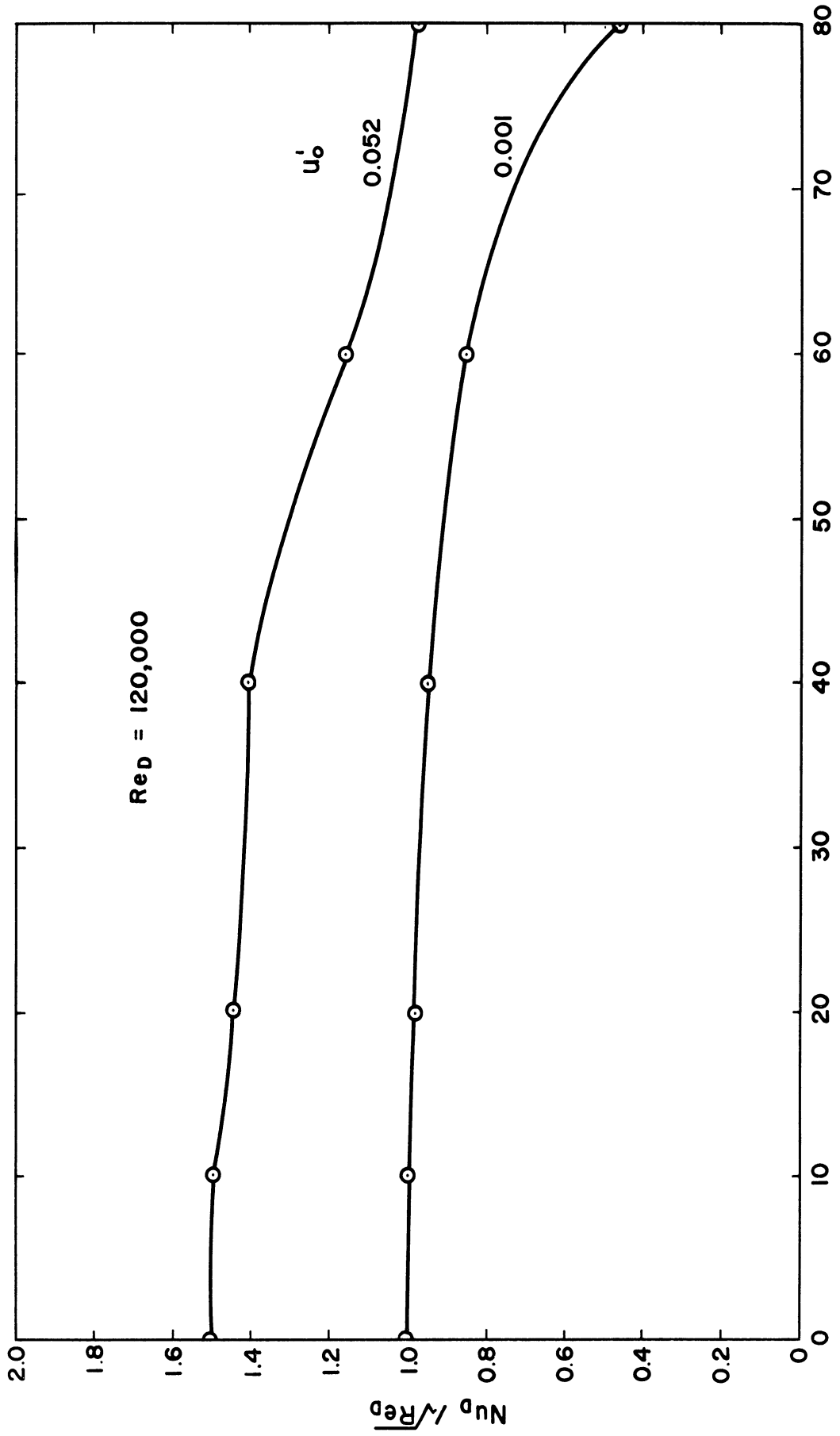

Figure 4-13. Heat Transfer Data with 8 Inch Cylinder, R_{e_D} = 120,000.

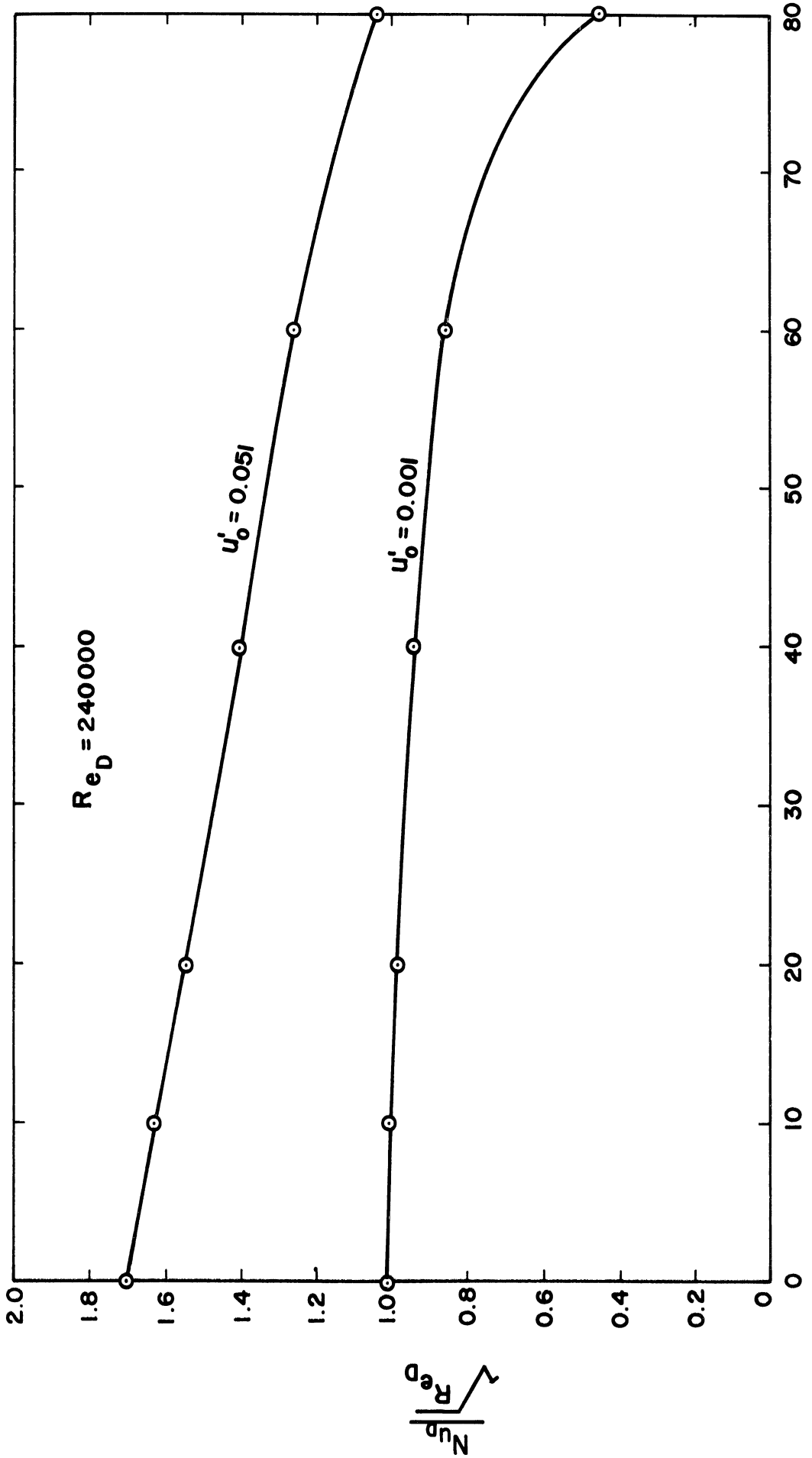

Figure 4-14. Heat Transfer Data with 8 Inch Cylinder, R_{e_D} = 240,000.

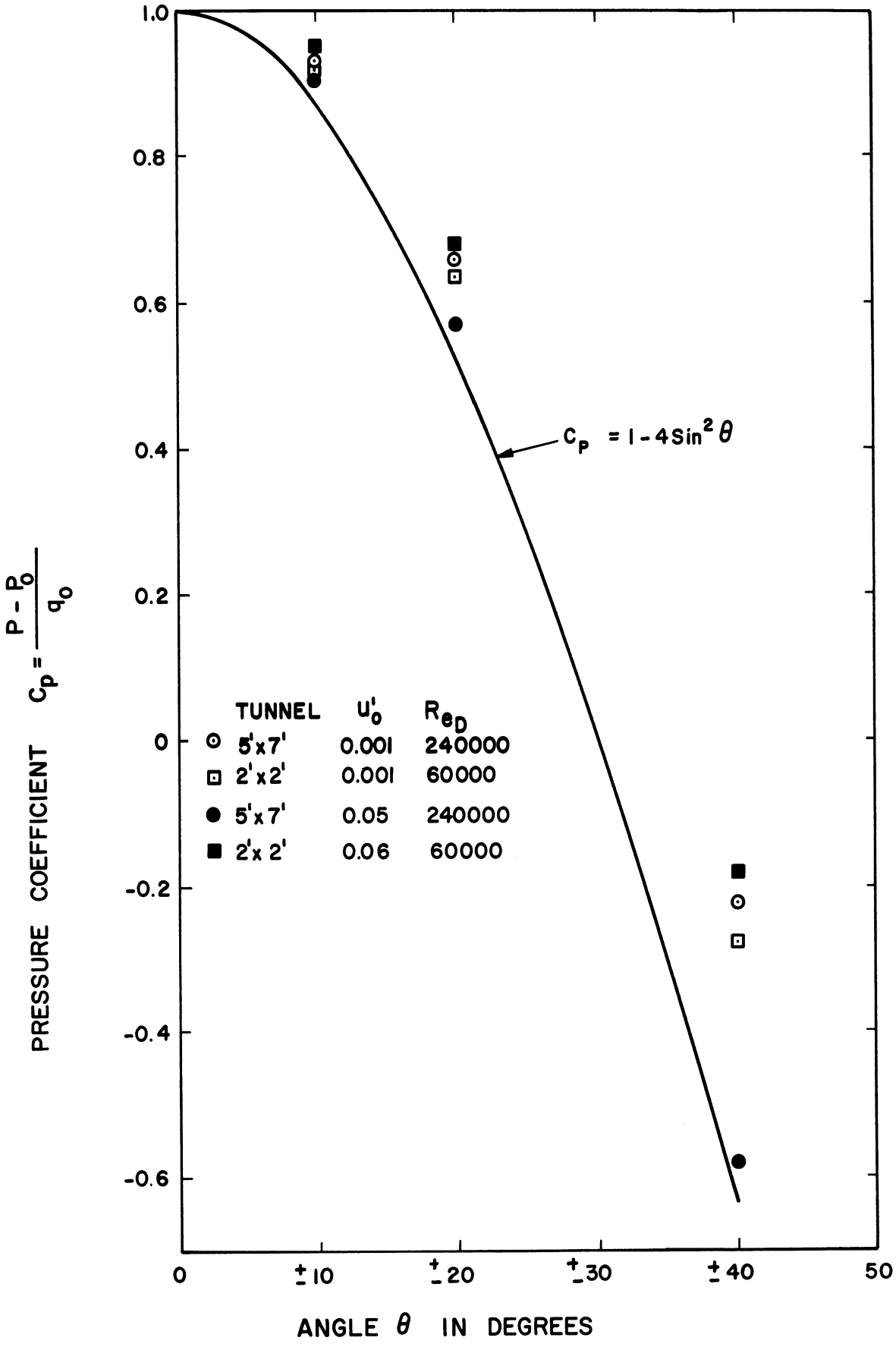

Figure 4-15. Cylinder C_p vs θ .

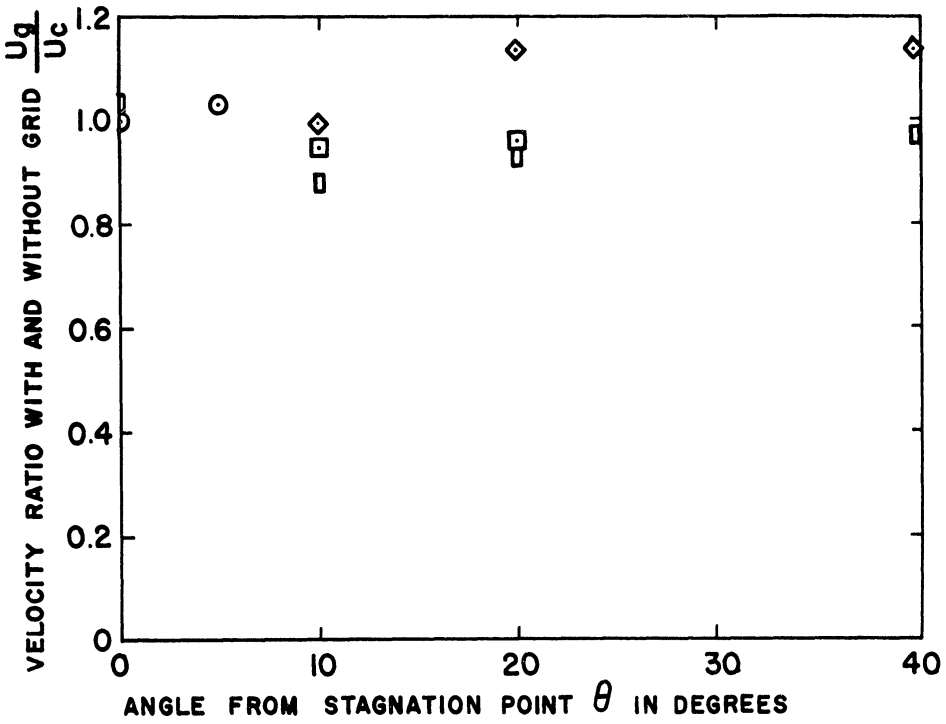

⊙	Hot Wire @ y = 0.5"	R_{eD} = 30,000	2'x2' Tunnel
◈	Static Pressure	R_{eD} = 60,000	2'x2' Tunnel
⊡	Hot Wire @ y = 0.13"	R_{eD} = 30,000	2'x2' Tunnel
▯	Static Pressure	R_{eD} = 240,000	5'x7' Tunnel

Note: All grid locations at 15-1/2" upstream of leading edge of cylinder.

Figure 4-16. Mean Velocity Ratio Outside the Boundary Layer.

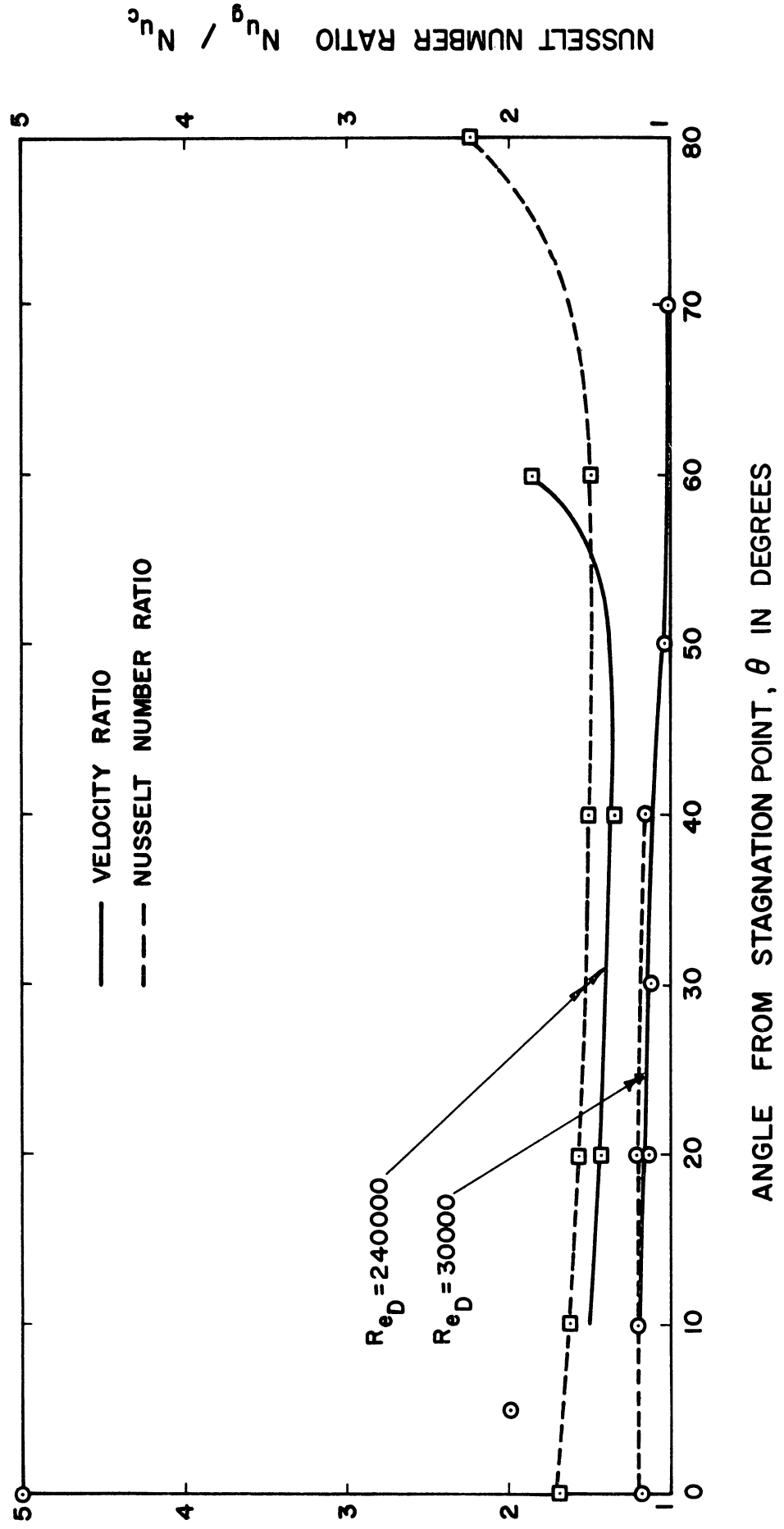

Figure 4-17. Velocity Ratio and Nusselt Number Ratio.

	$\theta = 10°$	$\theta = 20°$
U/U_o	0.51	0.66
α	19.0°	7.3°
y	0.10"	0.07"

NOTE: U/U_o and α were obtained from potential theory.

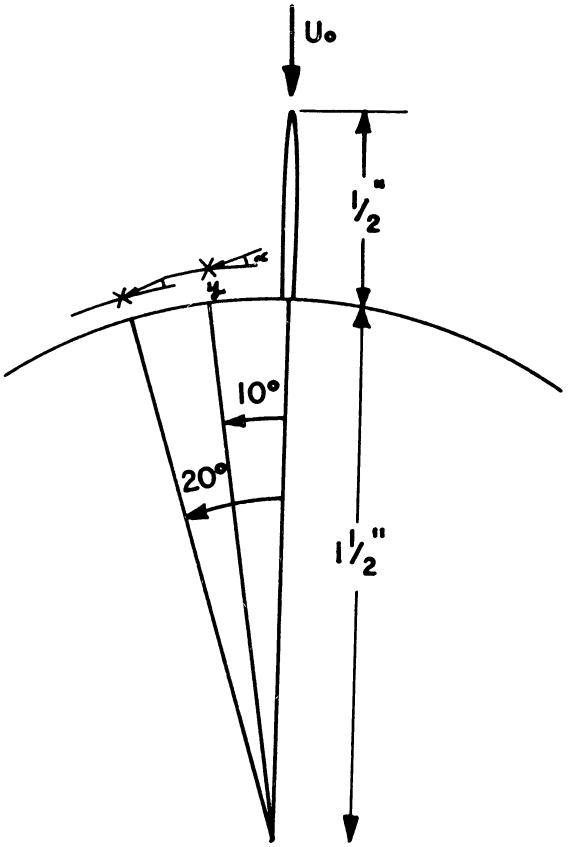

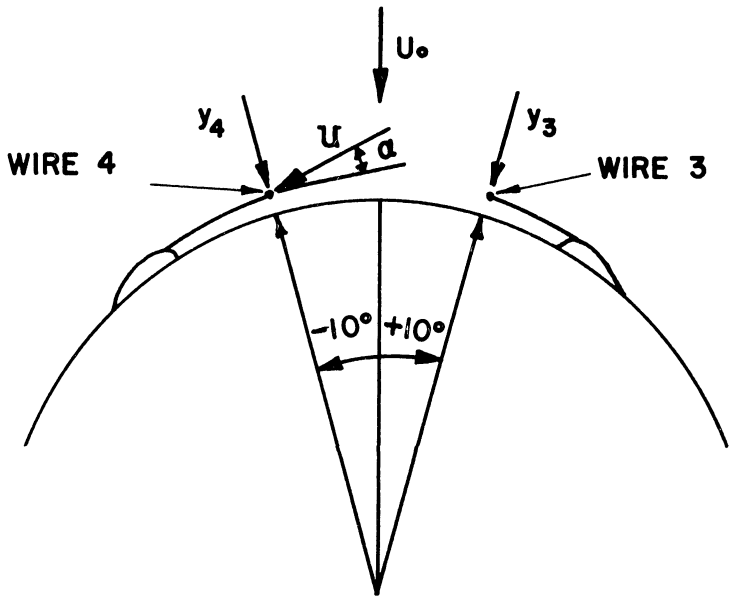

$y_3 = y_4 = 0.04"$

$\alpha \sim 8°$

Figure 4-18. Hot Wire and Flow Geometry.

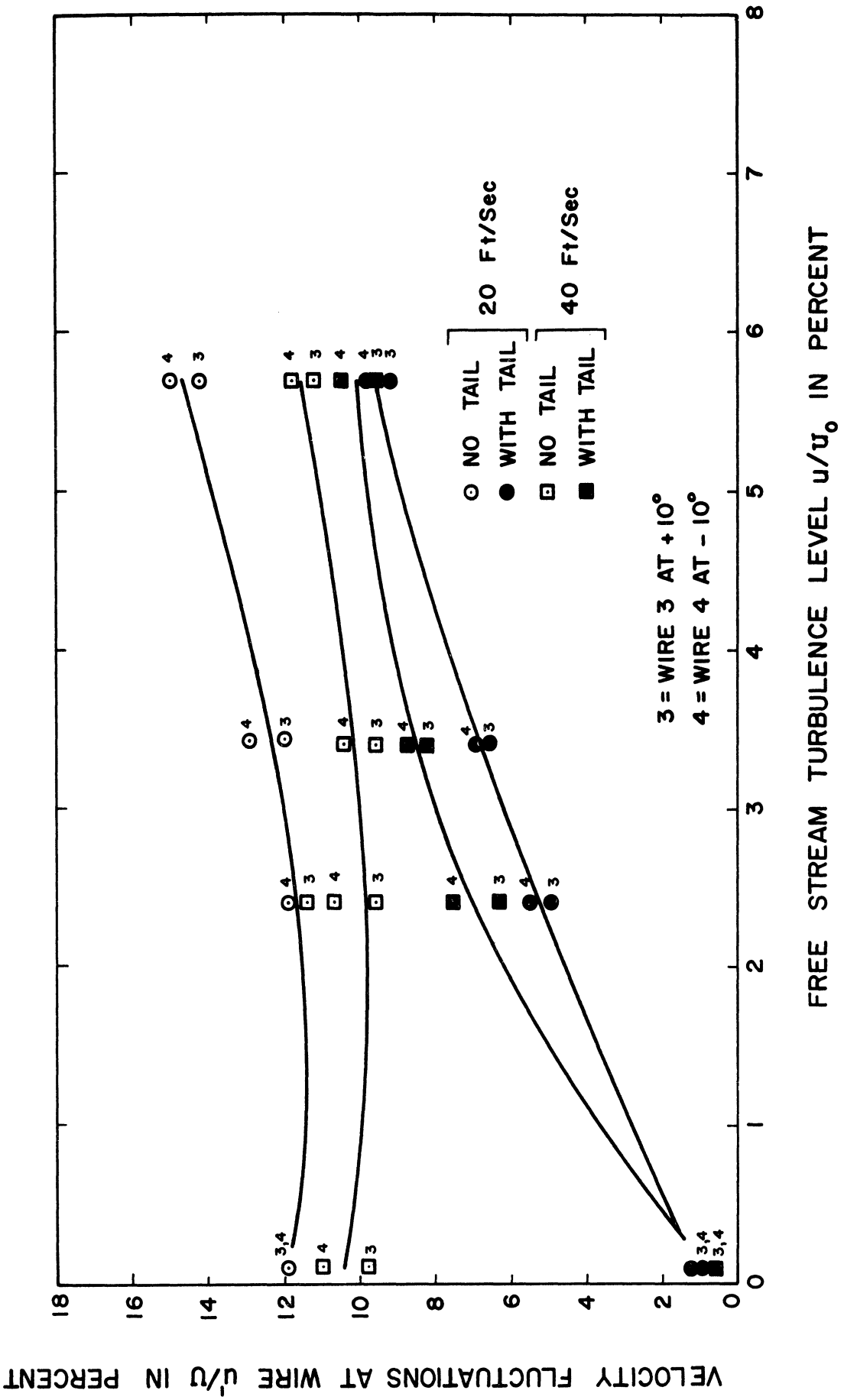

Figure 4-19. Velocity Fluctuation at $\theta = \pm 10°$.

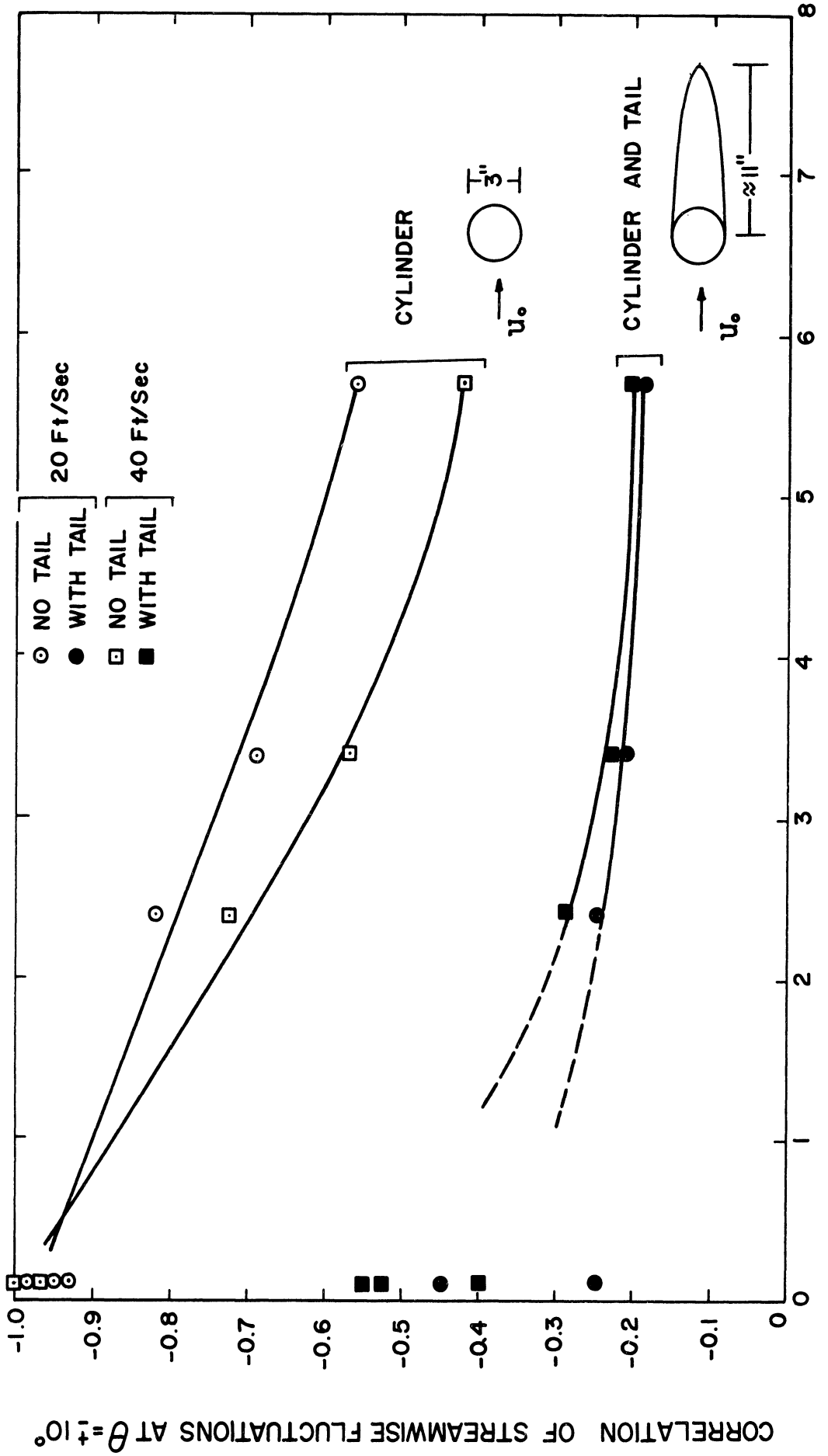

Figure 4-20. Velocity Correlations at $\theta = \pm 10°$.

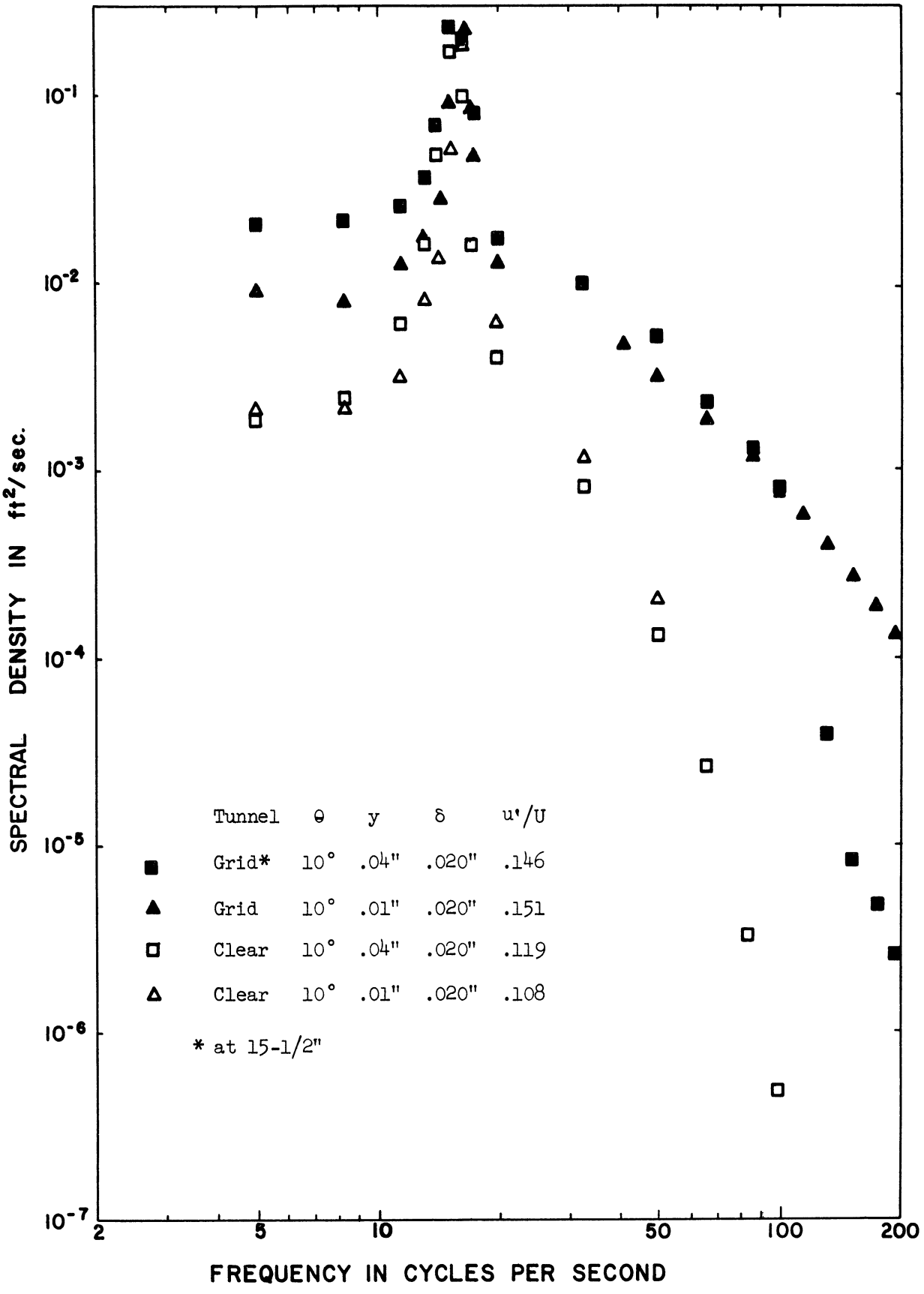

Figure 4-21. Cylinder Spectra at 20 ft/sec.

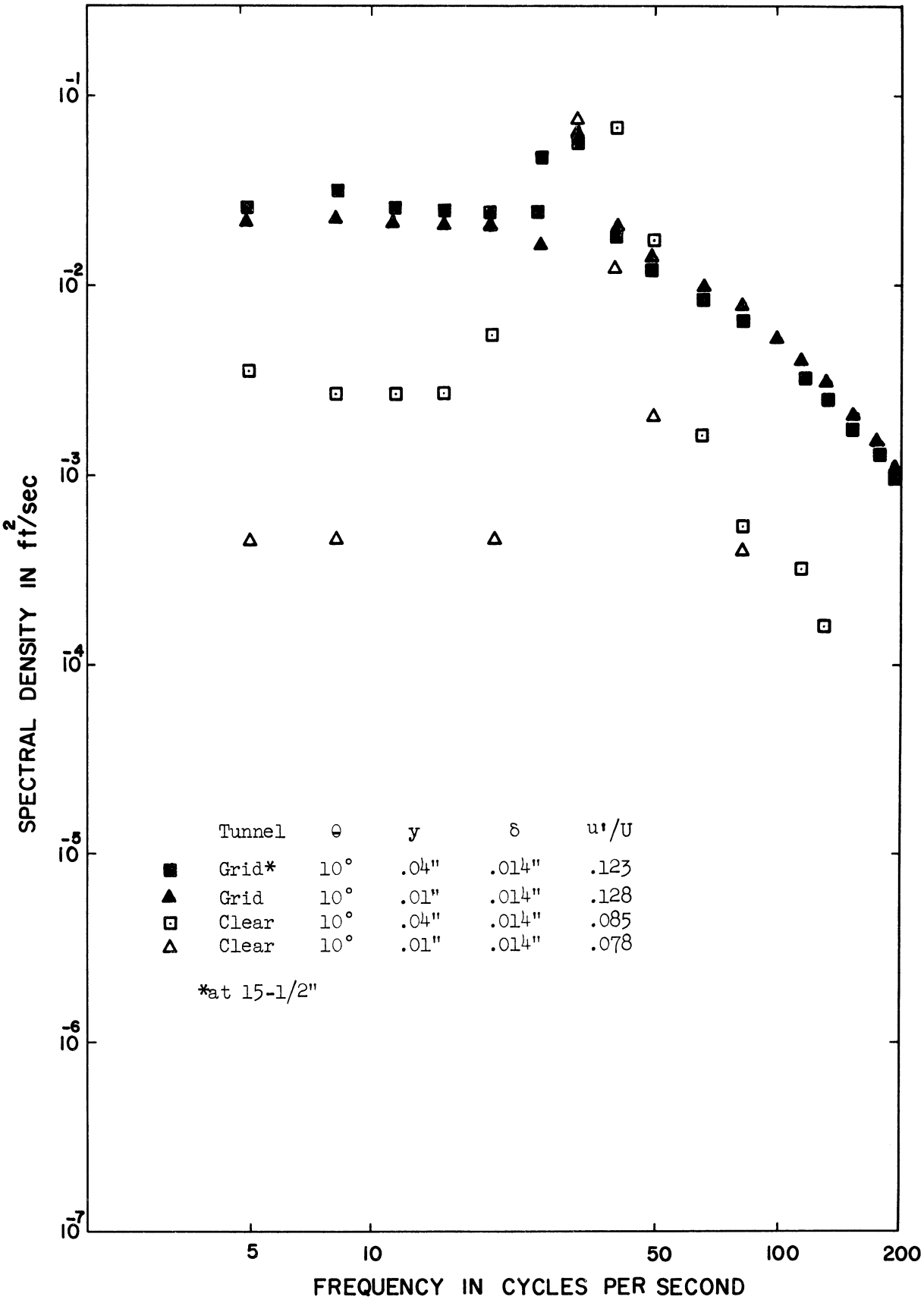

Figure 4-22. Cylinder Spectra at 40 ft/sec.

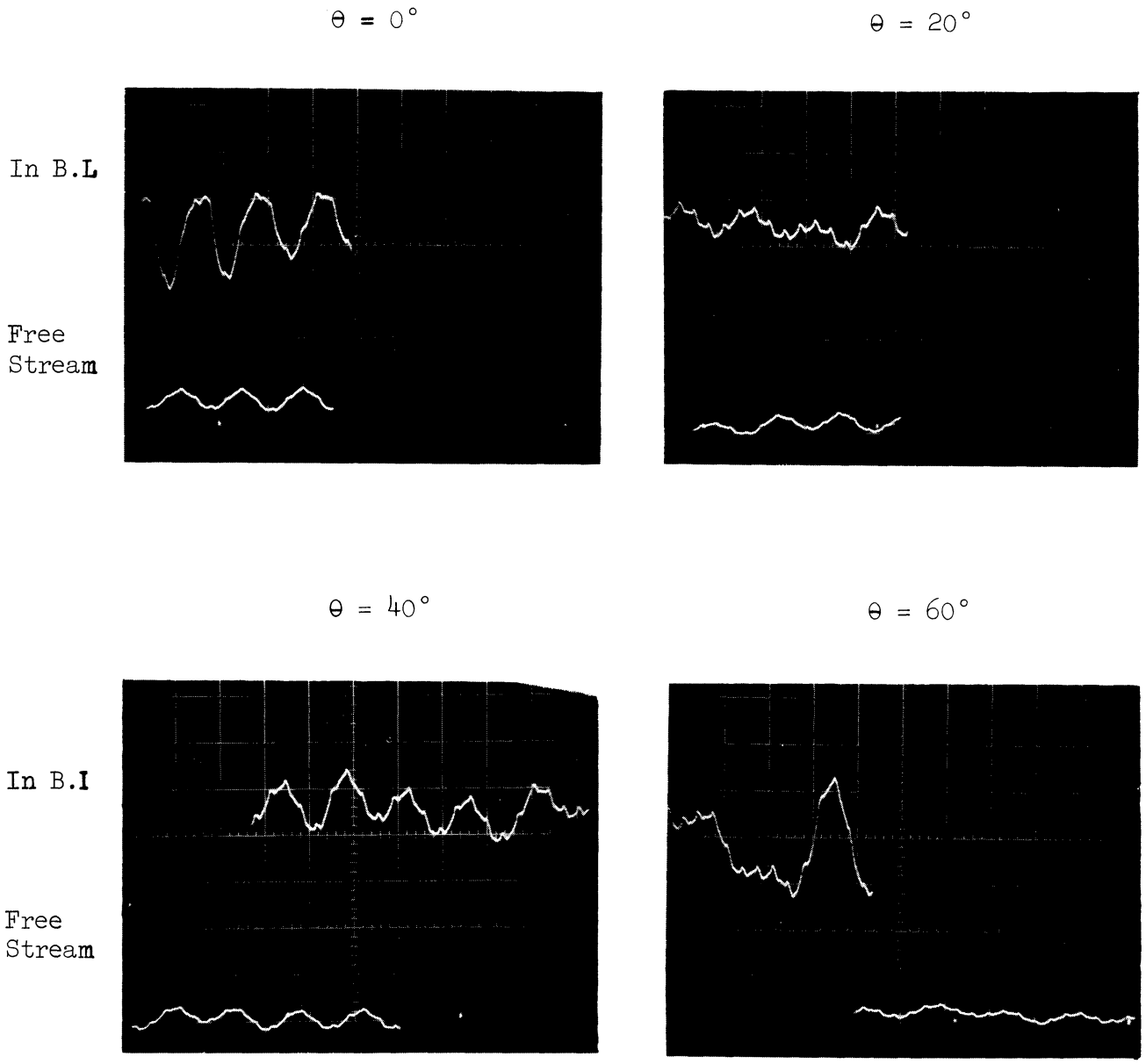

Note: Gain constant; sweep at 50 msec/cm.

Figure 4-23. Clear Tunnel Cylinder Oscillograms. R_{e_D} = 240,000; y = 0.001".

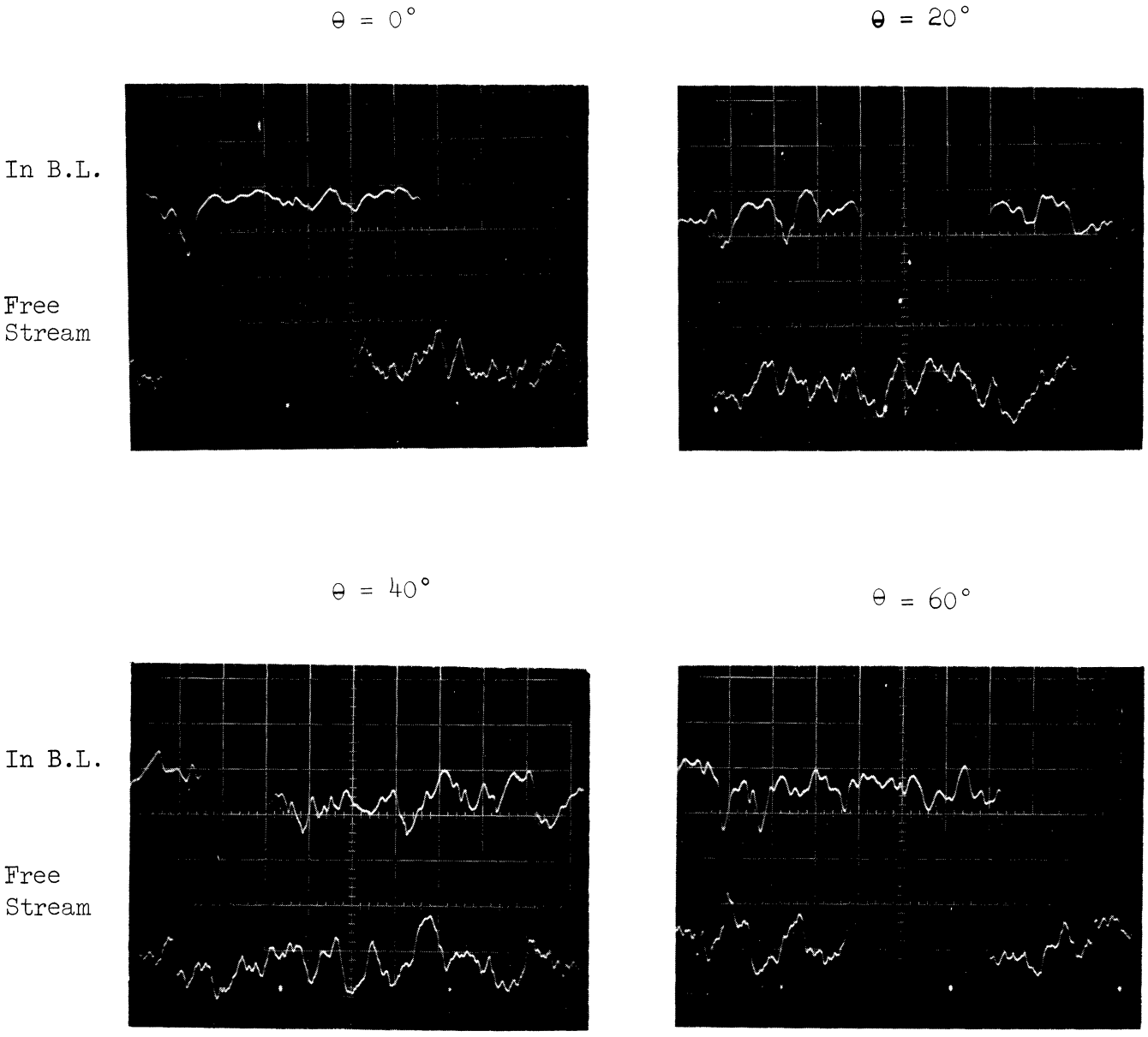

Note: Gain constant at 0.2 that of Figure 4-23. Sweep at $5\frac{\text{msec}}{\text{cm}}$.

Figure 4-24. Cylinder Oscillograms with Grid at 15-1/2 Inches. R_{e_D} = 240,000; y = 0.001".

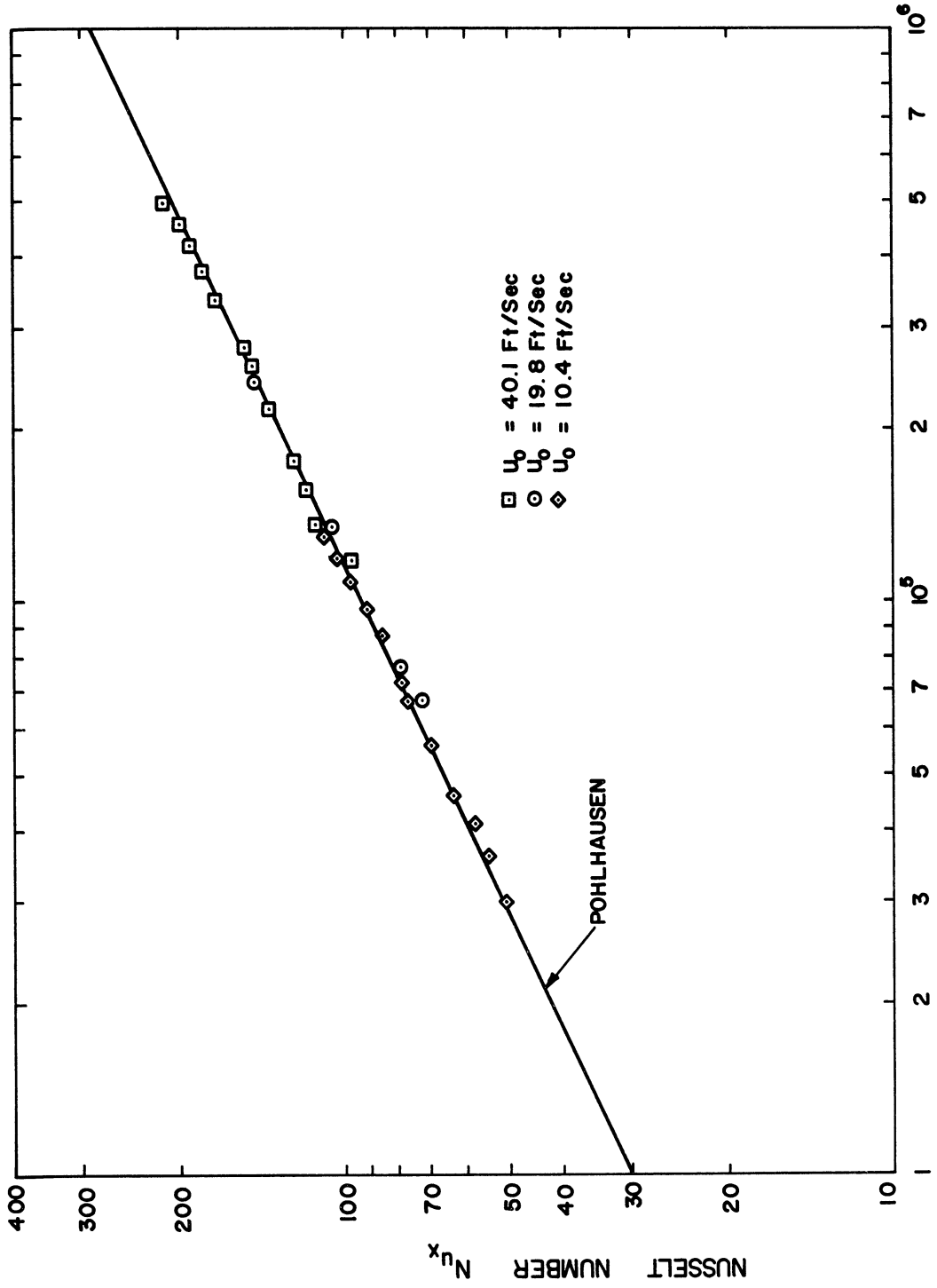

Figure 5-1. Constant Temperature Plate Heat Transfer Clear Tunnel.

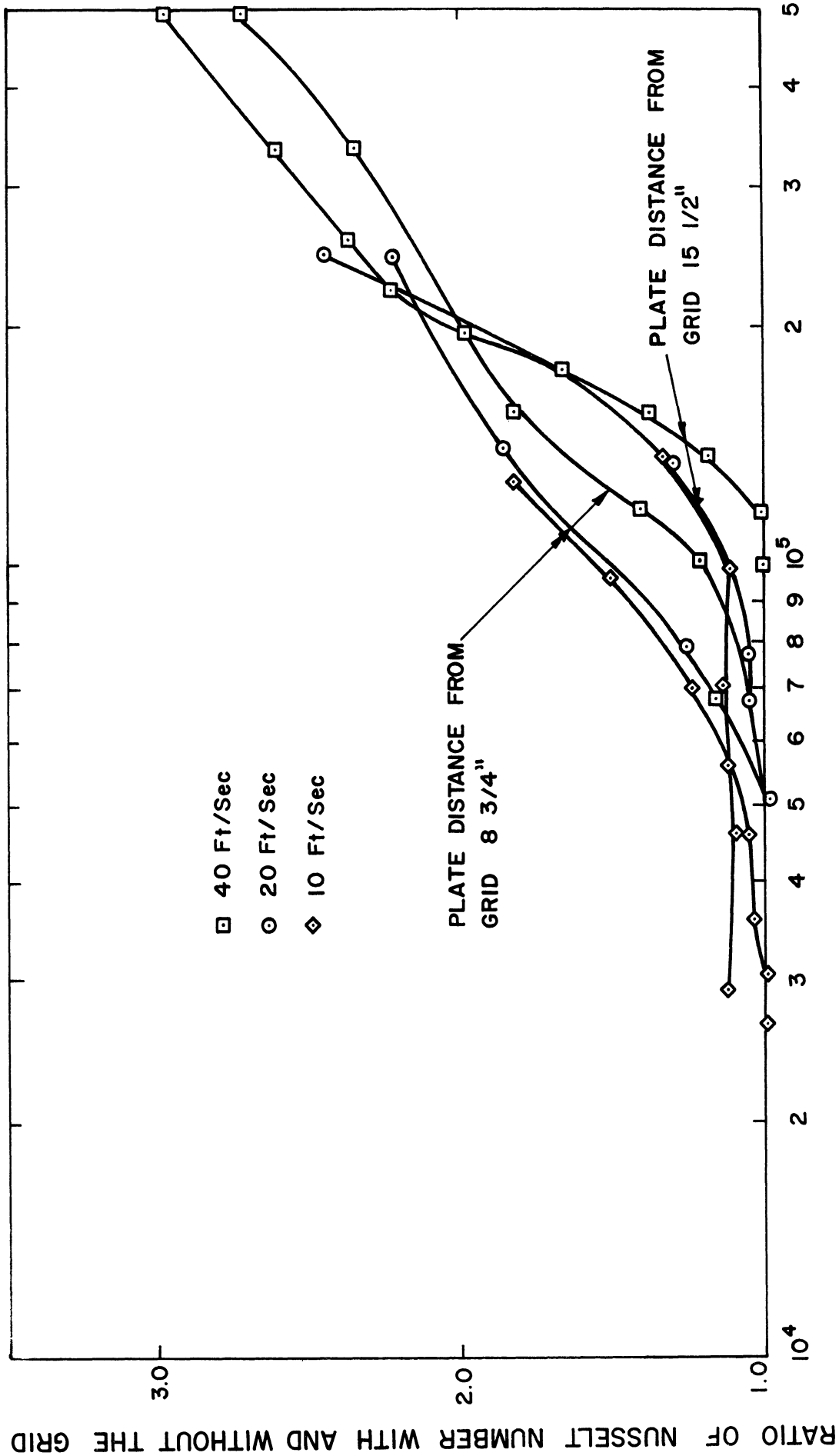

Figure 5-2. Effect of Free Stream Turbulence on Flat Plate Heat Transfer.

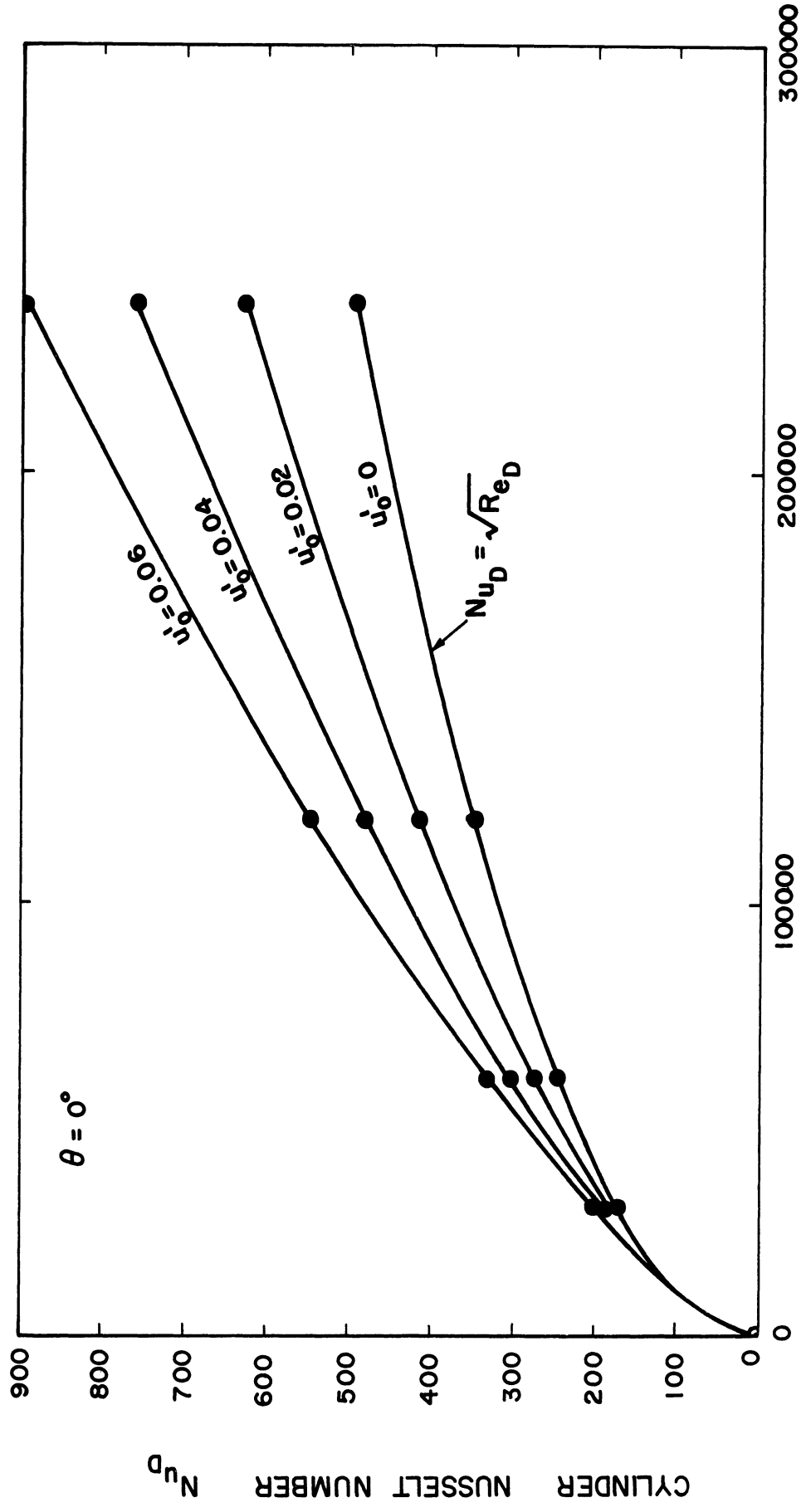

Figure 5-3. Cylinder Heat Transfer Faired Data $\theta = 0°$.

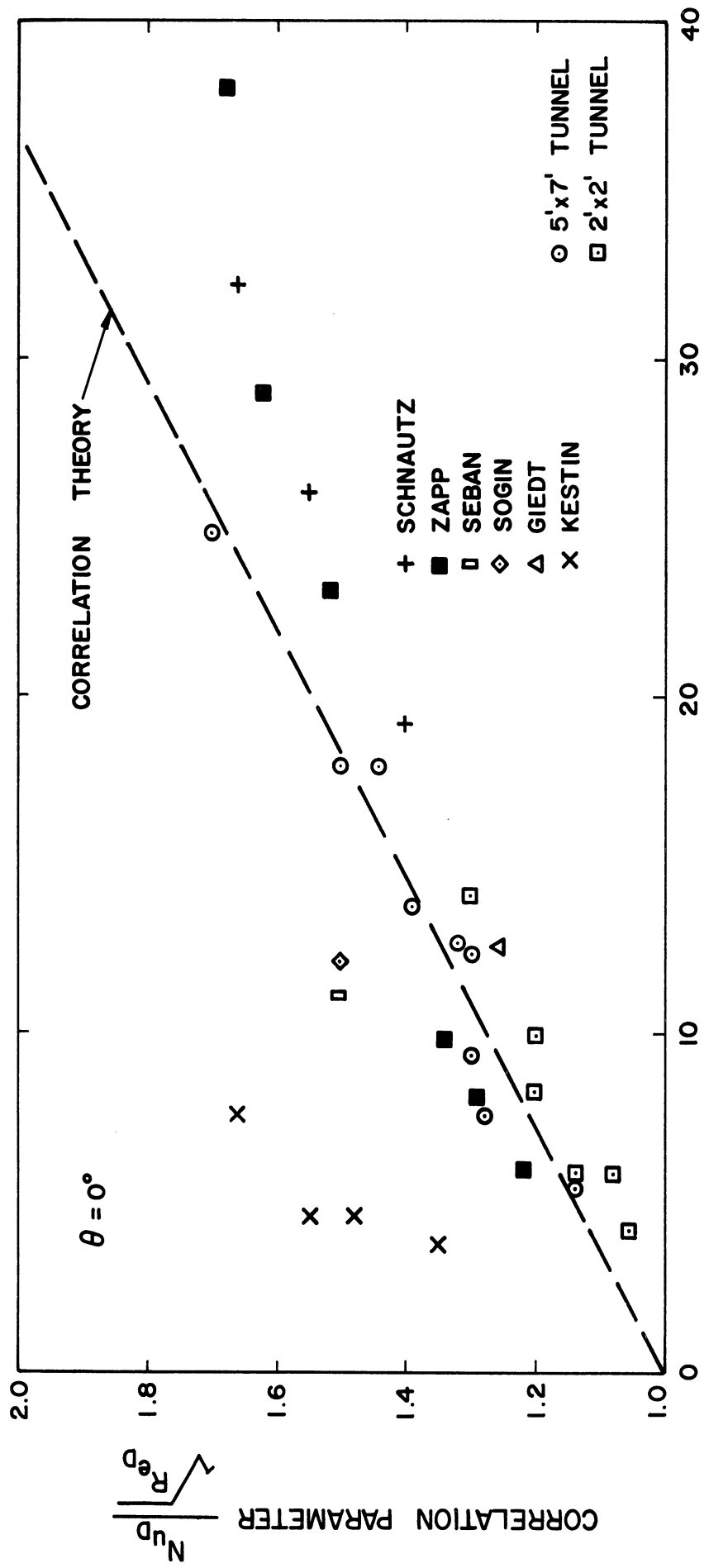

Figure 5-4. Cylinder Heat Transfer Correlation $\theta = 0°$.

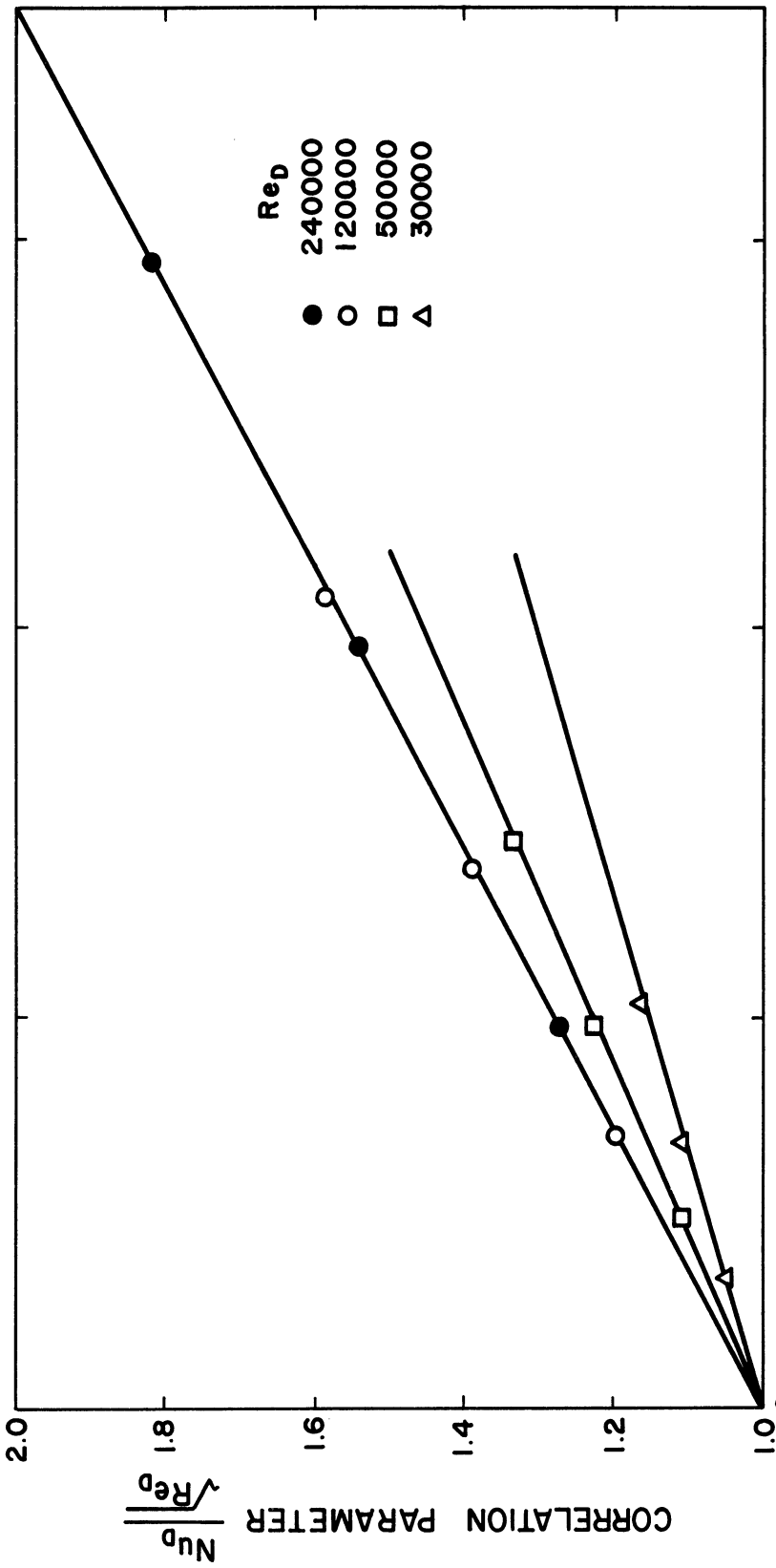

Figure 5-5. Correlation of Faired Data $\theta = 0°$.

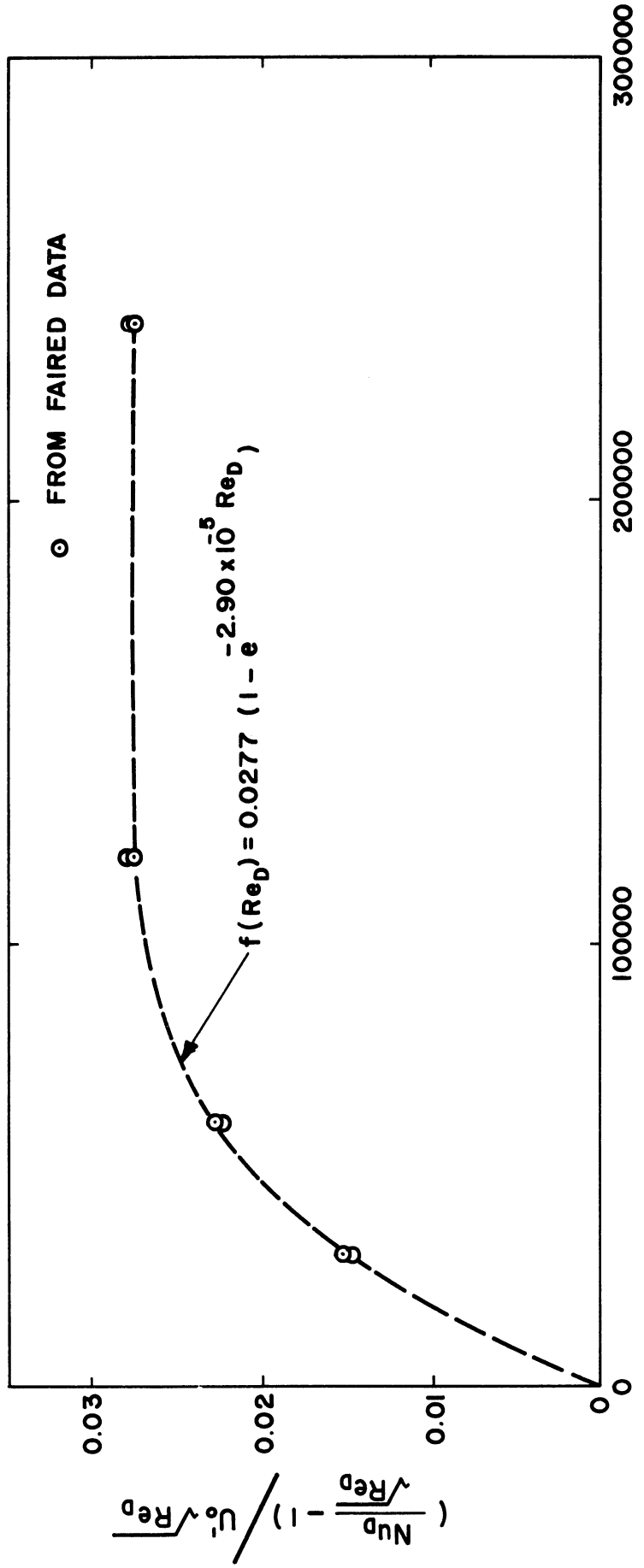

Figure 5-6. Exponential Correlation Function $\theta = 0°$.

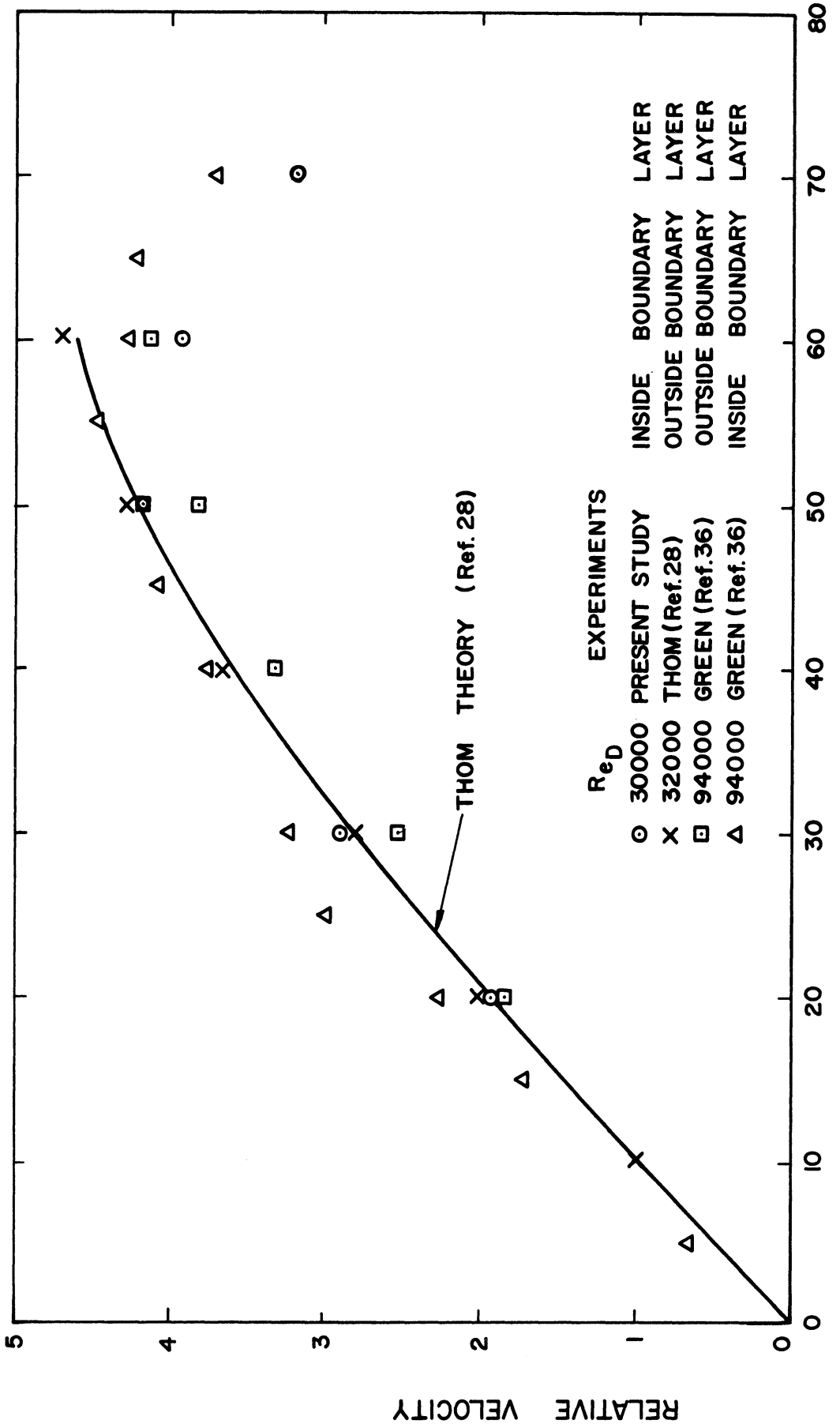

Figure 5-7. Thom Theory and Experimental Data.

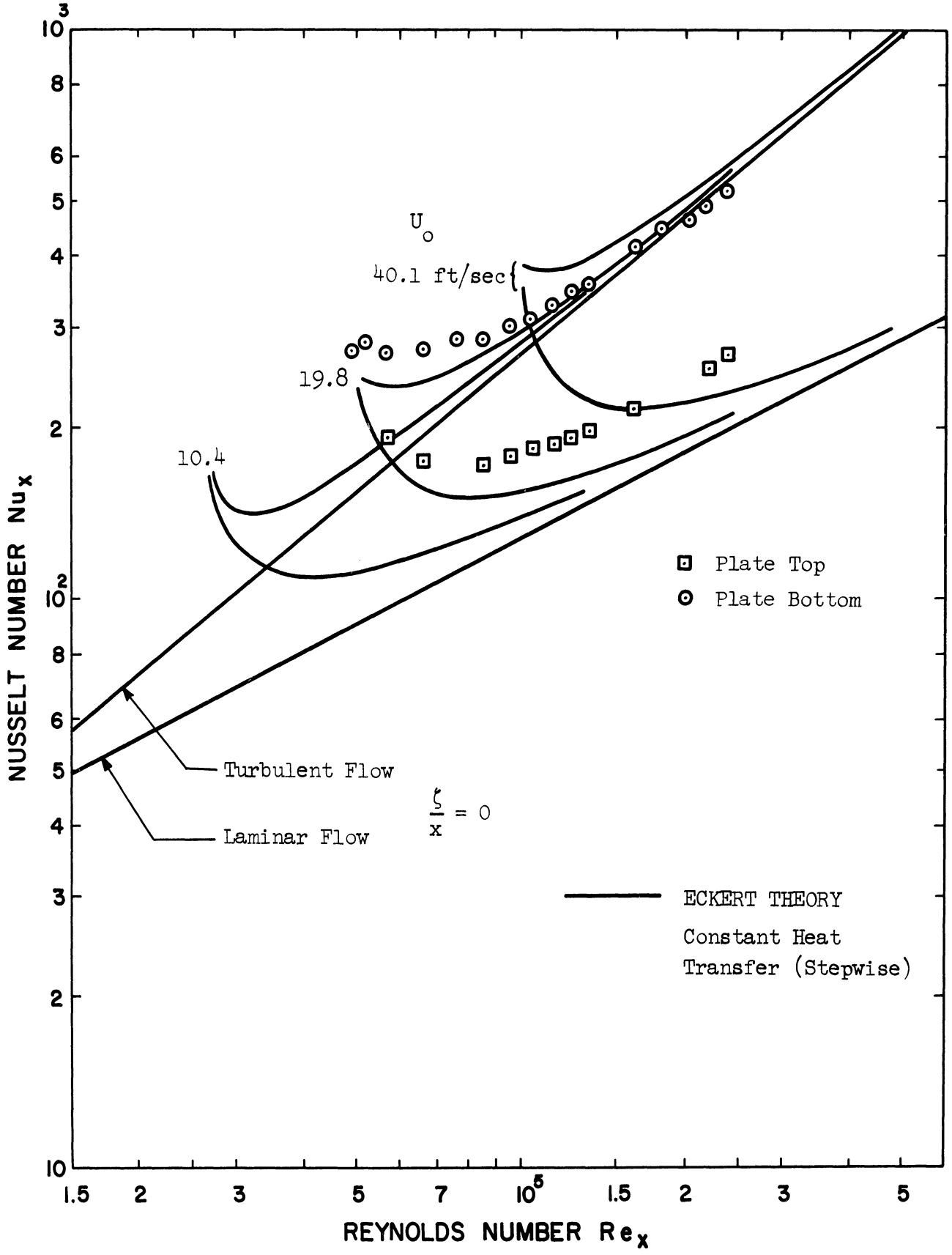

Figure 7-1. Sharp Leading Edge With Vortex Generators.

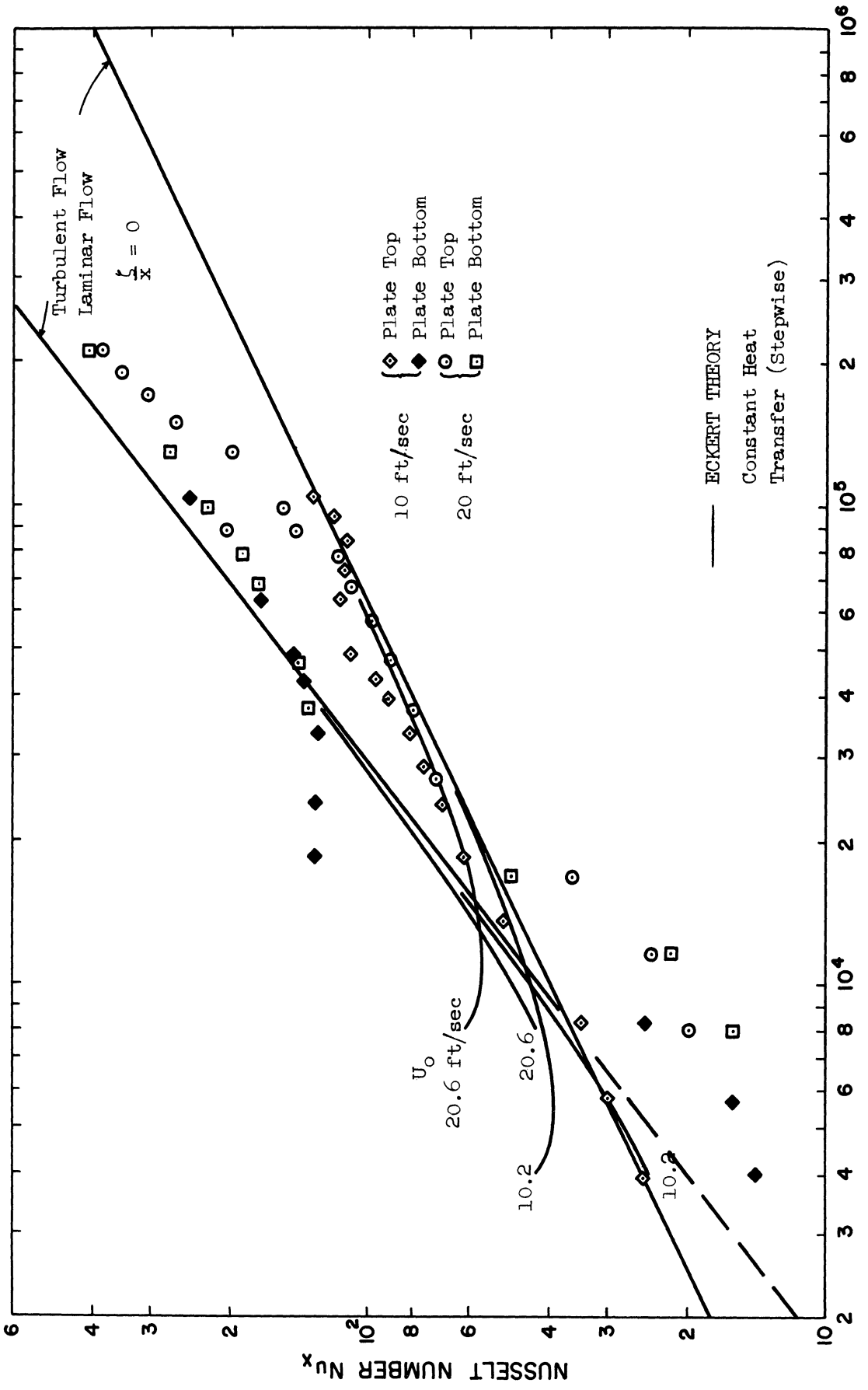

Figure 7-2. Hemicylindrical Nose in Clear Tunnel.

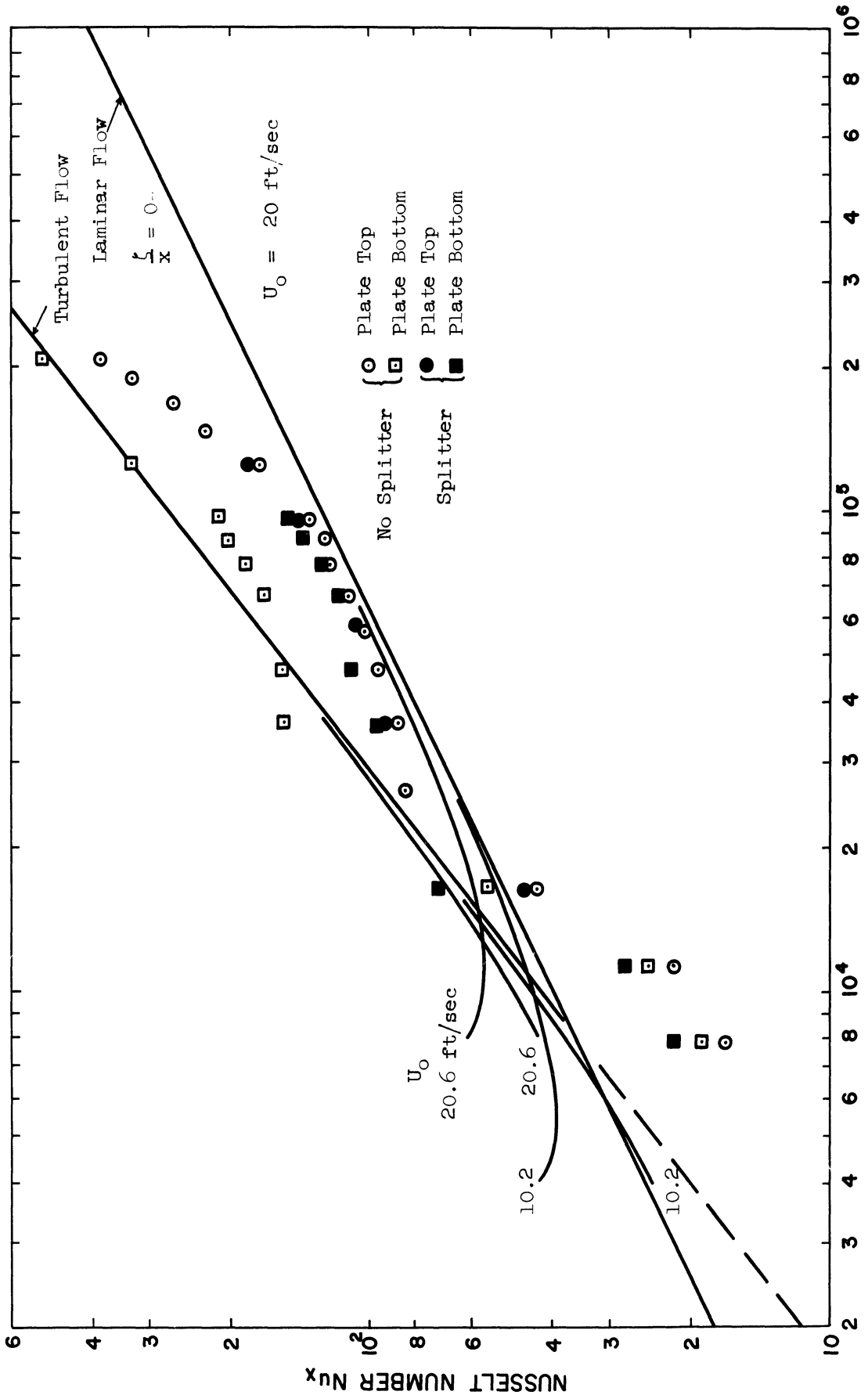

Figure 7-3. Hemicylindrical Nose with Splitter.

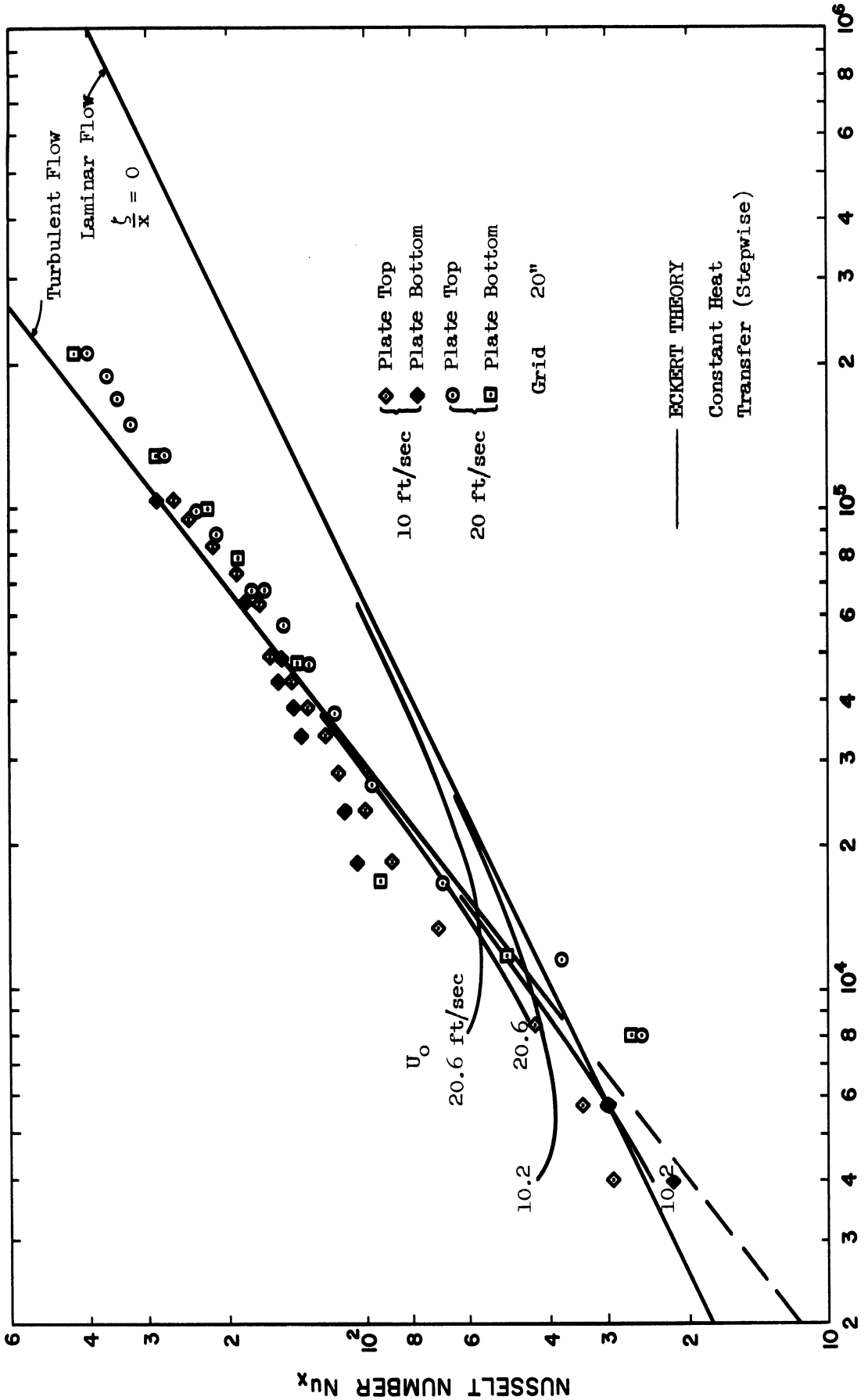

Figure 7-4. Hemicylindrical Nose with Grid.

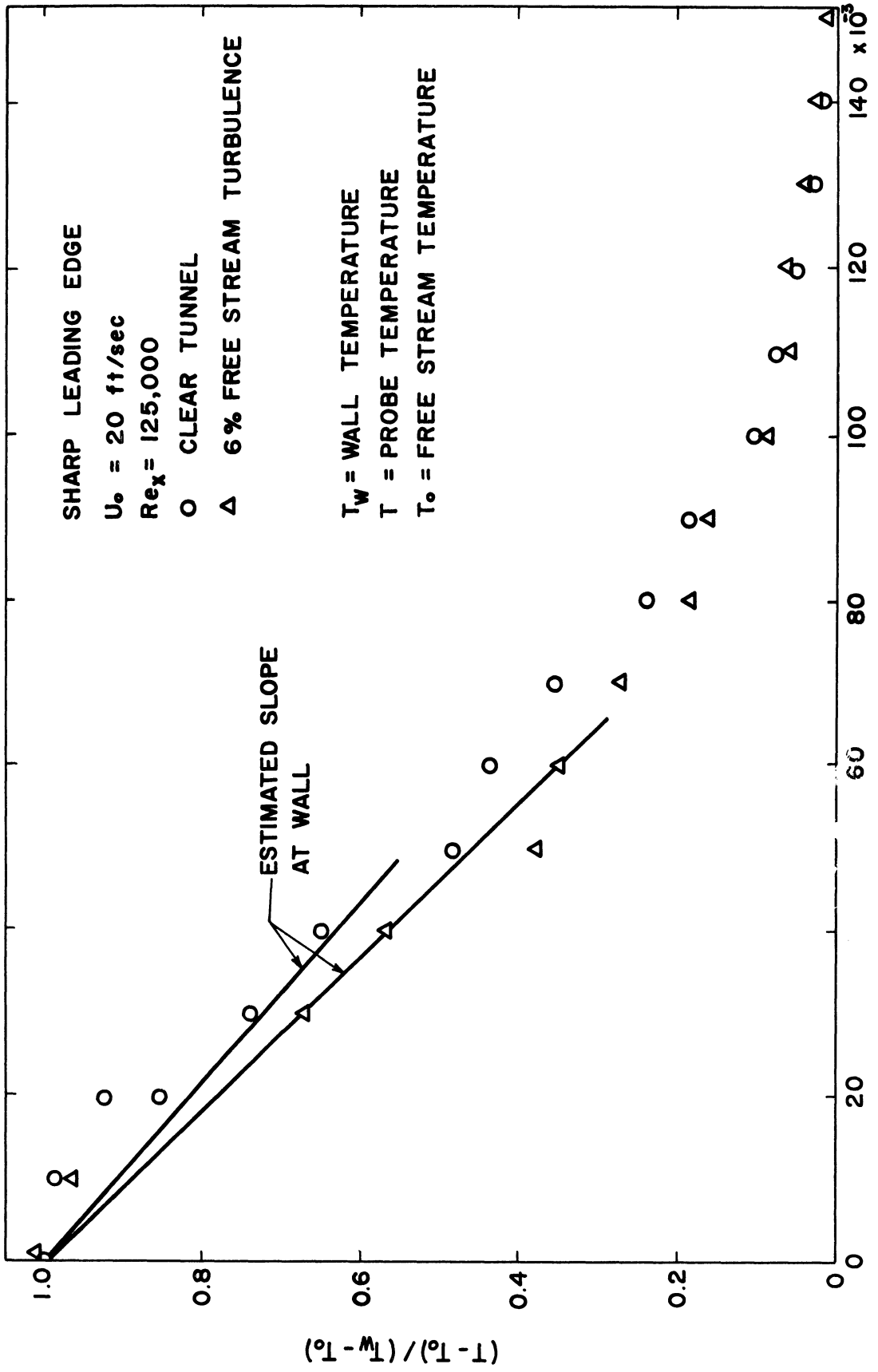

Figure 7-5. Flat Plate Temperature Profile.

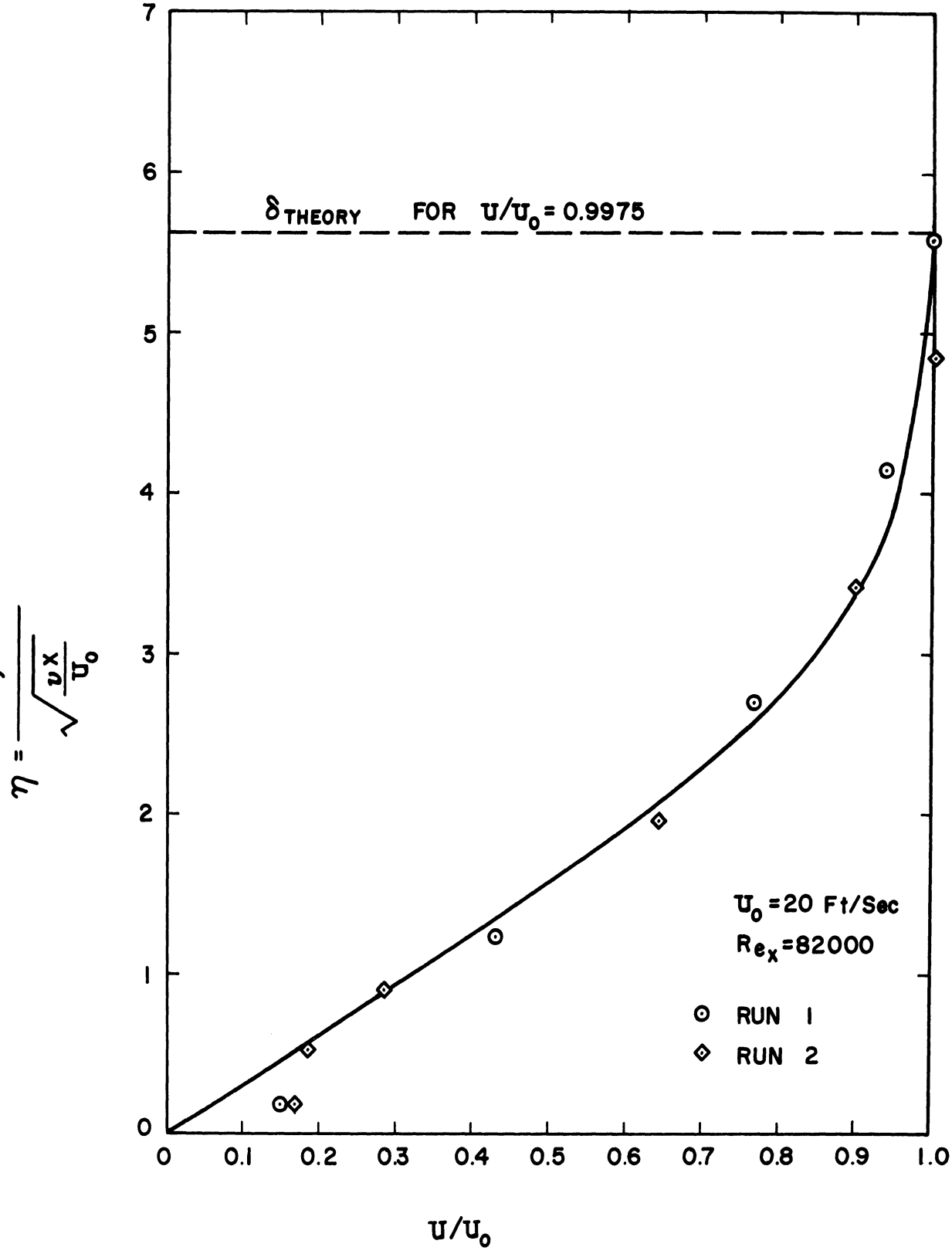

Figure 7-6. Flat Plate Velocity Profiles
Hemicylindrical Nose - Clear Tunnel.

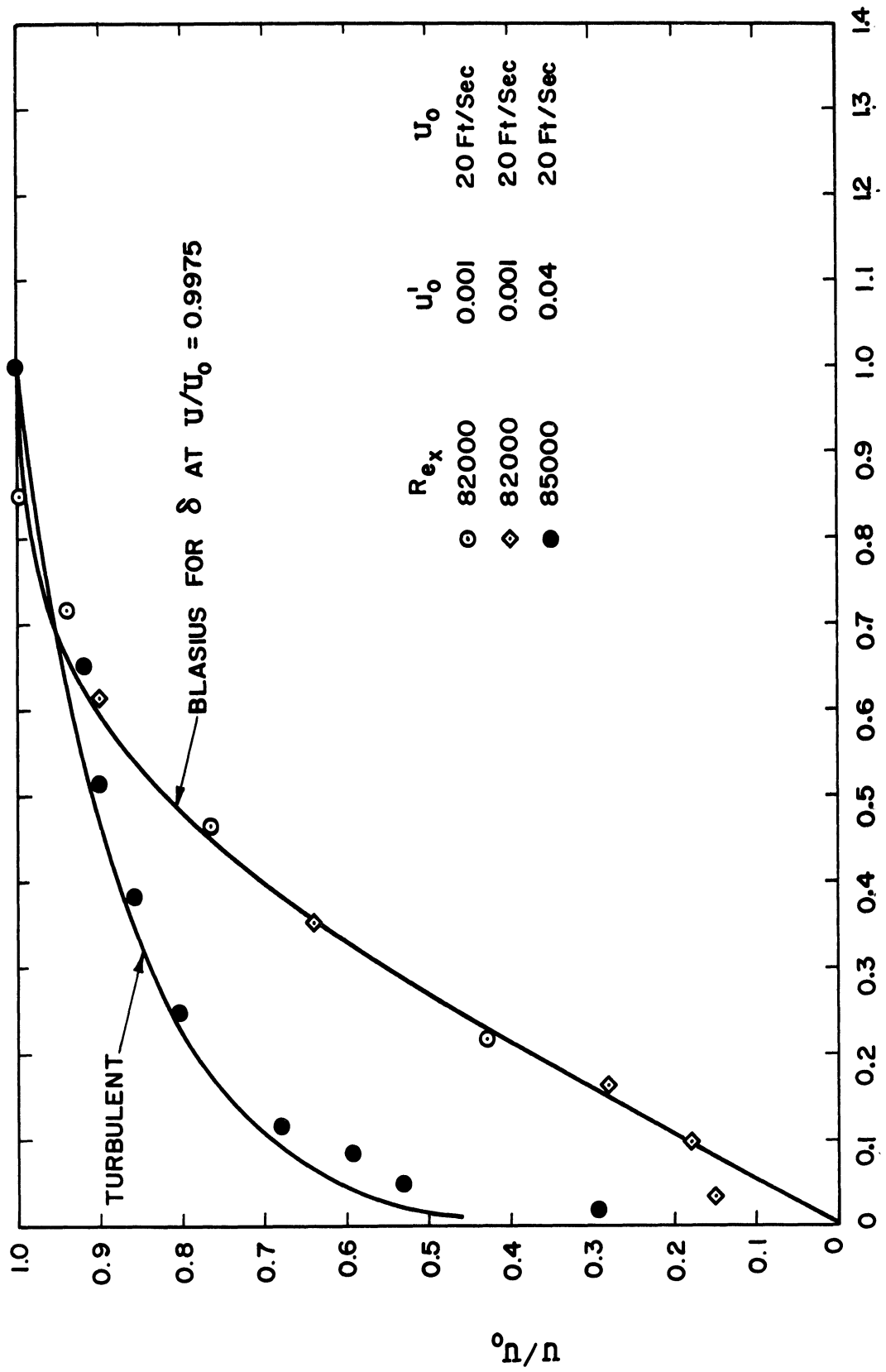

Figure 7-7. Flat Plate Velocity Profiles - Hemicylindrical Nose with Grid.

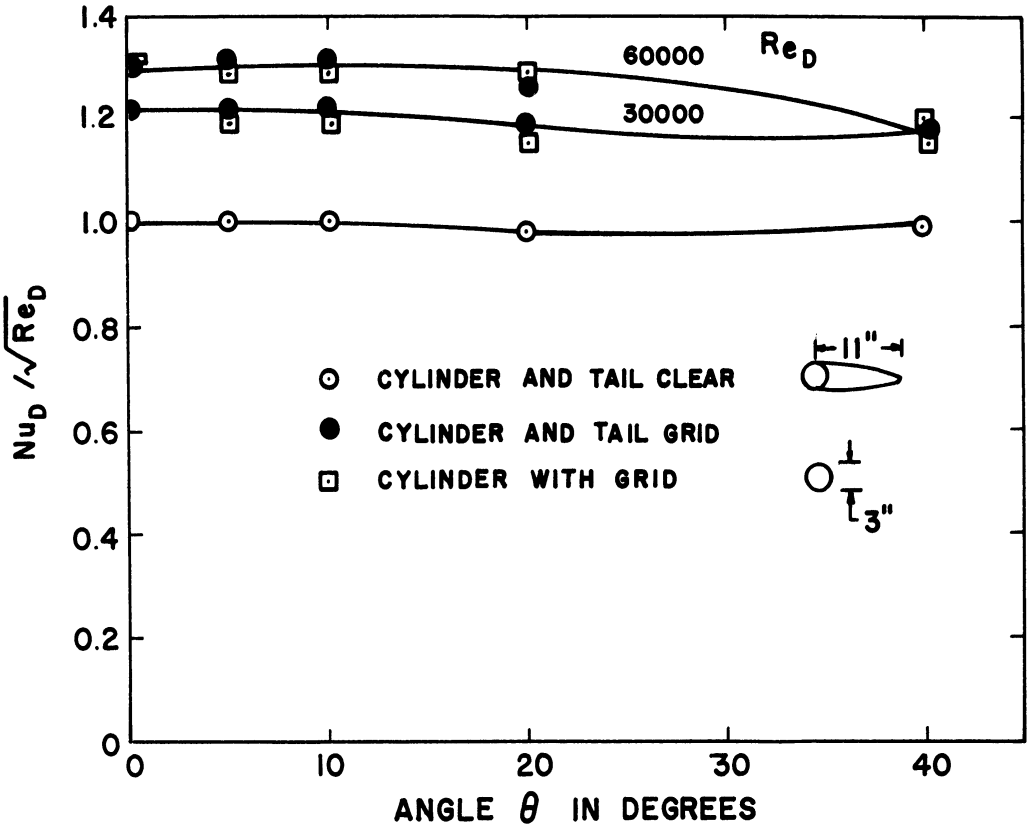

Figure 7-8. Nusselt Number for Cylinder with Tail.

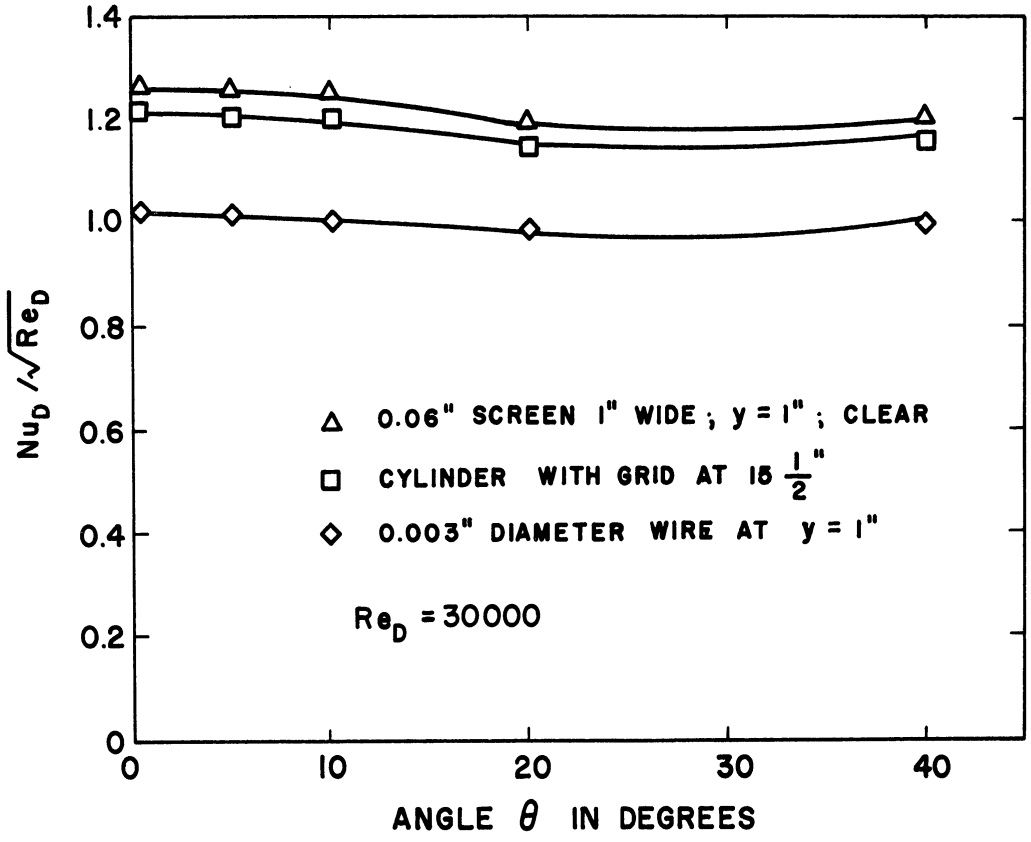

Figure 7-9. Nusselt Number with Flow Disturbances.

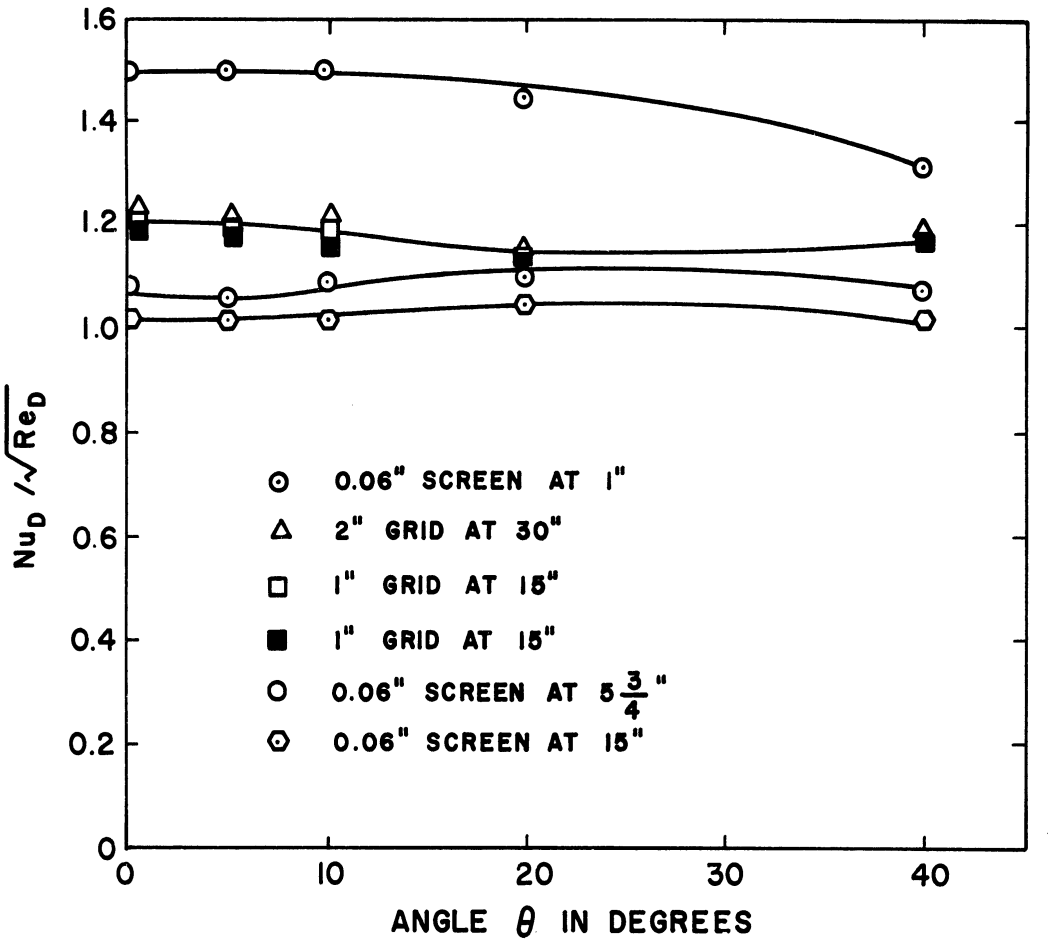

Figure 7-10. Nusselt Number with Screen and Large Grid.

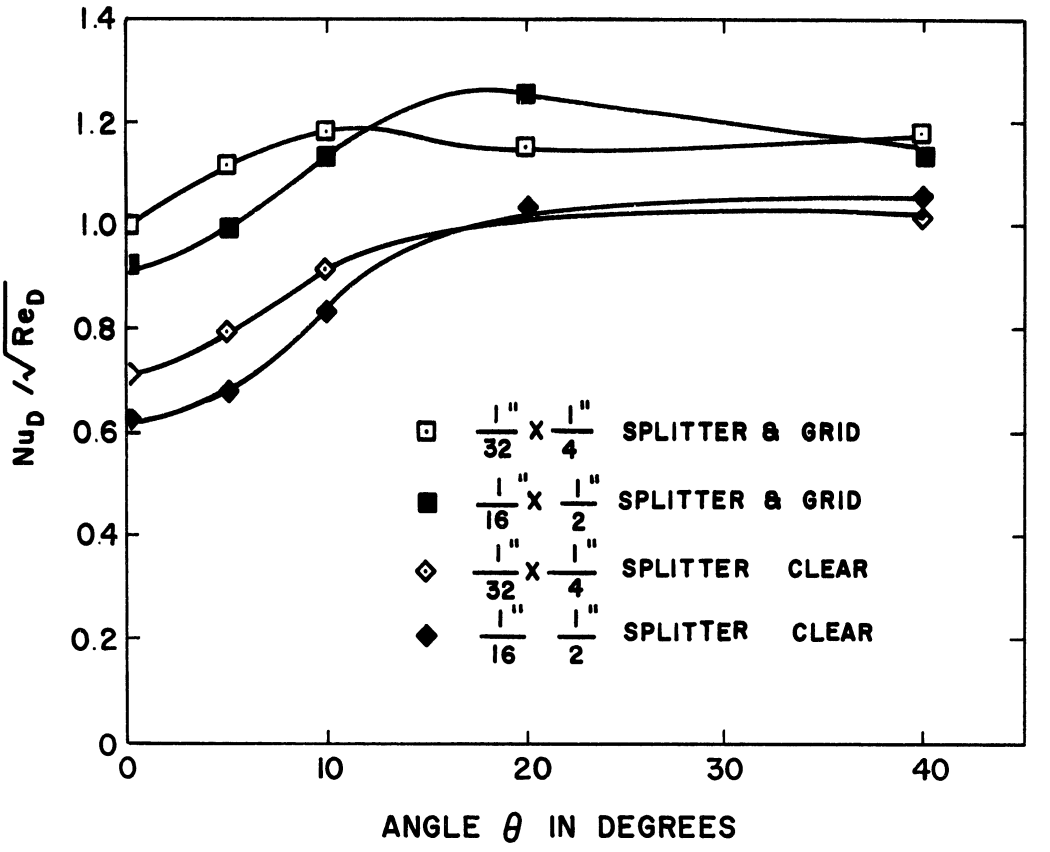

Figure 7-11. Nusselt Number with Splitter.

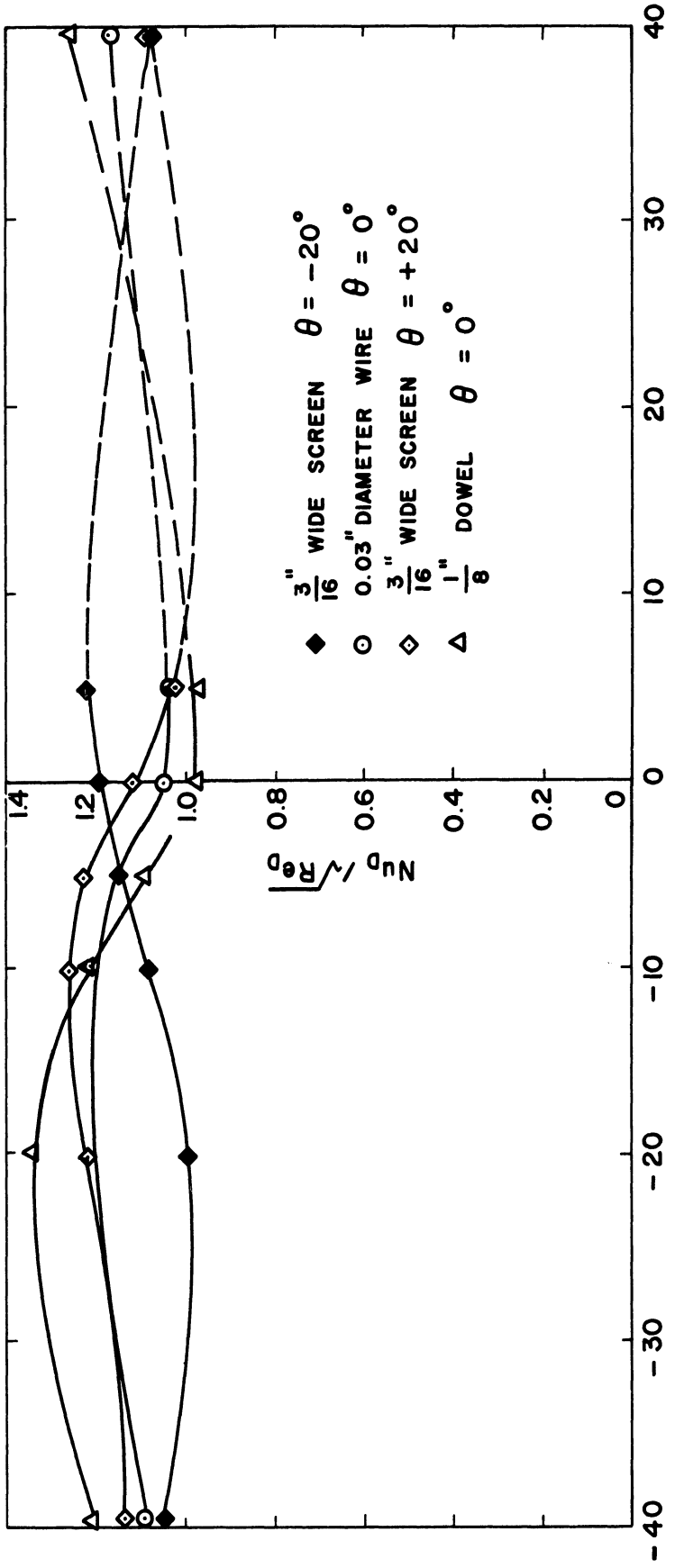

Figure 7-12. Nusselt Number with Local Unsymmetrical Disturbances.

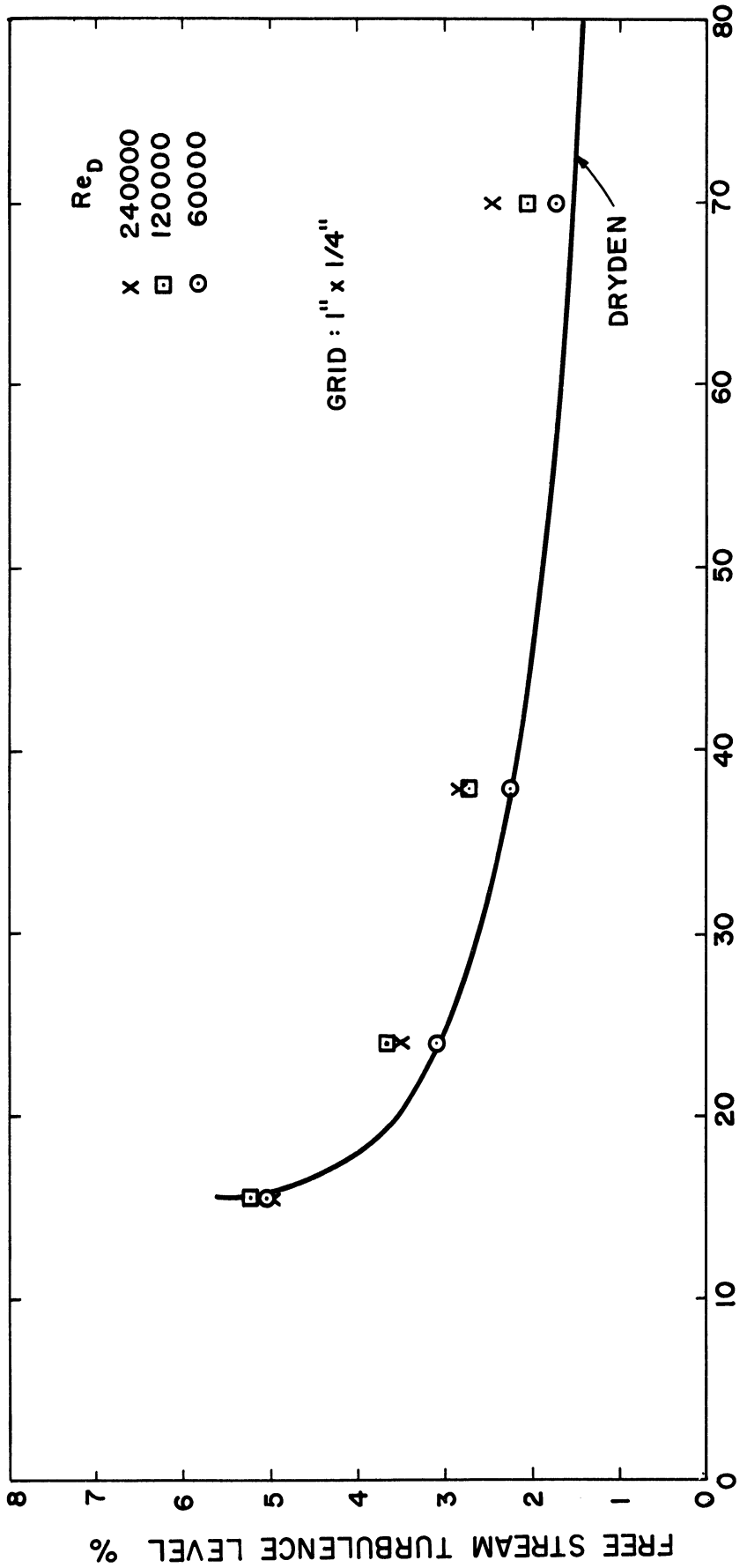

Figure 7.13. Turbulence Level in 5' x 7' Tunnel.

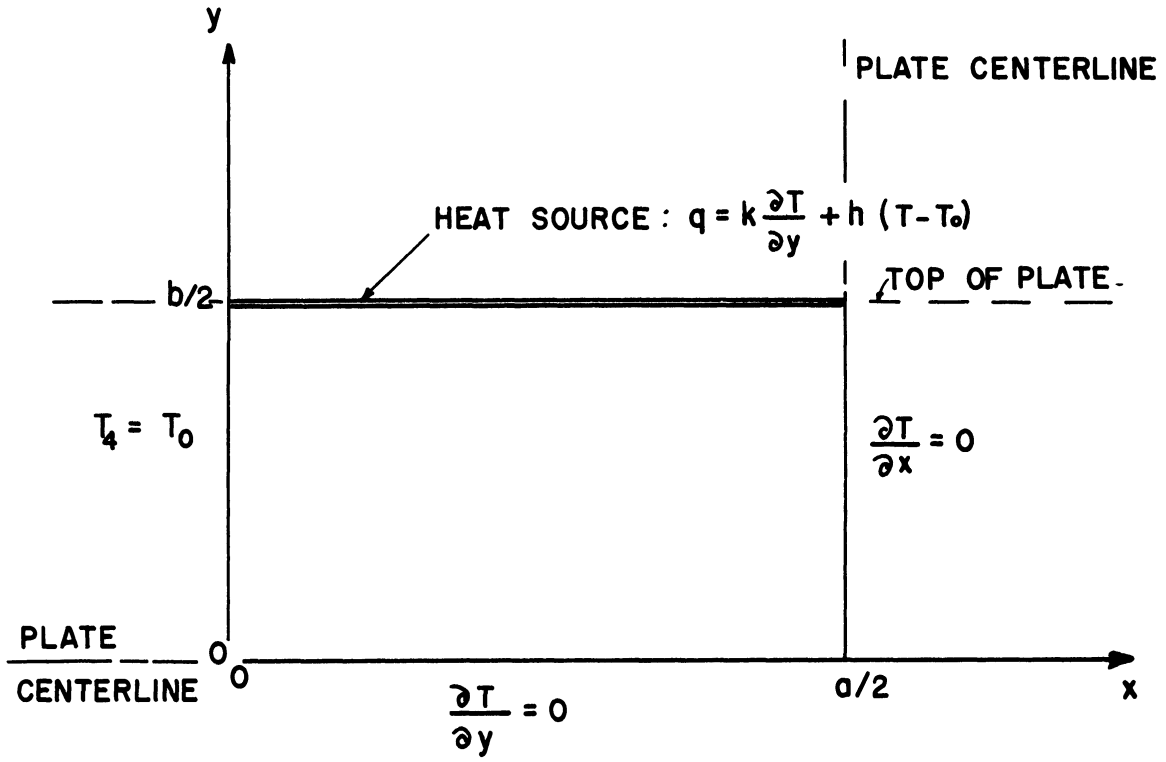

Figure 7-14. Homogeneous Plate Heat Conduction.

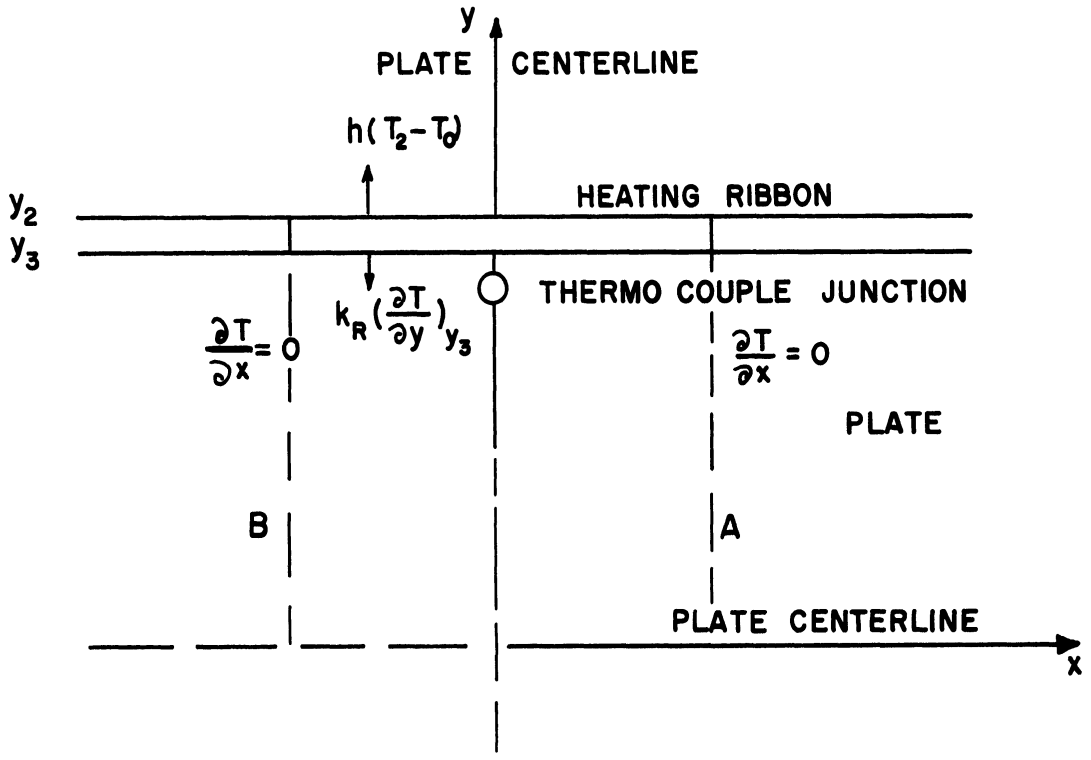

Figure 7-15. Thermocouple Error Due to Junction Location.

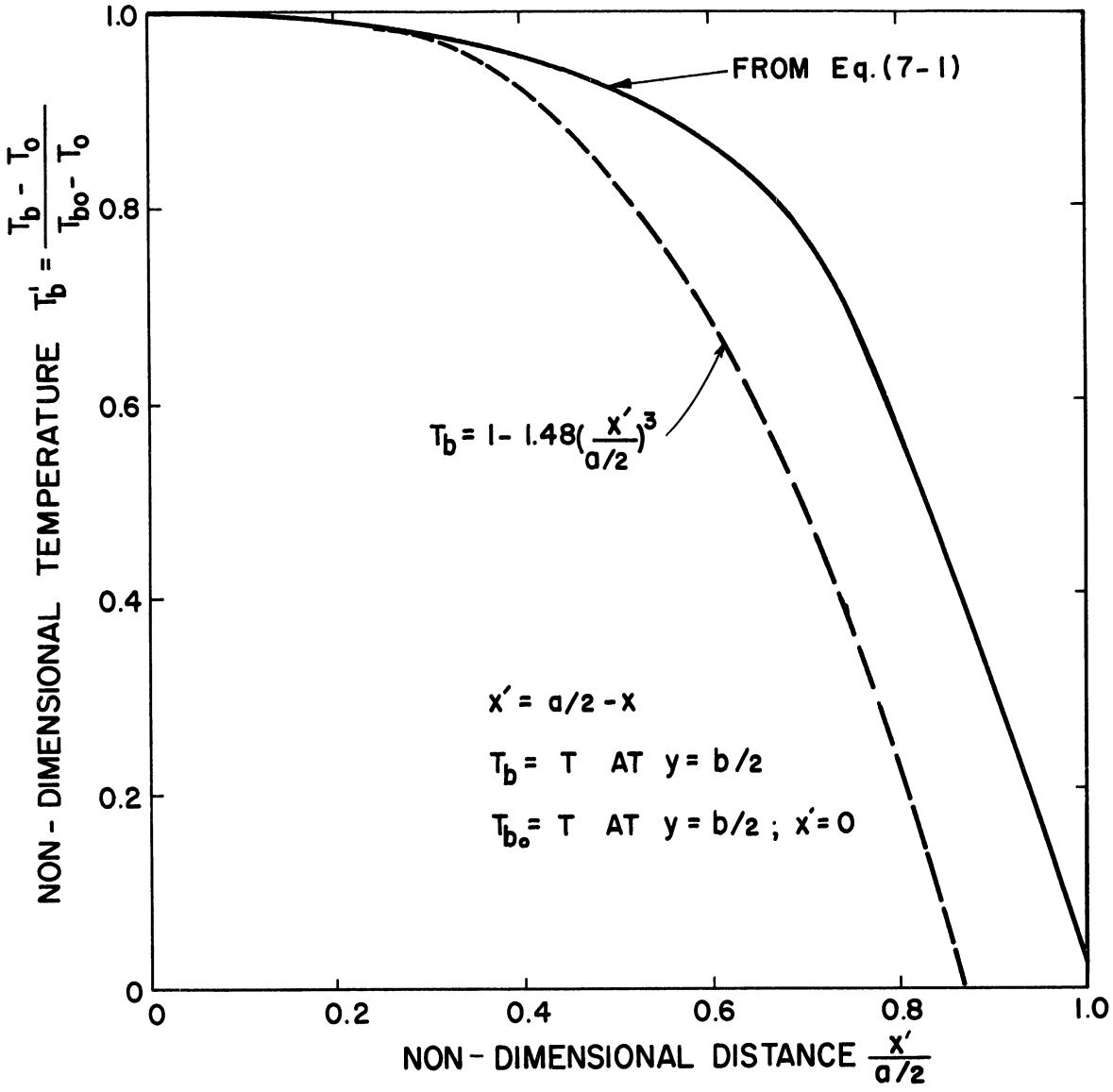

Figure 7-16. Homogeneous Plate Temperature Distribution.

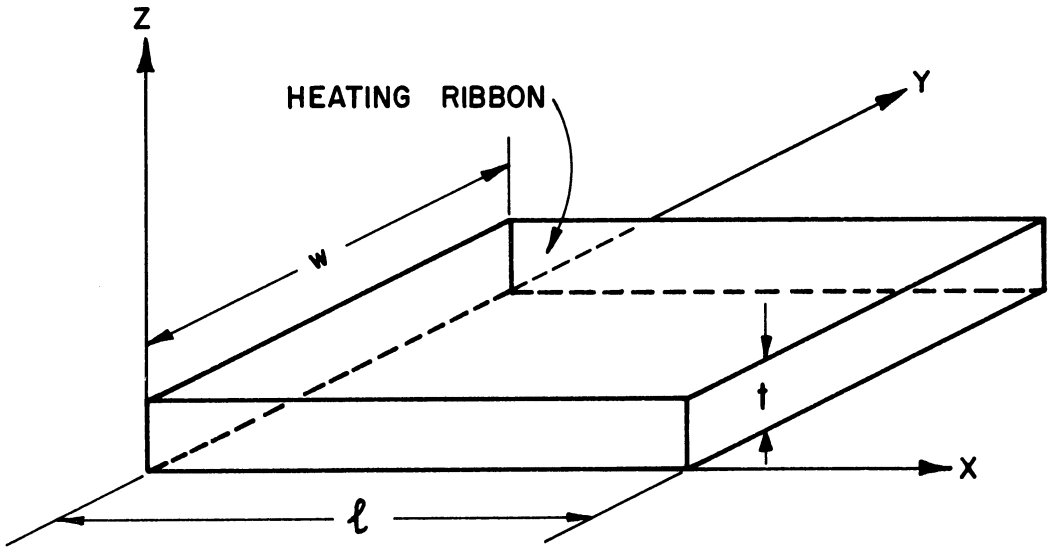

Figure 7-17. Alternating Current Plate Heating Nomenclature.

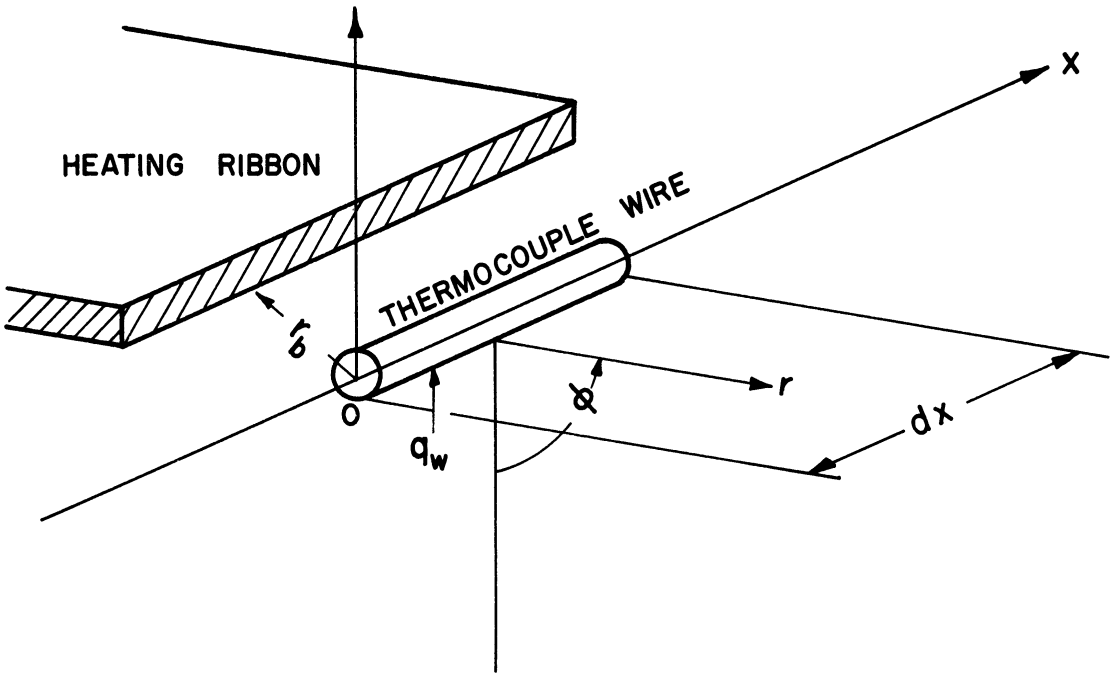

Figure 7-18. Thermocouple Heat Conduction Nomenclature.

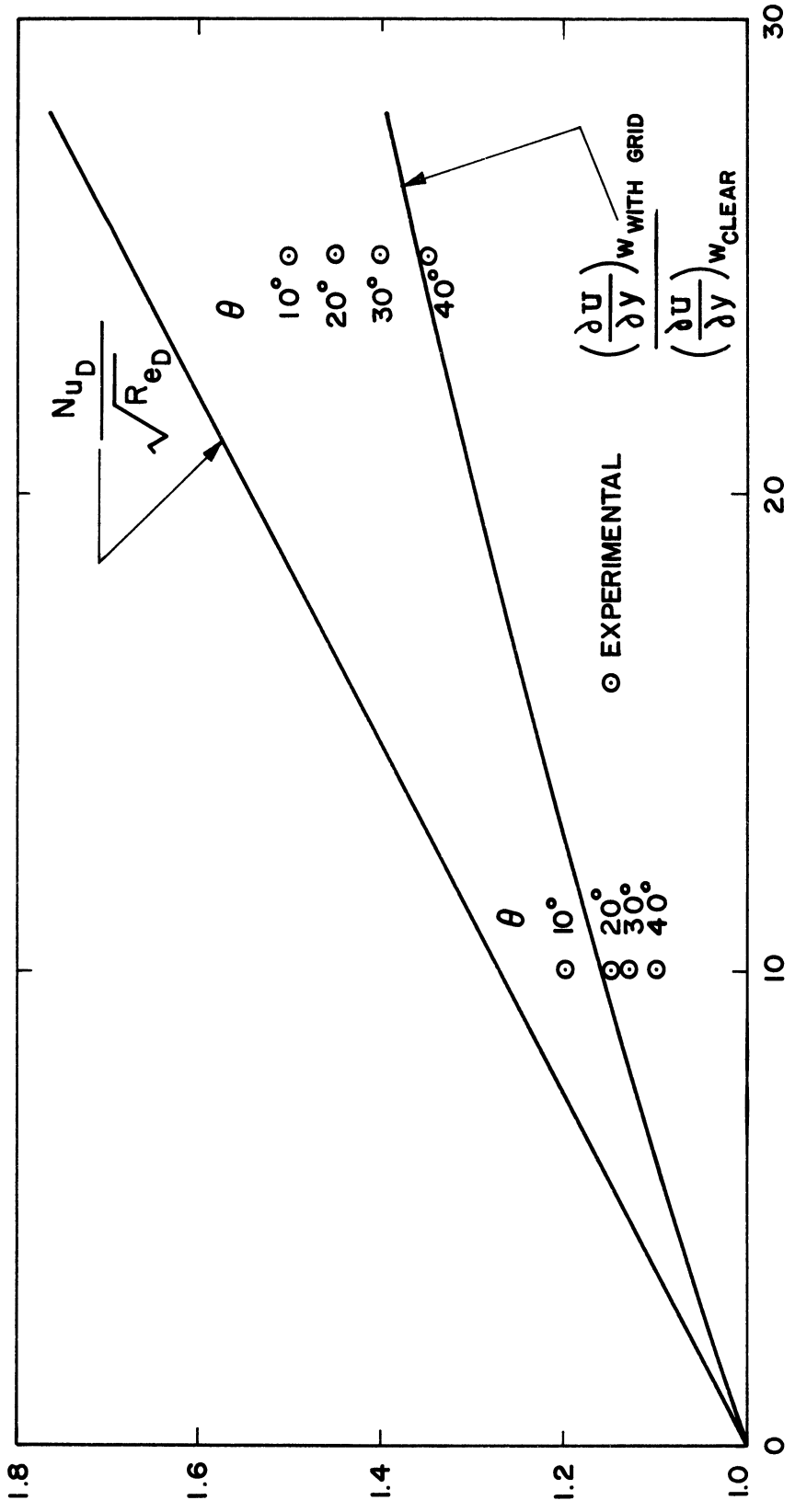

Figure 7-19. Results of Correlation Theory Calculations. (Theory for $\theta = 0°$)

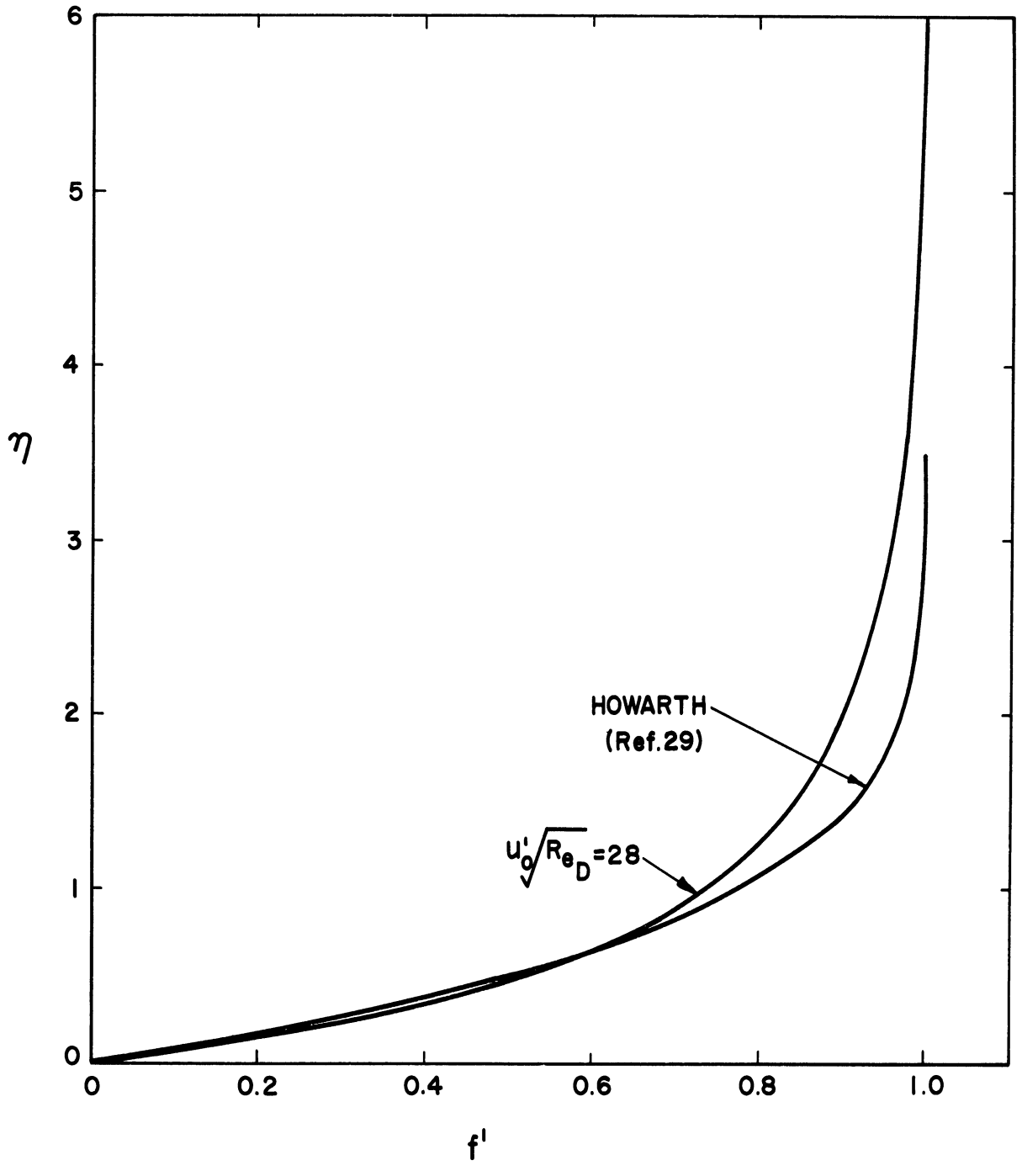

Figure 7-20. Theoretical Velocity Profiles, f' .

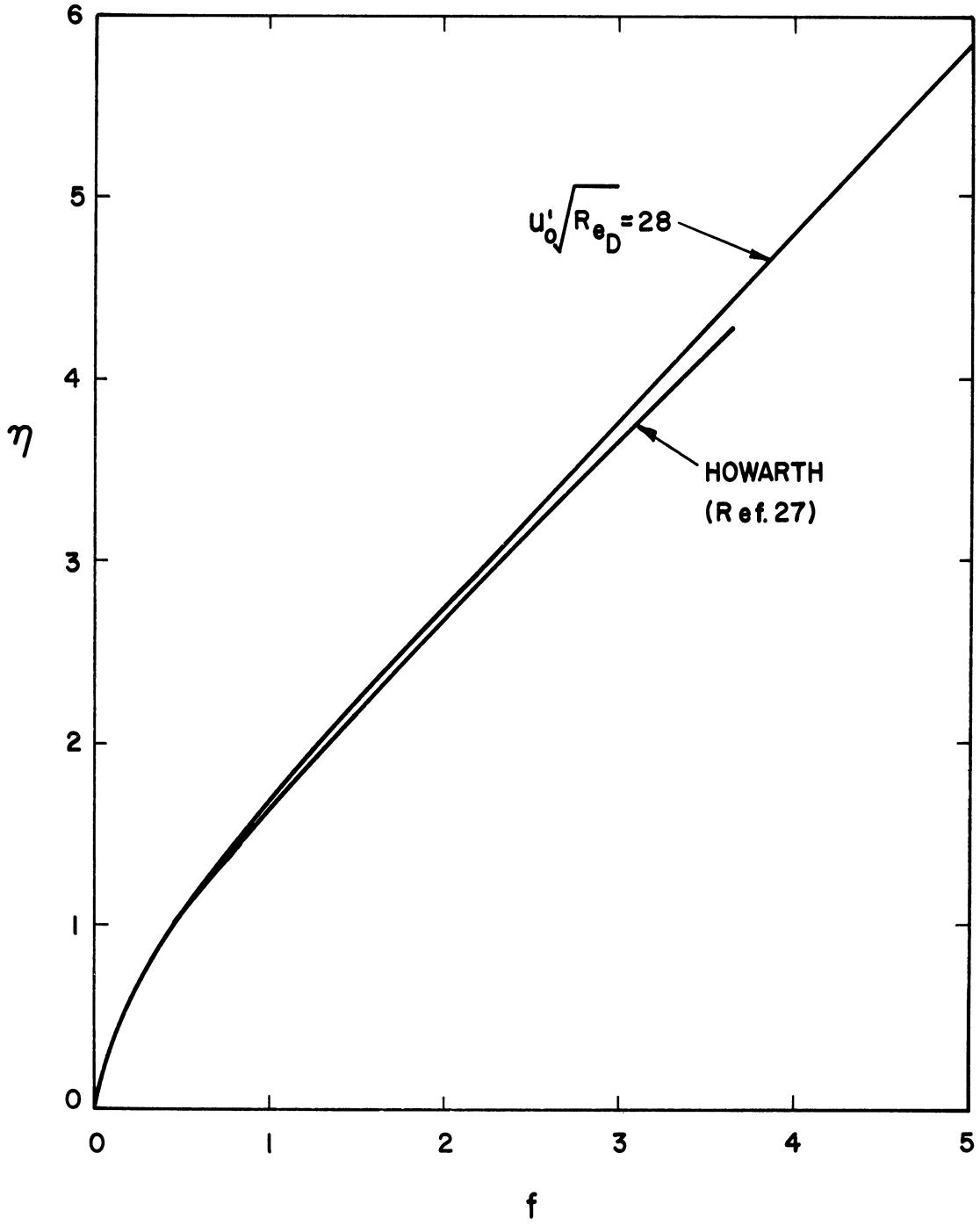

Figure 7-21. Theoretical Velocity Profiles, f .

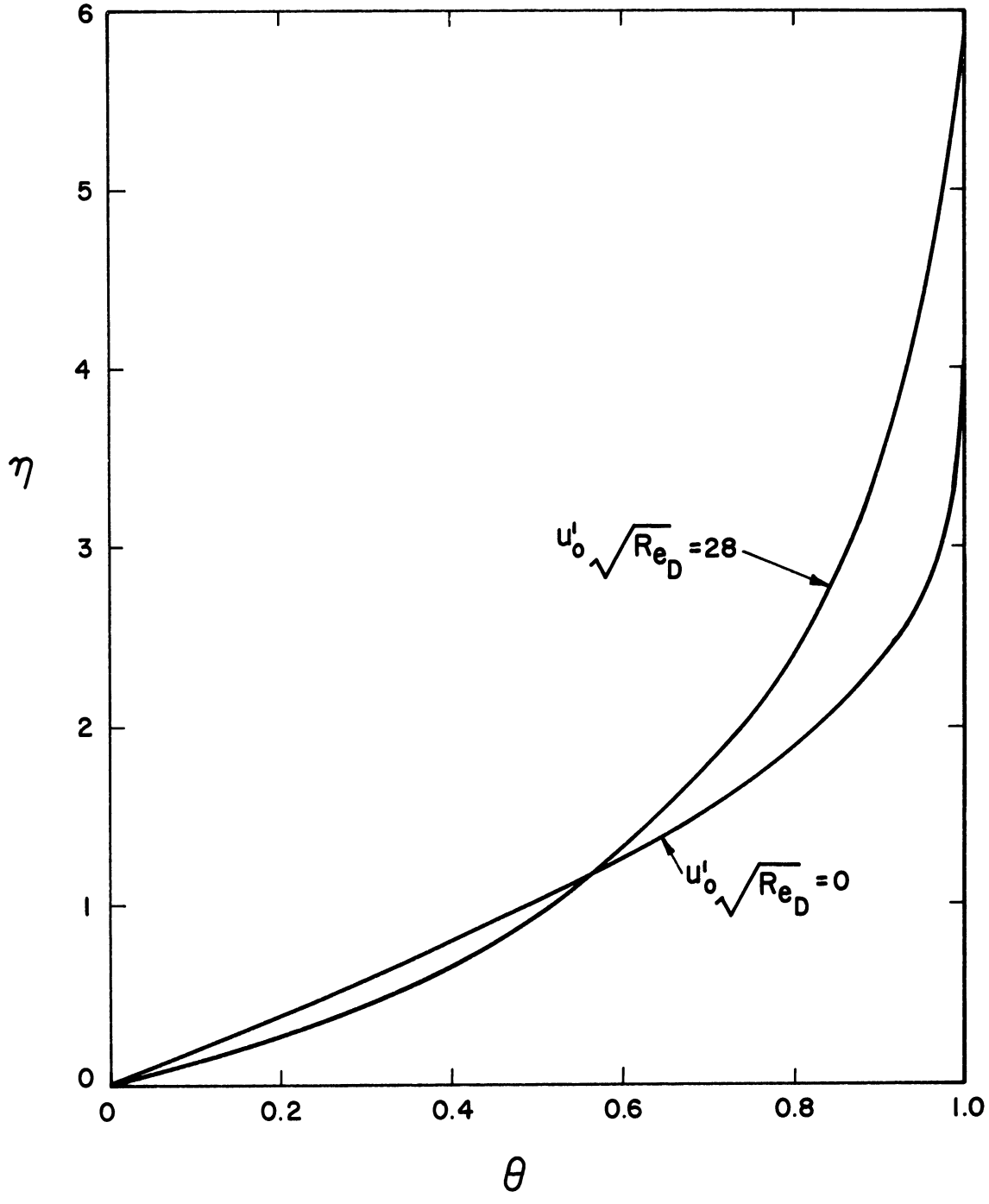

Figure 7-22. Theoretical Temperature Profiles.